POLITECNICO DI TORINO

Dipartimento di Ingegneria Meccanica e Aerospaziale

Master's Degree in Biomedical Engineering

Master's Degree Thesis

Multi-channel integration and analysis of an sEMG-based hand gestures recognition systems for rehabilitation applications

Supervisors
Prof. Danilo DEMARCHI
Ph.D. Fabio ROSSI
M.Sc. Andrea PRESTIA

Candidate
Edoardo FERRARO

Torino, March 2024

Abstract

Hand rehabilitation represents a significant priority for individuals with tetraplegia and stroke survivors, given the debilitating impacts of these conditions that persist in 45 % of cases after 18 months. However, current rehabilitation practices, e.g. repetitive Transcranial Magnetic Stimulation (rTMS), show limited evidence of their effectiveness. Therefore, the need for new approaches, such as using Functional Electrical Stimulation (FES) systems, emerges. This active rehabilitation technique uses low-intensity electrical pulses to stimulate skeletal muscles, acting on the nervous system by promoting new synaptic connections.

The purpose of the thesis is the development of an event-driven sEMG-based system for real-time FES control, aimed at recovering hand functionalities. The project focused on identifying the muscles required for hand motor control, defining the integration of the devices into the acquisition system, and their placement. For synchronous operation of the acquisition units, a control unit, from an existing version, was developed that employs Object-Oriented Programming (OOP) in Python programming language and controls a Graphical User Interface (GUI).

The surface ElectroMyoGraphic (sEMG) signal is extracted using two types of devices, made available by the eLiONS Lab. research group. The first is a wearable device, and four of them were used, while the second is a circular ring made up of seven units designed to fit around the forearm.

The acquisition units acquire the sEMG signals, which go through direct processing using the Average Threshold Crossing (ATC) technique. Subsequently, ATC data are wirelessly transmitted to the control unit where they are used to compute the stimulation parameters. The ATC paradigm is considered optimal for the sEMG-based FES system as it maintains a high correlation with muscle contraction.

The FES system operates with therapist-patient as the main usage mode. This modality enables patients to replicate rehabilitative movements performed by the therapist, as the stimulation patterns applied to the patient's muscles are defined based on the muscle activation of the therapist.

To select the stimulation channels based on the movement performed by the therapist, a classifier was developed. At this stage, an artificial neural network was developed for the multi-class classification of executed movements. These movements were systematically organized within a carefully defined acquisition protocol, delineating the precise timing and execution mode. This protocol includes a selection of nine movements chosen to enhance motor recovery and hand functionality.

Data collection was required for the training and testing phases of the classifier. Two types of datasets were then generated: the first comprised signals acquired from 12 subjects, while the second contained data from a single subject, a scenario that could simulate the use of the system personalized to a specific therapist.

The classifier's performance was evaluated in terms of average accuracy, reaching 59.3% and 86.1% for multi-subject and single-subject datasets, respectively. In the first case, accuracy shows high variability in individual movements and overall does not reach an appropriate level for the use of the model. Instead, the results on the single subject enable the integration of the classifier into the control unit. Therefore, hand movement recognition was tested in real-time, showing promising prospects for integration into the FES system.

Contents

List of Tables

List of Figures

Chapter 1

Introduction

1.1 Anatomy and Function of the Hand

The distinctive features of humans, setting them apart from other primates within the biological taxonomy as "higher-level mammals" or Homo sapiens, are intricately linked to the remarkable anatomy of the hand.

With more than 20 degrees of freedom [1] and the opposable thumb, the hand serves as a highly sophisticated and complex grasping organ. This intricate structure allows for a diverse range of movement combinations, facilitating the adaptation of force, speed, and dexterity. Additionally, the hand boasts a specialized sensory and tactile capacity, crucial for humans to perceive and evaluate themselves and their surroundings.

To achieve the mobilization of hand functionality, an exceptional interaction is required between the central control system and anatomical structures such as bones, muscles, joints, tendons, nerves, and blood vessels. This intricate coordination renders the hand an exceptionally complex organ. The distal region of the lower arm encompasses the distal radioulnar joint, thumb and finger carpometacarpal (CMC) joints, palm, and fingers. Comprising a total of 27 bones with 36 articulations and 39 active muscles, these structures must harmonize for the hand to translate its wide range of motor capabilities into complex motion.

1.1.1 Proximal and Distal Radioulnar Joints

The forearm skeleton consists of two bones: the ulna (elbow bone) and the radius. These two bones form two radioulnar joints, one near the elbow (proximal radioulnar joint) and one near the wrist (distal radioulnar joint), as shown in Figure 1.1.

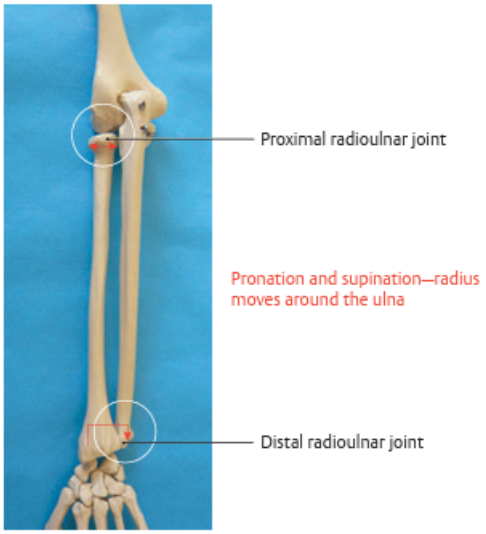

Figure 1.1: Distal and Proximal radioulnar joints [2]

In functional terms, both the proximal and distal radioulnar joints function as pivot joints. The distal radioulnar joint comprises the convex semicylindrical surface of the ulnar articular circumference, fully covered with cartilage, and the corresponding concave joint surface of the ulnar notch on the distal radius.

Stabilization of the distal radioulnar joint occurs on the palmar side, primarily by the pronator quadratus muscle, the tendon, and tendon sheath of the extensor carpi ulnaris muscle, and mostly by the triangular fibrocartilage complex (TFCC).

The TFCC serves to stabilize the distal radioulnar joint during pronation and supination movements and supports the carpal side of the ulna, along with its associated ligaments, during proximal and distal wrist movements. Additionally, it regulates pressure in the wrist.

Pronation and supination movements are facilitated by these two joints, with the shoulder joint also contributing to these motions.

1.1.2 Wrist Joint

Structure and Function of the Wrist Joint

From a functional perspective, the wrist is considered a singular joint. However, morphologically, it is comprised of two distinct joints: the proximal and distal wrist joints. These joints, each having two degrees of freedom, consist of eight carpal bones shown in Figure 1.2, including seven "regular" bones and one sesamoid bone. The proximal row includes the scaphoid, lunate, triquetrum, and pisiform, while the distal row comprises the trapezium, capitate, trapezoid, hamate.

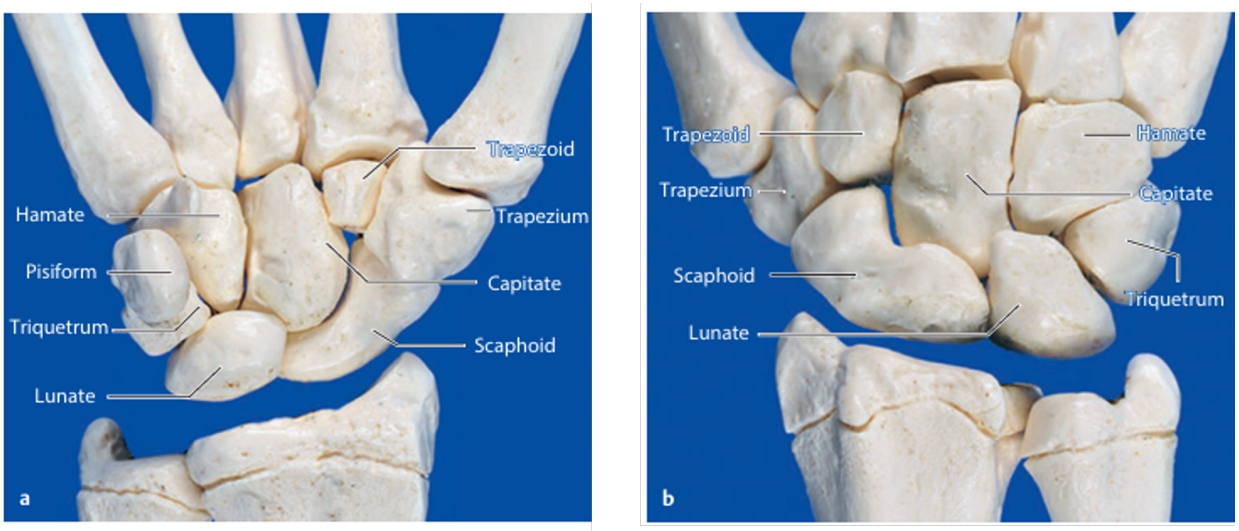

Figure 1.2: Carpal bones [2]: (a) Right hand and palm in the palmar view. (b) Right hand and palm in the dorsal view

The proximal wrist joint links the hand to the forearm's two bones, the radius and the ulna, involving the ulnocarpal disc. Together, these bones form the proximal biconcave socket, primarily from the bifaceted radial surface (scaphoid and lunate facets) and secondarily from the concave surface of the ulnocarpal disc. Approximately three-quarters of this surface corresponds to the radius, and one-quarter to the ulna. The distal ovoid convex joint head is comprised of the scaphoid, lunate, and triquetrum bones, which are covered by hyaline cartilage. Ligaments such as the scapholunate and lunotriquetral ligaments are responsible for holding these bones together, giving the illusion of a uniform cartilage covering. Although not directly involved in arthrokinematics, the pisiform serves as a sesamoid bone that aids in stabilizing the joint through the action of ligaments and muscles [2].

Muscles of the Wrist

Muscles play a pivotal role in stabilizing, regulating pressure, and influencing wrist kinematics during radial and ulnar deviation of the hand.

Carpal muscles are categorized into those involved in flexion and ulnar deviation, and those engaged in extension, radial deviation, and joint rotation.

1. Muscles Involved in Flexion and Ulnar Deviation of the Wrist:

   The most important muscles involved in flexing the wrist are the flexor carpi ulnaris and flexor carpi radialis, along with the palmaris longus muscle. The muscle primarily responsible for ulnar deviation is the extensor carpi ulnaris, with the involvement of the flexor carpi ulnaris and the extensor digitorum

communis muscles. Some of the finger flexor muscles are also involved in these movements to some extent.

(a) *Flexor Carpi Ulnaris*

(b) *Flexor Carpi Radialis*

(c) *Palmaris Longus*

(d) *Extensor Carpi Ulnaris*

2. Muscle Involved in Extension and Radial Deviation of the Wrist:

   The extensor carpi radialis brevis and extensor carpi radialis longus muscles are the most important wrist extensors. In contrast, radial deviation is performed only by the extensor carpi radialis longus muscle.

   (a) *Extensor Carpi Radialis Longus*

   (b) *Extensor Carpi Radialis Brevis*

   The muscles mentioned are shown in the following Figure 1.3 showing the muscle structure of the dorsal and palmar forearm.

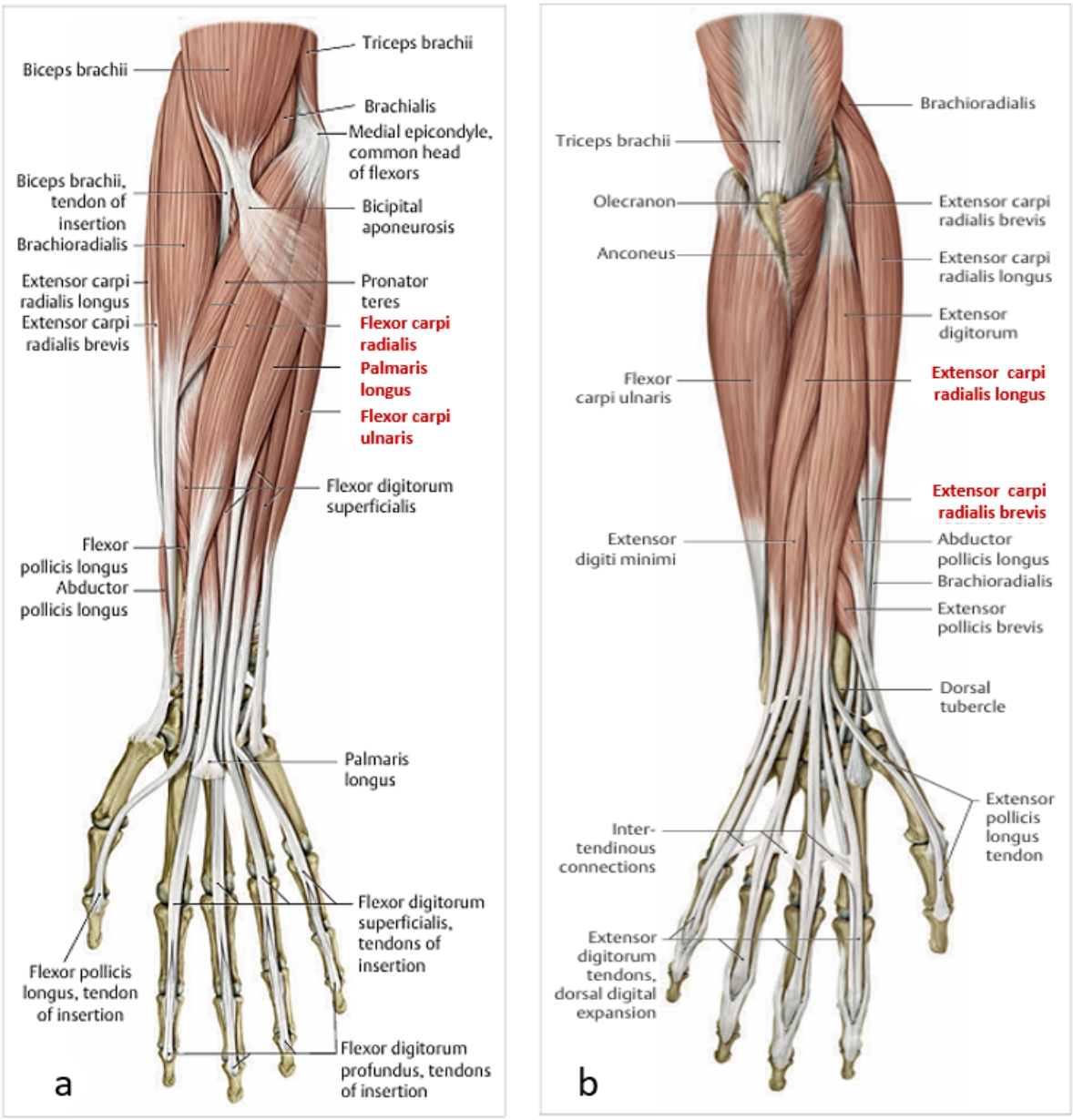

Figure 1.3: (a) Forearm palmar muscles. (b) Forearm dorsal muscles [2]

1.1.3 Thumb Joint

In contrast to nonhuman primates, whose thumbs can only adduct but not oppose, the human thumb signifies a significant evolutionary advancement. As the foremost and most robust digit of the hand, it holds a unique status due to its extensive range of motion capabilities.

Movements and Range of Motion

The opposition capability of the thumb enables powerful fist closure, making it an essential grasping tool [3]. When using a pinch grip, the force exerted is approximately one-fourth that of a full fist closure. Overall, the thumb significantly enhances both gross motor and fine motor grasping functions of the hand. This complexity arises from the thumb's carpometacarpal (CMC) joint and the diverse functions of its nine muscles, distinguishing it from the other fingers. Moreover, the brain areas responsible for thumb movement and sensitivity exhibit greater prominence compared to those of the wrist and other fingers.

The functional joints of the thumb are divided into the CMC joint of the thumb, which belongs to the wrist joint, and the thumb metacarpophalangeal (MCP) and interphalangeal (IP) joints, which belong to the digit itself.

Kapandji (1982) distinguished three functional units between the thumb and the other fingers of the hand:

Movements of the Thumb , Figure 1.4:

1. The first degree of freedom comprises abduction and adduction around an axis through the base of the first metacarpal.

2. The second degree of freedom comprises flexion and extension. The axis for this movement takes a radiopalmar toulnodorsal course through the trapezium.

3. The most typical movements of the thumb involve opposition a repositioning. In the opposition movement, the thumb, together with the first metacarpal, is opposed to the other fingers.

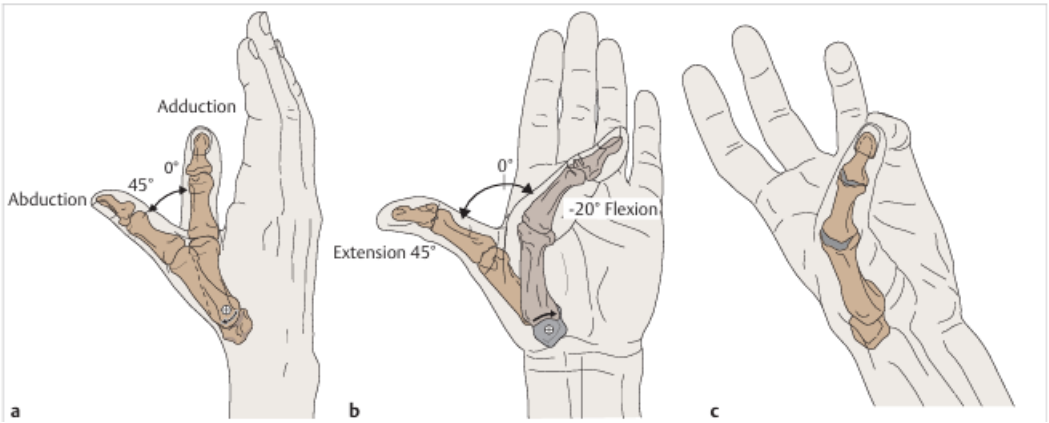

Figure 1.4: Thumb Movements [2] (a) Abduction and adduction. (b) Extension and flexion. (c) Opposition.

Thumb CMC Joint

- Structure and Function of the Thumb CMC Joint:

  Numerous studies [4] [5] have examined the structure and function of the carpometacarpal joint (CMC) of the thumb. The CMC joint is commonly described as a saddle joint, with the articular surface of the trapezium ranging from convex to concave. During opposition, the contact surface between the two joints is maximum (53 %), decreasing during adduction (28%) and radial deviation (25%). The capsule of the CMC joint is broad, allowing a wide range of movements despite its low stability, thanks to various stabilizing ligaments.

- Muscle of the Thumb CMC Joint:

  Nine muscle act on the thumb CMC joint. Each movement sequence is performed by at least two muscles groups. The muscles are divided into an extrinsic group and an intrinsic group.

  The first muscles of the thumb are located outside the hand in the area of the forearm, the latter are places in the hand and originate in the wrist or carpus.

Table 1.1: Thumb intrinsic and extrinsic muscles

Extrinsic Muscles	Intrinsic Muscles
• Abductor Pollicis Longus • Flexor Pollicis Longus • Extensor Pollicis Brevis • Extensor Pollicis Longus	• Flexor Pollicis Brevis • Opponens Pollicis • Abductor Pollicis • Adductor Pollicis

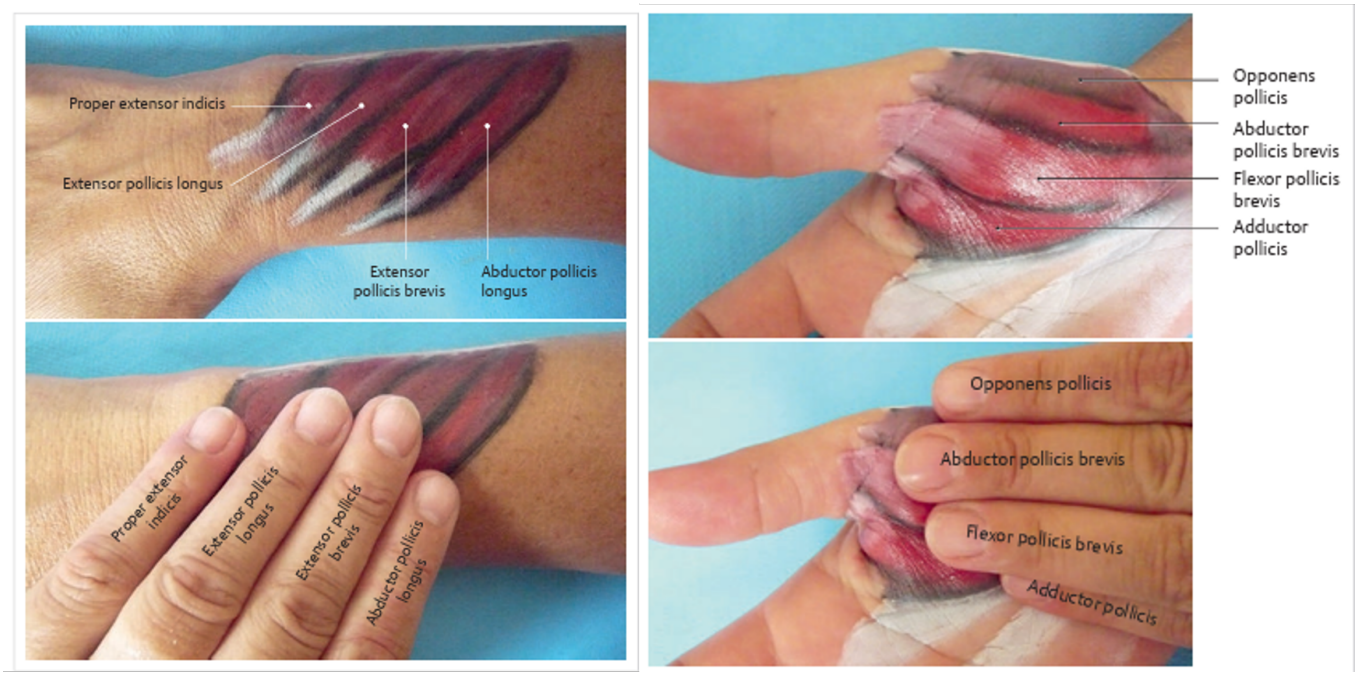

Figure 1.5: Thumb intrinsic and extrinsic muscles [2]

The depicted Figure 1.5 illustrates the muscles involved in thumb control. Notably absent from the illustration is the Flexor Pollicis Longus muscle, which stands out from the rest due to its distinct positioning. This flexor muscle is situated adjacent to the finger flexors on the palmar side of the forearm. Additionally, the figure includes the extensor of the index finger, positioned near the other extrinsic muscles associated with thumb movement.

Thumb MCP and IP Joints

- Structure and Function of the Thumb MCP and IP Joints:

  The thumb MCP and IP joints are involved in all movements of the thumb. The opposition of the thumb is only possible through the combination of extension and flexion with abduction and adduction of the MCP joint in cooperation with the IP joint. Without the thumb MCP and IP joints, opposition of the thumbnail would not be possible. In contrast to the fingers, the thumb has only two anular ligaments with a Y-shaped ligament in between.

1.1.4 Palm

The palm comprises five short tubular bones known as metacarpal bones, situated adjacent to the angular carpal bones. These metacarpal bones are divided

into three segments: the base, body, and head, each featuring articular surfaces facilitating connections with both the carpal bones and neighboring metacarpals. Notably, the thumb metacarpal articulates with the carpal bones through a saddle joint.

The primary function of the metacarpal bones is to provide structural support for the hand's grasping function. Together with the palm, they offer a stable foundation for gripping and holding objects securely. Additionally, they create space for the two vascular arches and serve as conduits for sensory nerves and tendons to reach the finger joints. Moreover, the metacarpal bones serve as attachment sites for the intrinsic muscles of the hand, essential for finger movement and joint stabilization.

Structure and Function of the Second to Fifth Metacarpals

Incorporating the thumb, the hand comprises five metacarpal bones, which are short tubular bones of different lengths. The bases of the third to fifth metacarpals exhibit a rectangular shape, whereas the base of the second metacarpal is triangular. This comparatively rigid structure gives rise to a convex arch on the dorsal aspect and a concave arch on the palmar side, collectively referred to as the palmar carpal arch, as depicted in the accompanying Figure. 1.6. This concavity flattens out to some extent at the level of the metacarpal heads or the metacarpal arch.

The first to fifth metacarpal bodies are somewhat convex dorsal wards and have a strongly concave shape palmar ward, which reinforces the formation of the palm. The metacarpals fan out from proximal to distal, which additionally increases the breadth of the hand's grip. With their convex heads, they form the proximal sections of the second to fifth MCP joints.

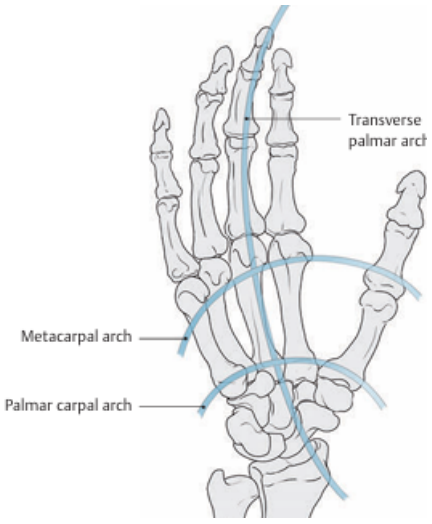

Figure 1.6: Function of the Palm: palmar arch [2]

Muscles of the Metacarpals

Various muscles insert onto the bases of the metacarpals (e.g., extensor carpi ulnaris), while other muscles arise from these bones. These include the dorsal and palmar interossei and adductor pollicis with its transverse head, which arise from the shaft. In addition, some intrinsic muscle bellies lie on the metacarpal bones in order to insert into the fingers further on (lumbricals, abductor digiti minimi, flexor digiti minimi brevis and opponens digiti minimi muscles).

1. Dormsal and Palmar Interossei
2. Lumbricals
3. Abductor Digiti Minimi

1.1.5 Finger Joints

The fingers contribute to providing various functionalities, such as the sense of touch and the ability to grasp objects. Specifically, the fingers are the five terminations of the human hand named: thumb, index finger, middle finger, ring finger, and little finger. The thumb consists of two phalanges, while each of the fingers is composed of three phalanges: proximal, middle, and distal phalanges.

Structure and Function of the MCP Finger Joints

The metacarpal bones allow various movements including abduction-adduction, extension-flexion, and circumduction. They facilitate precision grip and grasping objects. The second metacarpal's prominence decreases towards the ulnar direction, leading to ulnar deviation of the proximal phalanx. Supination of the fourth and fifth metacarpals enlarges the circumduction movement of the corresponding MCP joints, aiding in grasping larger objects. Conversely, for precision grip, the second metacarpal assumes a somewhat pronated position, causing the index finger to rotate slightly into supination during flexion.

Structure and Function of the PIP Finger Joints

The proximal interphalangeal joints (PIP joints), together with the MCP joints, are the most important functional unit for grasping, gripping, and making a fist, and play a significant role in the undisturbed movement of the fingers and the hands. The PIP joint is a hinge joint and it allows only flexion and extension, although slight side-to-side and rotational motions are also possible. The PIP joints of the index and middle fingers exhibit ulnar deviation in flexion and the PIP joints of the ring and little fingers exhibit radial deviation. The second, third, and fifth PIP joints supinate slightly and the fourth PIP pronates slightly. Therefore, only

the PIP joint of the little finger with the fifth metacarpal rotates in the form of supination, which tends to move the little finger palmar ward, brings it closer to the ring finger and can contribute significantly to forcefully making a fist.

Structure and Function of the DIP Finger Joints

The DIP joints are similar to the PIP joints. On the whole, the joint structures are smaller. As with the PIP joints, the distal bases of the DIP joints have two concave facets, although the eminences are not pronounced and therefore allow for lateral translation. In addition, the base of the distal phalanx is somewhat wider than the head of the middle phalanx.

Extrinsic Muscles Finger Joints

In addition to the interossei and the lumbricals muscles, the extrinsic muscles of the finger (flexors and extensors) are particularly important.

- The extensors of the finger comprise the Extensor Digiti Minimi, the Extensor Digitorum Communis and the Proper Extensor Indicis, the latter was previously shown in Figure 1.5.
- The extrinsic flexors of the fingers are divided into four layers. The Flexor Digitorum Superficialis muscle lies in the second layer and the Flexor Digitorum Profundus muscle lies in the third layer.

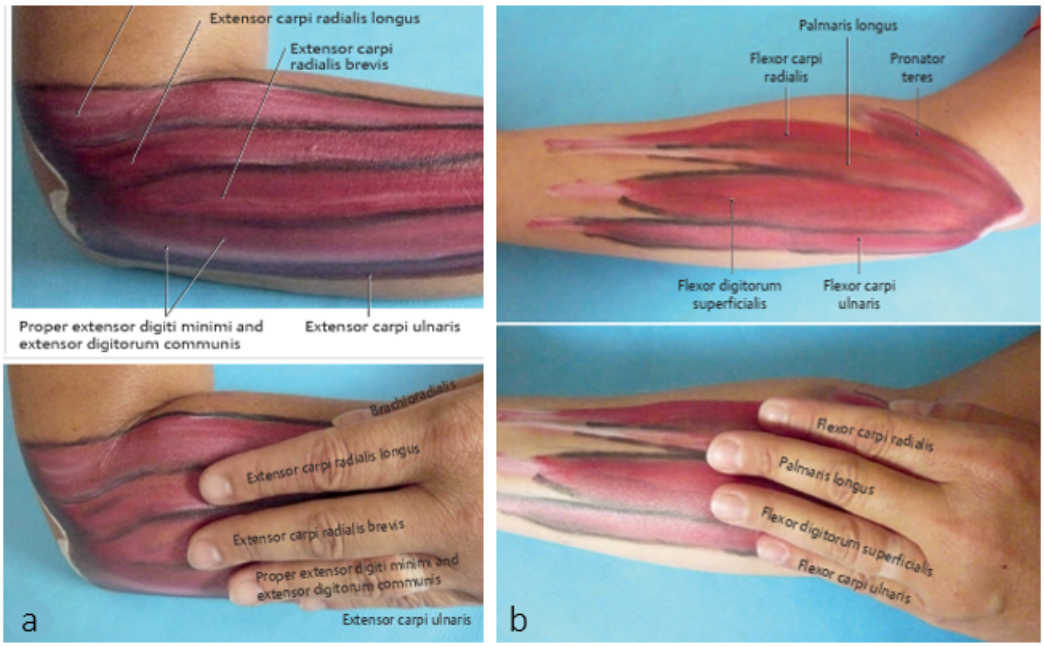

Figure 1.7: Finger extrinsic muscles [2] (a) Extensors (b) Flexors

1.2 Skeletal Muscle

There are three different types of muscles in the human body: skeletal, cardiac, and smooth. Skeletal muscles constitute the majority of our muscle mass, approximately 40% of body weight. They are attached to the bones of the skeleton via tendons and are responsible for posture and movement of skeletal bone segments.

Skeletal muscle, like cardiac muscle, is classified as striated due to its characteristic alternating light and dark bands visible under the microscope. Skeletal muscles only contract in response to stimuli from motor neurons, and when two bones attached to a muscle are connected by a movable joint, the muscle contraction causes skeletal movement.

There are flexor muscles, which bring the centers of bones closer together during contraction, and extensor muscles, which cause the opposite movement. These two categories of muscles are found in numerous joints. Indeed, the contraction of a muscle can move the skeletal segment it is attached to, but it cannot return it to the starting position. The flexor-extensor muscle pair is referred to as antagonistic: as in the case of the biceps acting as flexor and the triceps as extensor.

This chapter will describe the anatomy and contractile mechanism of skeletal muscle.

1.2.1 Skeletal Muscle Architecture

The skeletal muscle is composed of muscle cells or muscle fibers, each characterized by a large number of nuclei arranged superficially along the elongated cylindrical structure of the fiber [6]. Within the muscle, the fibers are arranged with their longitudinal axes in parallel. Each fiber is surrounded by connective tissue, called endomysium, which groups together a set of muscle fibers forming fascicles. Among the various fascicles are collagen, elastic fibers, blood vessels, and nerves.

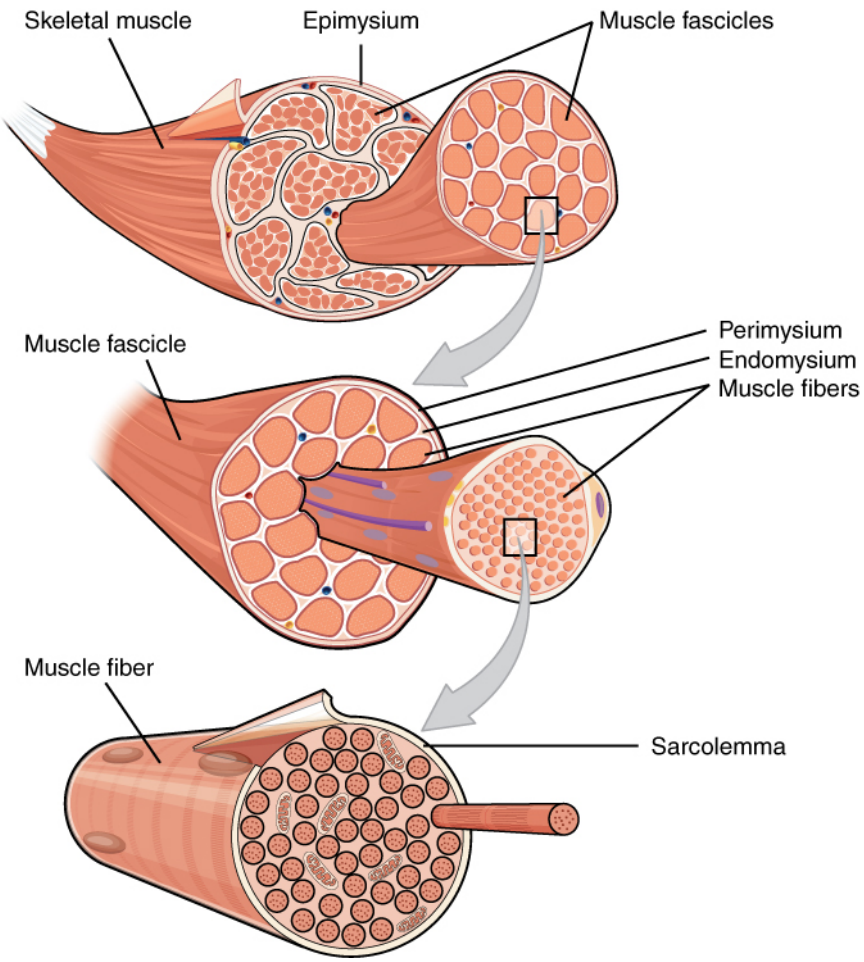

Figure 1.8: Skeletal muscle architecture [7]

Anatomy of Muscular Fibers

Striated muscle fibers are cylindrical and vary in length from a few millimeters to several centimeters, with a diameter ranging from 10 to 150 µm. Each fiber is enveloped by the sarcolemma, a specialized plasma membrane involved in the transport, exchange, and reception of synaptic signals at the neuromuscular junction [6].

The main intracellular structure consists of myofibrils, bundles of contractile and elastic proteins responsible for contraction. Furthermore, skeletal muscle cells contain a sarcoplasmic reticulum (SR), composed of terminal cisternae, which surrounds each myofibril. The SR manages the concentration of calcium ions (Ca2+) with the help of the enzyme Ca2+-ATPase, providing signals crucial for contraction.

Closely associated with the terminal cisternae is an intricate network of transverse tubules known as T-tubules. The membranes of the T-tubules derive from

invaginations of the sarcolemma, allowing the lumen of these tubules to be in direct communication with the extracellular fluid. These T-tubules facilitate the rapid propagation of action potentials from the cellular surface into the interior of the fiber, thus playing a crucial role in the dynamics of muscle cell function.

To conclude, the sarcoplasm, the cytoplasm within muscle fibers, contains numerous mitochondria, essential in the process of oxidative phosphorylation of glucose that produces ATP for muscle contraction.

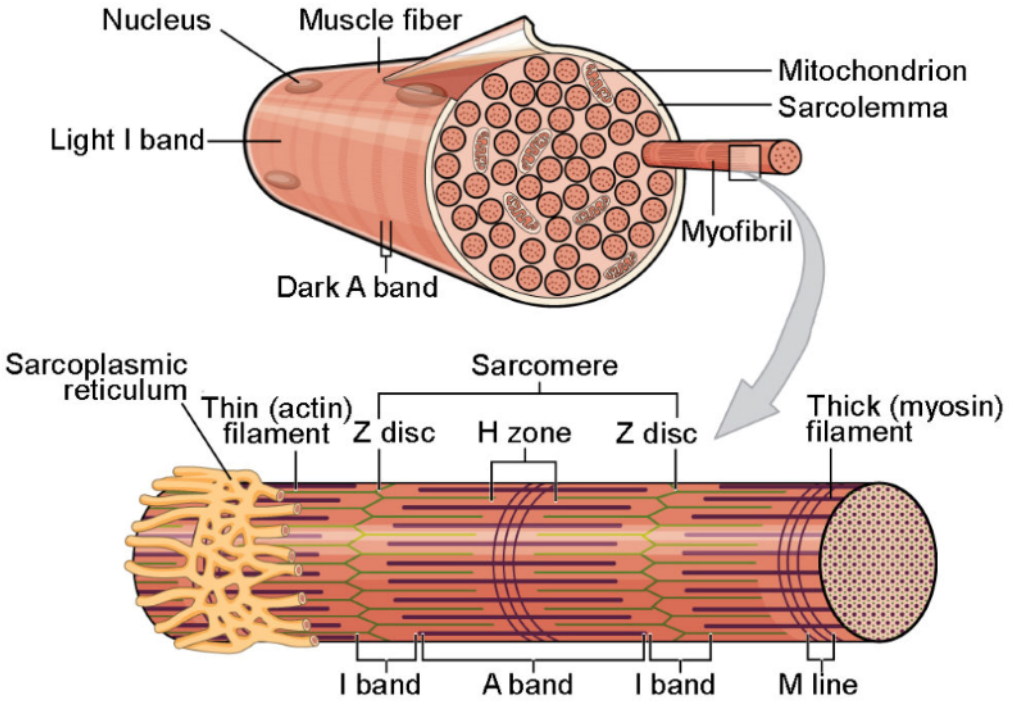

Figure 1.9: Skeletal muscle fiber [7]

Myofibrils: The Fundamental Contractile Structures of Muscle Fibers

Each myofibril is composed of several proteins organized into repeated contractile structures called sarcomeres. The proteins involved include the motor protein myosin, which forms the thick filaments, and the actin microfilament, the main component of the thin filaments.

Myosin provides movement, and its various isoforms differentiate muscle types and characterize contraction speed. A myosin filament is composed of a pair of protein chains that intertwine to form a long tail with two globular heads. Together, these myosin molecules create a thick filament.

Actin is the protein that makes up the thin filament in the muscle fiber; it is a globular protein and polymerizes to form long filaments called F-actin, which,

when wrapped together, form the filament.

The most common configuration assumed by the described filaments involves them being interconnected by means of cross-bridges, where the bridge forms when the myosin head binds to the actin site. The repeated arrangement of the filaments gives rise to the alternating light and dark bands, visible under the optical microscope, which characterize the myofibril. Each repetition of the bands constitutes a sarcomere, in turn formed by the following elements [6]:

- Z-line or Z-disc: A sarcomere is formed by the filaments located in the area delimited by two successive Z-lines.
- I-bands: These bands are exclusively formed by thin filaments and are lighter. Each of these bands is crossed by the Z-disc.
- A-band: They are the longest part of the sarcomere and cover the entire length of the thick filament.
- H-zone: The central region of the A-band, occupied solely by myosin filaments.

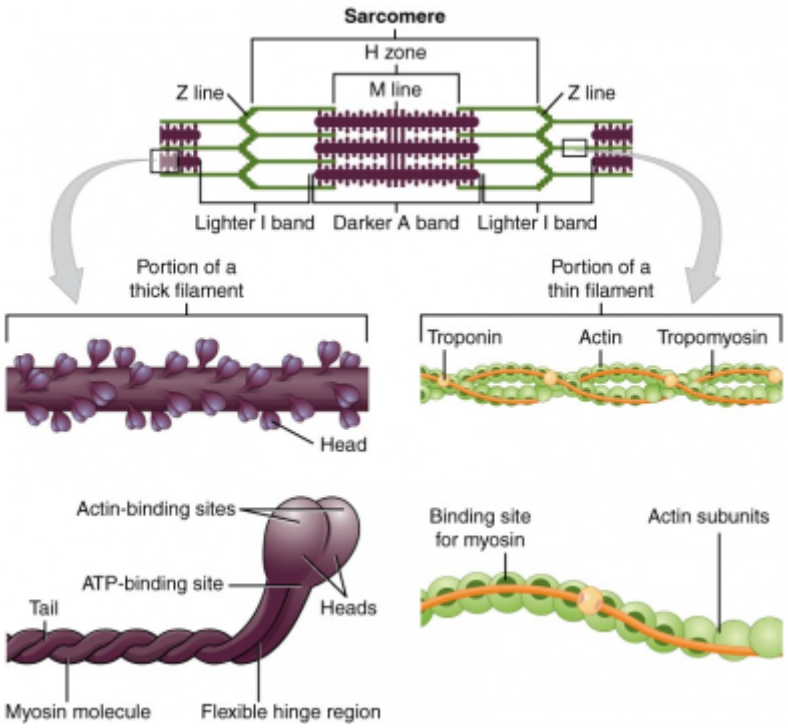

Figure 1.10: The Sarcomere, functional unit of skeletal muscle fiber [7]

1.2.2 Muscolar Contraction Mechanism

Muscle contraction, namely the generation of tension by the muscle, is an active process that requires energy produced from the hydrolysis of ATP. The steps leading to the contraction of skeletal muscle are:

1. The release of acetylcholine by a somatic motor neuron at the neuromuscular junction. This event is converted into an electrical signal, called an action potential, in the membrane of the muscle cell. The action potential induces the release of calcium from the sarcoplasmic reticulum.

2. Increase in intracellular calcium concentration that initiates the excitation-contraction coupling by binding to troponin.

3. Contraction-relaxation cycle, individually termed a twitch, explained by the sliding filament theory. According to this model, the actin and myosin filaments, overlapping and of fixed length, slide past each other, and the Z-discs of the sarcomere move closer together.

Muscle contraction is initiated by the release of calcium ions from the sarcoplasmic reticulum, triggering a series of events that lead to the interaction between actin and myosin filaments. A protein called troponin controls the position of tropomyosin, an elongated protein polymer that, in the resting muscle situation, is positioned along the groove of the thin filament, covering the binding sites for myosin (tropomyosin 'off'). For contraction to begin, tropomyosin must transition to the 'on' conformation, a situation that occurs when the intracellular calcium concentration increases, triggering a process called the cross-bridge cycle theory.

The initial state of the cycle is defined as the rigor state, in which myosin heads are tightly bound to G-actin molecules, while no nucleotides such as ATP or ADP are bound.

1. ATP binds to the binding site present in the head of the myosin, causing the detachment of myosin from actin.

2. ATP hydrolysis provides the energy for the extension of the myosin head and its reattachment to the actin site. The ATPase site of myosin binds and hydrolyzes ATP into ADP and inorganic phosphate (Pi), and the two elements remain bound to myosin. The release of energy allows the rotation of actin, forming a 90° angle with the longitudinal axis of the filament. In this way, the formed bridge is weak because tropomyosin is partially occupying the actin site. Nevertheless, the bridge represents an accumulation of potential energy, ready to trigger contraction upon an increase in calcium concentration.

3. The power stroke initiates following the calcium-troponin binding, releasing the binding sites. The binding force between actin and myosin is increased,

resulting in the release of inorganic phosphate, allowing the head to rotate towards the M line, generating greater force.

4. Myosin releases ADP, and myosin is again strongly bound to actin in the rigor state, and the cycle can begin again.

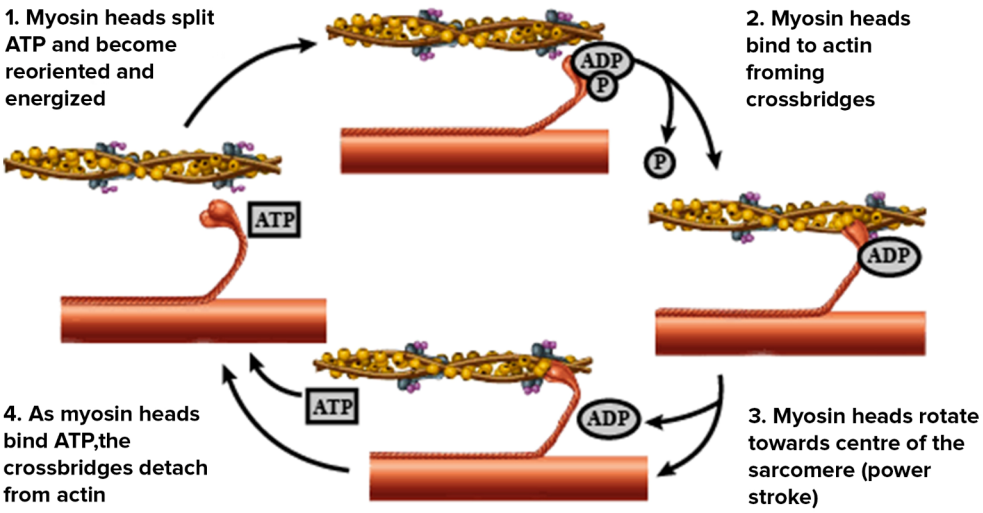

Figure 1.11: Cross Bridge Cycle [8]

1.2.3 Skeletal Muscle Classification

Skeletal muscle fibers can be classified based on their contraction speed and resistance to fatigue following repeated stimulation. Currently, the classification depends on the isoform of the thick filament myosin ATPase:

- Slow-twitch fibers, type I fibers
- Fast oxidative-glycolytic fibers, type 2A fibers
- Fast glycolytic fibers, type 2X fibers

Further sources of differentiation among muscle fiber types relate to their resistance to fatigue. Glycolytic fibers utilize anaerobic glycolysis as their source of ATP. The hydrolysis of glycolysis contributes to the accumulation of H+ ions, leading to acidosis, a condition of fatigue.

Conversely, oxidative fibers preferentially utilize oxidative phosphorylation as their ATP source. These fibers are more densely vascularized, enhancing the efficiency with which they receive oxygen, thereby favoring their preferred metabolic cycle for glucose. ATP production in this case occurs within mitochondria, reached by oxygen diffusing into muscle fibers through a protein called myoglobin, which imparts a characteristic red coloration.

Due to the abundance of myoglobin within them, oxidative fibers are termed "red" fibers. Conversely, glycolytic fibers, with lower myoglobin concentrations, are also referred to as "white" fibers.

The distribution of these fiber types within the human body adapts according to the subject's lifestyle.

1.2.4 Force generated during a contraction

The fundamental unit for skeletal muscle contraction is called a motor unit and consists of a somatic motor neuron and the muscle fibers it innervates, all of the same type. The generation of an action potential by the motor neuron triggers the contraction of all fibers associated with it. The number of fibers constituting a motor unit varies and allows for the gradual regulation of force developed in movements.

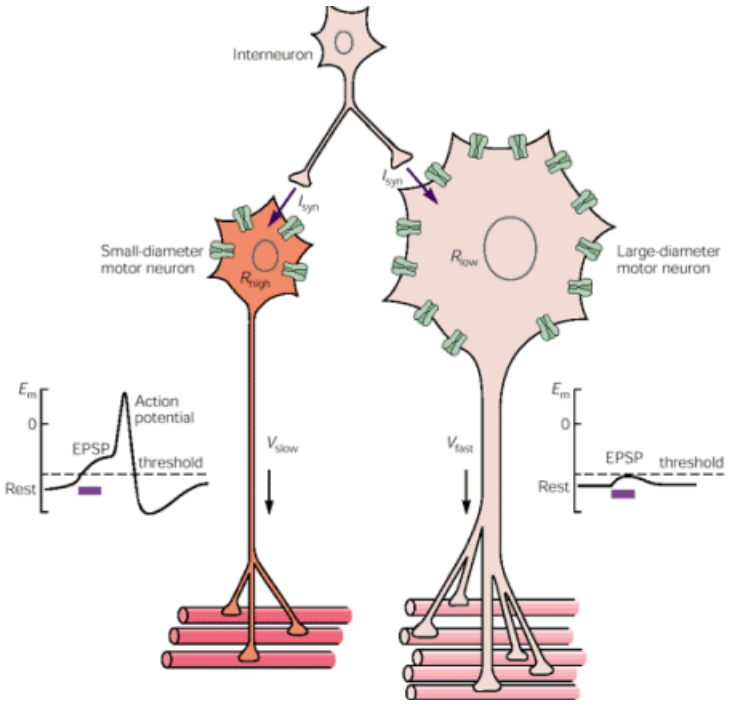

Figure 1.12: Motor Unit [9]

The force generated by a single fiber can be increased by increasing the frequency of action potentials that stimulate it. In this way, the fiber does not have enough time to relax, and the phenomenon of summation is initiated, culminating in tetanus. Therefore, the tension developed by a single fiber is modulated by the frequency of action potentials.

The motor units of skeletal muscle fibers are capable of contracting exclusively in an all-or-none manner. How, then, is the modulation of force and duration of contractions achieved?

The modulation of force and duration of contractions is achieved using two mechanisms [10]:

1. Recruitment of motor units of different types
2. Variation in the number of motor units activated at the same time

Recruitment is under the control of the central nervous system and depends on the intensity of the stimulus. Starting from low-threshold stimuli, slow-twitch fibers, which are fatigue-resistant and develop little force, are initially recruited. As the intensity of the excitatory stimulus increases, motor neurons innervating fast oxidative-glycolytic fibers are also activated.

At this point, in order to maintain contraction over time by attenuating the onset of fatigue, the mechanism of asynchronous recruitment comes into play. The nervous system modulates the recruitment of motor neurons whose activation occurs alternately.

1.2.5 Types of contraction

A muscle contraction can manifest in two distinct ways: isometric or isotonic. In an isometric contraction, muscle tension equals the applied load. During this phase, the muscle length remains constant, and no movement occurs. Therefore, no work is performed as there is no change in position. Conversely, isotonic contraction involves movement as muscle tension exceeds the applied load. If the muscle shortens to support the load, the contraction is termed concentric. If, on the other hand, the muscle lengthens, the contraction is considered eccentric.

1.3 Electromyographic signal

During a muscle contraction, the activation of motor units can be controlled, with each unit generating a single motor unit action potential (MUAP). Each motor unit is associated with its own MUAP, thus the electromyographic (EMG) signal is an interfering signal, resulting from the summation of action potentials from all motor units that activate asynchronously [11] [12]. By studying the EMG signal, it is possible to distinguish between central (CNS) and peripheral control information.

EMG signals can be acquired in two modes [13]:

- Invasive: Needle electrodes are used to record a signal very close to the source in a limited volume, but the global view of the muscle is lost.
- Surface: Electrodes are placed on the skin, allowing for a global view of muscle activation but creating a signal rich in interference.

The sEMG signal contains information from a large number of motor units, making it difficult to distinguish between central or peripheral information [14]. In order to obtain optimal results from sEMG, it is crucial to have a thorough understanding of the muscles from which the EMG signal is being extracted. Additionally, proper electrode placement on the skin requires careful consideration and skin preparation beforehand.

1.3.1 sEMG Signal Morphology

The peak-to-peak amplitude of the electromyographic signal reaches values up to 10 mV. The bandwidth is up to 500 Hz, but the predominant energy content is between 50 and 150 Hz [15]. The nature of the signal is stochastic and this makes it mathematically describable through Gaussian probability distribution functions.

Figure 1.13: Raw sEMG signal [15]

1.3.2 sEMG Acquisition Electrodes

Surface EMG sensors are electrochemical transducers that can detect potential differences generated by ionic currents associated with muscle contraction. They employ metallic conductors placed on the skin, creating the metal-electrolyte interface (the skin being rich in electrolytes such as synovial fluid and sweat).

By placing a conductive material within an electrolyte, an oxidation-reduction reaction occurs. Some surface atoms of the metal go into solution in ionic form, leaving electrons in the conductive bar. At their interface, a potential difference forms, known as the half-cell potential.

The potential of a single electrode cannot be directly determined and is expressed relative to a reference value, such as the Standard Hydrogen Electrode (SHE). Therefore, another electrode must be used. The most commonly used electrodes are Ag/AgCl electrodes due to their stability, tissue tolerance, and ease of modeling [16].

1.3.3 Electrode-skin interface

In order to accurately model the electrode-skin contact, it is necessary to understand the structure of the skin. The skin consists of three layers: the epidermis, dermis, and subcutaneous tissue.

Of particular interest for our analysis is the epidermis, as it is in direct contact with the electrode. The epidermis itself is composed of three layers:

1. Corneum layer, composed of cells at the end of their life cycle and with relatively low conductivity. This layer can be considered insulating, which is why the use of conductive gels is sometimes required.

2. Granular layer

3. Basal layer, where epidermal cells are generated.

At the dermal level, the presence of sweat glands with ducts is important, making this layer of skin highly conductive.

Finally, the layer of conductive gel, often used as an interface between the electrode and epidermis, must be considered. Based on this information, it is possible to accurately model the electrode-skin interface[17][18].

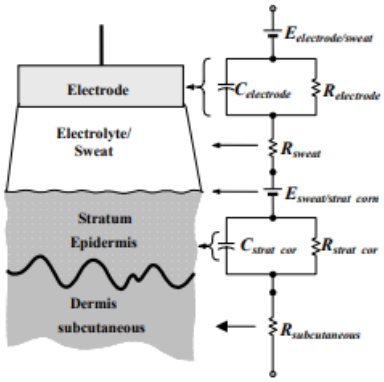

Figure 1.14: Electrode-skin interface model [18]

Considering, however, the current values involved in the extraction of the electromyographic signal and the frequencies of interest, it is possible to neglect the two parallel models.

Noise sources of the surface Electromyographic signal

During sEMG signal acquisitions, it is necessary to consider several factors that may contribute to an increase in signal noise.

- Power line interference (PLI): This disturbance is created by the acquisition equipment and is also known as Power Line Interference. It appears as a sinusoid with variable amplitude and a fixed frequency, which in European countries corresponds to 50 Hz. This problem can be addressed using selective filtering techniques, such as the Notch filter or more advanced adaptive algorithms. Additionally, it is recommended to twist the cables connected to the sampling electrodes to reduce the disparity in parasitic capacitances between the source of interference and the cables. If the capacitive effects on the two cables are similar, the interference will be treated as common mode and not subjected to differential amplification.

- Motion artifact: This consists of the formation of momentary potentials at the metal-electrolyte interface due to the reciprocal movement between the skin and the cables. It can typically be removed with careful skin preparation during electrode adhesion.

- Stimulation artifact: If the surface electromyographic signal is acquired during stimulation, this artifact occurs. Its characteristic is an initial peak followed by a tail. The peak is not problematic as long as it is recorded prior to the myoelectric response, while the tail may overlap with the signal. To attenuate this type of artifact, stimulators with voltage stimulation are preferred, with a faster discharge constant.

- ECG artifacts: The electrocardiographic signal, being based on biopotentials, can influence the sEMG signal during acquisitions. To remove this artifact, it is necessary to work on common mode rejection.

1.3.4 sEMG signal acquisition circuitry and configurations

After comprehensively understanding the characteristics of the target muscle, preparing the skin, and positioning the EMG electrodes, the next step involves the acquisition of the EMG signal.

The EMG signal is acquired using a differential amplification technique. This amplifier should ideally have high input impedance and very low output impedance. In an ideal scenario, a differential amplifier would possess infinite input impedance and zero output impedance.

The instrumentation amplifier accomplishes differential amplification by subtracting the voltages from two input sources (V1 and V2), Figure 1.15. This effectively eliminates common noise signals present at both electrode inputs, such as power line interference. The determination of a differential amplifier's capacity to dismiss signals shared between both inputs relies on its common mode rejection ratio (CMRR). A CMRR of 90 dB is generally sufficient for eliminating common signals in instrumentation amplifiers.

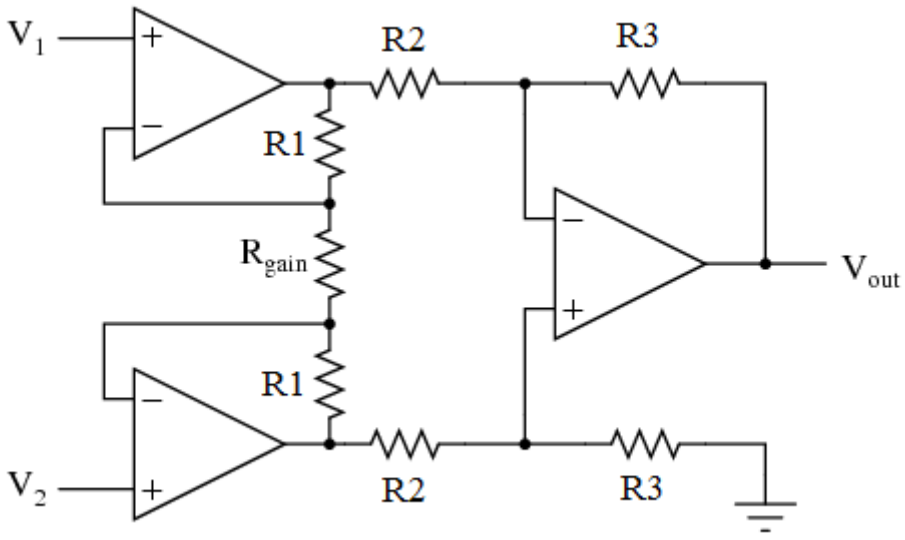

Figure 1.15: Instrumentation Amplifier Vout = (V2 - V1) x Gain [19]

The gain of the instrumentation amplifier can be adjusted using a single resistor (Rgain).

The placement of the EMG electrodes can be done using three different configurations: monopolar, bipolar, and multipolar.

- Monopolar configuration [20]: This configuration involves using a single electrode on the skin with respect to a reference electrode. While simple, this method is not recommended as it picks up all electrical signals in the vicinity of the detecting surface.

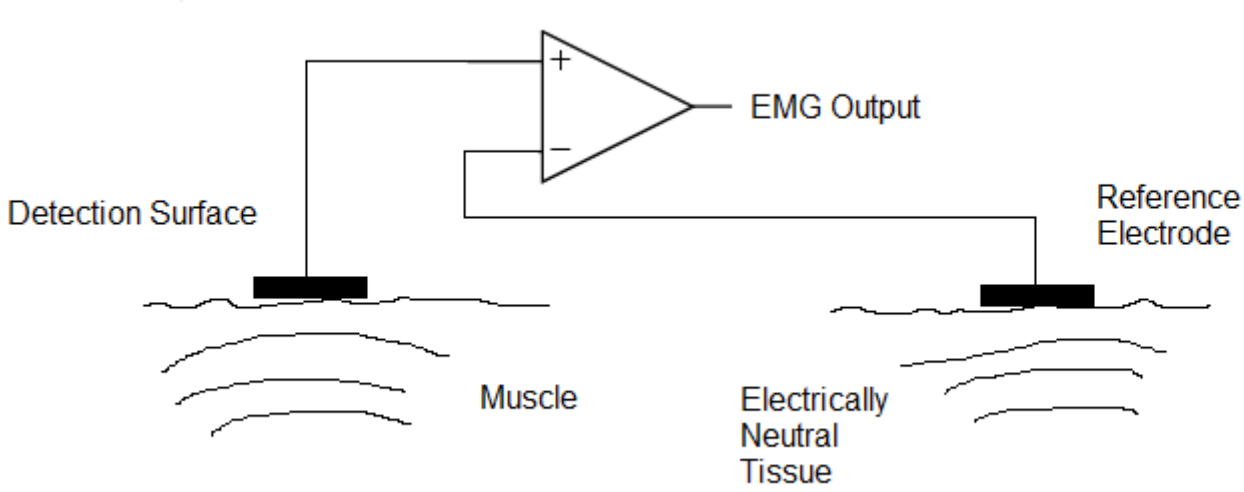

Figure 1.16: Monopolar Configuration [19]

- Bipolar configuration [20]: In the bipolar configuration, two EMG electrodes are used along with a reference electrode. The signals from these two electrodes are connected to a differential amplifier. The electrodes are placed approximately 1-2 cm apart. The differential amplifier suppresses common noise signals and amplifies the difference between the two inputs. This configuration addresses the limitations of the monopolar setup and is the most commonly used electrode configuration.

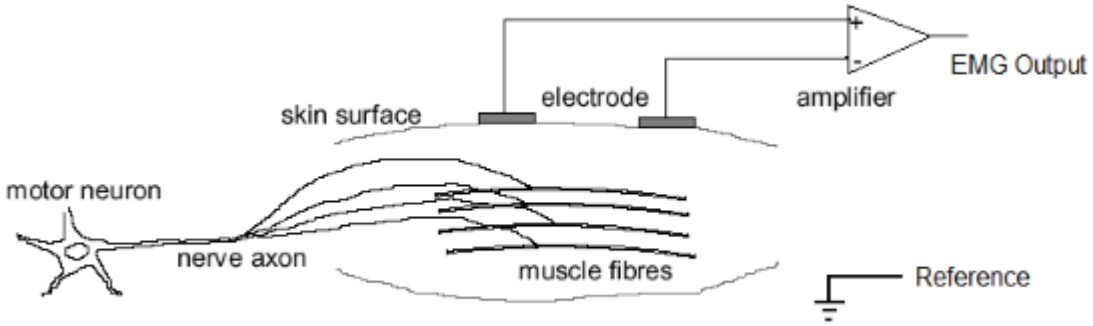

Figure 1.17: Bipolar Configuration [19]

- Multipolar configuration: This configuration utilizes more than two EMG electrodes along with a reference electrode. It further reduces crosstalk and noise concerns. The signals from three or more electrodes, placed 1-2 cm apart,

undergo multiple stages of differential amplification. This configuration is employed in comprehensive research studies aimed at studying EMG muscle fiber orientation, conduction velocity, and motor point localization.

1.4 Average Threshold Crossing (ATC)

The recognition of movements through the analysis of surface electromyographic signals (sEMG) is a significant area of research in the field of bio-potentials and human-machine interactions. In this context, it is crucial to synchronously acquire and process force levels from various muscles, preferably locally to minimize interference. The processed information is then transmitted to external hardware with robust computational capabilities for real-time gesture analysis. The use of wearable systems, powered by one or more batteries, emphasizes the critical consideration of power consumption, especially during prolonged continuous recording. This consumption is closely linked to circuit implementation, the number of channels, and the sampling frequency. A suitable methodology to meet these requirements is the Average Threshold Crossing (ATC).

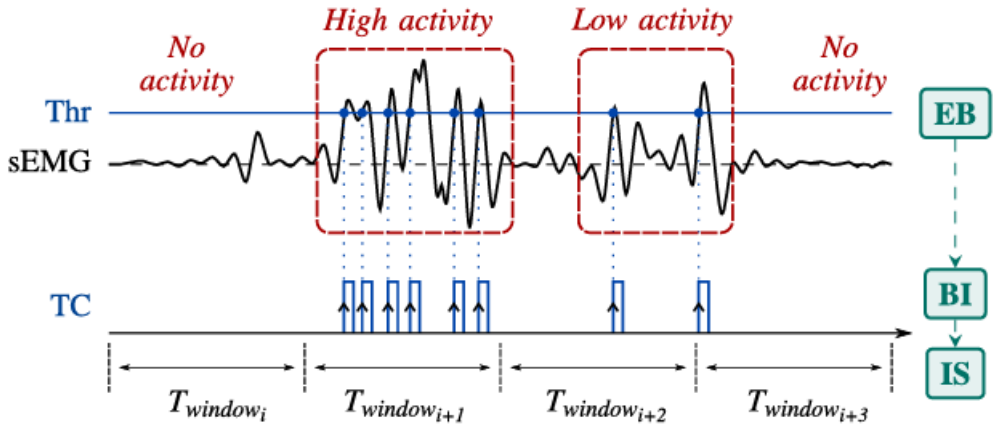

Figure 1.18: Average Threshold Crossing (ATC) technique: following the Event-Based (EB) paradigm, the threshold crossing (TC) points are identified as the events carrying the information of muscle activation, and they can be represented by a time distribution of electrical spikes, as it happens in the biological communication among neuron cells, i.e., a Bio-Inspired (BI) process. Information Synthesis (IS) is achieved by applying a time-window (Twindow) approach to the TC distribution to compute the ATC parameter, which summarizes the state of muscle contraction (e.g., high, low or no activity).

Figure 1.18 explains the process of generating an event, represented as a digital pulse in our system, every time the sEMG potential exceeds a predefined threshold. The resulting sequence of pulses constitutes an almost digital signal, referred to as "Threshold Crossing" (TC), which utilizes only the temporal dimension and disregards amplitude.

Subsequently, the TC signal information is compressed by counting how many events have been generated in an observation window, thus defining the ATC parameter[21] as in Eq.1.1, where *TC-events* represents the number of TC events, and *Twindow* normalizes the parameter to the duration of the observation window.

$$\mathrm{ATC} = \frac{TC_{\mathrm{events}}}{T_{\mathrm{window}}} \tag{1.1}$$

ATC has demonstrated a significant correlation with motor unit firing rates in muscles and, consequently, with generated force [22]. This unique feature allows for the monitoring of muscle activation by reducing the volume of data managed by the hardware, leading to a decrease in circuit complexity, size, and power consumption. The event-driven approach of Average Threshold Crossing (ATC) incorporates three design paradigms [23]:

1. Event-based: Designed to identify, capture, or respond to significant events rather than operate continuously or cyclically.

2. Bio-inspired: Transfers information from biological processes, encoding electronic signals as digital pulses, referring to neural spike communication.

3. Information synthesis: Significantly reduces the overall amount of acquired data through a feature extraction process directly on the sensor node to reduce transmission load and provide high-level user information.

The choice of the threshold value plays a crucial role in extracting Threshold Crossing (TC) events. Proper threshold calibration should enable the identification of the maximum number of sEMG events, capturing the entire informational content while maintaining high robustness against environmental noise and artifacts related to biological signals. From the results of various investigations, the strategy has emerged of setting the threshold slightly above the baseline of the sEMG signal during muscle rest, proving effective in detecting the most relevant muscle activation events with minimal effort.

1.5 Functional Electrical Stimulation (FES)

Damage to the central nervous system (CNS) due to injury or disease, in conjunction with other health problems (e.g., muscle atrophy, joint contractures, increased frequency of bladder infections, decreased cardio-vascular capacity), can lead to

decreased sensory–motor performance [24]. A sensory–motor disability directly affects the patient's lifestyle and limits life activities.

Functional electrical stimulation (FES) was introduced as a method to artificially trigger the sensory-motor system after a CNS injury/disease and alleviate the resulting disability. FES systems are often used in neural motor prostheses and can be engineered as surface or implantable stimulation units for upper limb control or for assistance in standing positions or walking. FES devices directly assist in the performance of disrupted functions in humans with CNS lesions; furthermore, FES causes changes in cortical excitability and stimulates cortical reorganization (carry-over effects). Electrical stimulation can act directly on the central nervous system or it can be applied to the peripheral nervous system.

FES devices aid in the performance of primary functions, in individuals with central nervous system lesions, aiming to restore muscle function and facilitate cortical reorganization. By utilizing electrical current, FES triggers muscle contraction in paralyzed muscles, ultimately aiming to activate specific nerve fibers and elicit motor responses. For efficient stimulation, FES must target the undamaged nerve fibers that connect the spinal cord to the muscles.

FES is a potential treatment option for individuals experiencing impaired limb movement due to various neurological. It is essential for the nerve fibers connecting the spinal cord to the muscles to remain intact for FES to be effective, allowing electrical impulses to travel along the nerves and stimulate the muscles. In such cases, FES holds promise as a rehabilitation tool.

FES is distinguished into three functional categories:

- FES neuroprosthetics
- FES training
- FES therapy

1.5.1 FES Therapy

FES therapy aims at neurostimulation and, as previously mentioned, cannot be utilized in patients with complete spinal lesions since it requires afferents reaching the CNS. Peripheral areas are stimulated to induce adaptations at the central nervous system level.

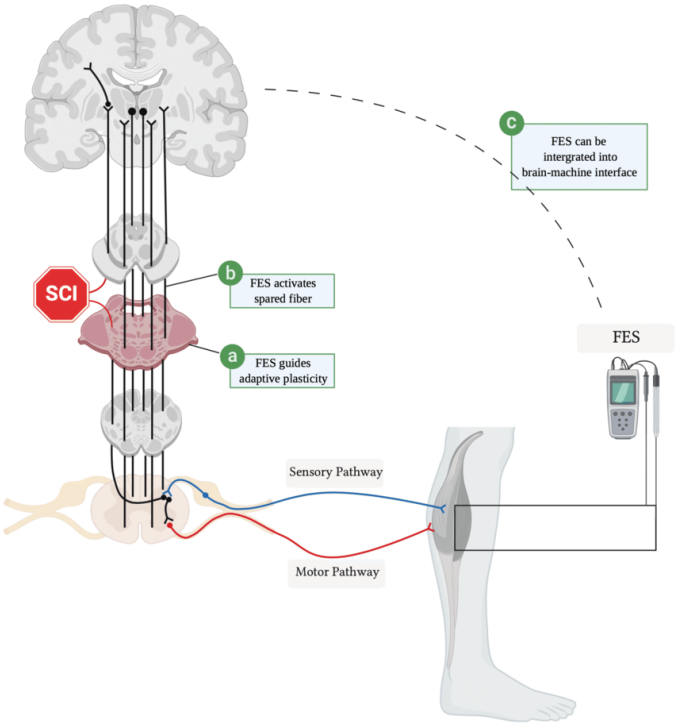

Figure 1.19: FES, in line with Hebbian theory [25], aims to strengthen the connections between the brain and affected muscles after Spinal Cord Injury (SCI). This involves guiding adaptive plasticity, activating damaged networks through spared fibers, and inducing neuronal plasticity via cortical neuron-controlled FES. FES facilitates the restoration of function by enhancing communication along sensory (shown in blue) and motor (shown in red) pathways, promoting recovery of paretic and paralyzed muscles.

It has been suggested that the advantages of functional electrical stimulation (FES) during rehabilitation partly arise from neuroplastic changes in motor circuits [26], as previously discussed. The Hebbian principle proposes that linking cortical and peripheral activity could reinforce intact descending pathways and result in sustained enhancement of motor function over time [25].

Moreover, employing electromyography (EMG) or motion tracking can help identify and monitor any residual movements, allowing for tailored customization of FES therapy for each individual.

The main issue with FES is fatigue. In the case of voluntary contraction, the neuromuscular system employs mechanisms to compensate for the reduction in performance:

- Increased firing frequency of motor units.
- Recruitment of new motor units.

- Substitution of active motor units.

In the case of electrically stimulated contraction, none of these strategies can be applied. Particularly, the recruitment order of muscle fibers does not follow the Henneman principle but is random or inverse. Another difference concerns the activation frequency of motor units which, in the case of stimulation, occurs synchronously. This creates greater variability in the force profile at the same frequency; therefore, to achieve tetanic force, a higher frequency is required.

1.5.2 FES Therapy for Hand Rehabilitation

In the context of functional electrical stimulation (FES) therapy for hand rehabilitation, the application focuses on retraining voluntary movements and grasping functions in individuals with conditions such as stroke and spinal cord injury. The FES therapy targets both proximal and distal muscles of the upper extremity to restore functional abilities.

Initially, the therapy begins with training proximal shoulder muscles, including the deltoid, biceps, and triceps. This phase aims to recover proximal function, with participants progressing to gain functional strength in these muscles. Once sufficient strength is attained, FES is applied to distal muscles of the forearm and hand.

A key aspect of the therapy involves training voluntary extension of the fingers, crucial for tasks requiring manipulation of objects. Participants are guided through exercises aimed at successfully opening their hand with assistance from FES. Low-amplitude stimulation of the finger flexors is then used to facilitate hand closing.

Throughout the treatment process, the intensity of FES assistance is gradually reduced as participants show improvement, eventually being phased out. Sessions typically last around 45 minutes, including electrode application and removal. Physiotherapists provide guidance and assistance to ensure movements are performed as close to physiological patterns as possible.

FES-reaching protocols have evolved to encompass various functional reach patterns, including sideways reaching, forward reaching and retrieving, reaching over opposite shoulder or knee, and hand-to-mouth movements. These protocols can be combined with grasping protocols to train reaching and grasping together, facilitating comprehensive hand rehabilitation.

Overall, FES therapy for hand rehabilitation utilizes a combination of targeted muscle stimulation and functional tasks to promote recovery of voluntary movement and grasping function, to improve independence and activities of daily living for individuals with neurological impairments.

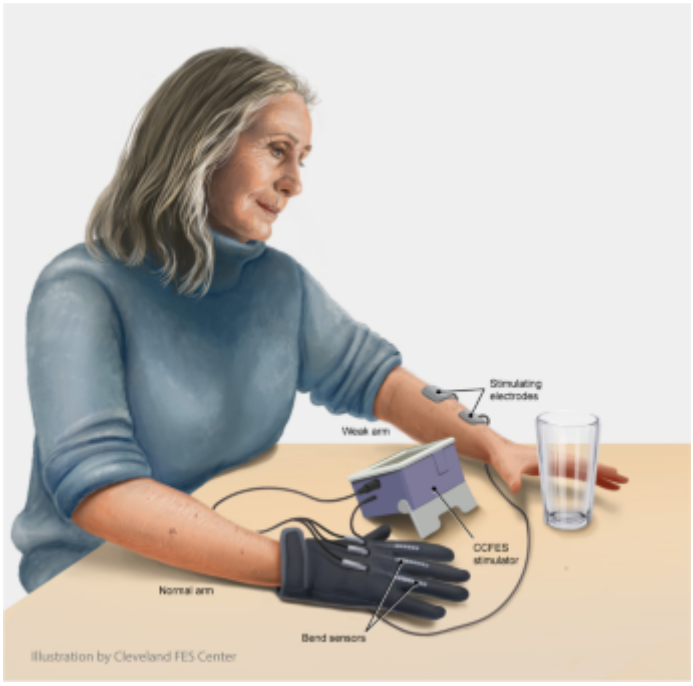

Figure 1.20: The contralaterally controlled functional electrical stimulation (CCFES) enables stroke survivors to open their paretic hand. The stroke survivor controls the rate of hand opening using a CCFES glove worn on the non-impacted hand, which controls the strength of electrical stimulation provided to the extensor muscles of the fingers and thumb of the paretic hand. [27]

1.5.3 Fatigue reduction methods applied to FES

In the context of research activities, the issue of random recruitment of motor units (MUs) during stimulation has been encountered, highlighting the need for a more physiological approach. The proposal focuses on inducing stimulation through the activation of reflexes, particularly leveraging the patellar reflex. In this scenario, the tap applied to the tendon generates stretching of muscle receptors, known as muscle spindles, resulting in a train of afferent stimuli. This process selectively activates motor neurons, based on the Hennemann theory, which suggests the activation of muscle fibers in relation to their recruitment threshold.

The practical implementation of this methodology involves stimulating the afferent nerve, aiming to activate the pathway of type I fibers. The main challenge lies in ensuring exclusive stimulation of afferents while avoiding efferent activation. This distinction is based on the different intensity-duration curve of afferents compared to motor axons. It is crucial to find an optimal balance in stimulation to generate a reflex response with Hennemann-type recruitment, but without causing complete

muscle contraction, limiting motor axon recruitment to 20-30

Despite the promising outlook of this approach, an additional challenge related to intra- and inter-subject variability has been identified, making the method less repeatable. Therefore, further avenues are explored to refine the effectiveness of stimulation, ensuring a controlled response of sensory afferents and minimizing unwanted activation of motor axons. This study aims to contribute to the understanding and optimization of physiological stimulation techniques in research in the field of muscle neurophysiology.

1.6 Machine Learning and Neural Network

This section introduces the process of implementing a classifier using machine learning techniques, with a specific focus on Artificial Neural Networks (ANNs). ANNs serve as potent and flexible tools, drawing inspiration from the complex workings of the human brain. By utilizing ANNs, we aim to harness their capability to learn intricate patterns from data and generalize acquired knowledge, thereby facilitating the classification process.

Neural networks, inspired by the intricate workings of the human brain, are powerful and versatile tools for approximating real-valued, discrete, and vector-valued target functions. They excel in handling complex input data and have demonstrated remarkable success across various domains, including handwritten character recognition, speech recognition, object recognition, and natural language processing tasks. Conceptually, neural networks can be viewed as mappings from input space X to output space Y, functioning as classifiers or function approximators for real-valued functions. Despite being named and inspired by biological systems, neural networks primarily function as machine learning algorithms with distinct architectures, lacking substantial parallels to actual neural systems.

In recent years, there has been a resurgence of interest in neural network architectures, driven by advancements in computer architecture (e.g., GPUs, parallelism) and the availability of vast amounts of data. While minor algorithmic tweaks have been made since the late 1980s, particularly in optical character recognition, the recent resurgence owes much to architectural innovations. An intriguing emerging perspective on neural networks revolves around the significance of intermediate representations. Previously viewed merely as function approximators, neural networks are now being recognized for the meaningful representations they develop at hidden layers during learning.

1.6.1 Artificial Neuron

The artificial neuron serves as a fundamental unit within artificial neural networks, inspired by the structure and functionality of biological neurons found in biological neural networks like the brain, spinal cord, and peripheral ganglia. While the biological neuron receives information through dendrites, processes it within the soma, and transmits it via the axon, the artificial neuron receives inputs, each weighted individually, processes them along with a bias using a activation function, and produces outputs as shown in Figure 1.21. This simplified model of artificial neurons allows facilitating their incorporation into neural network architectures.

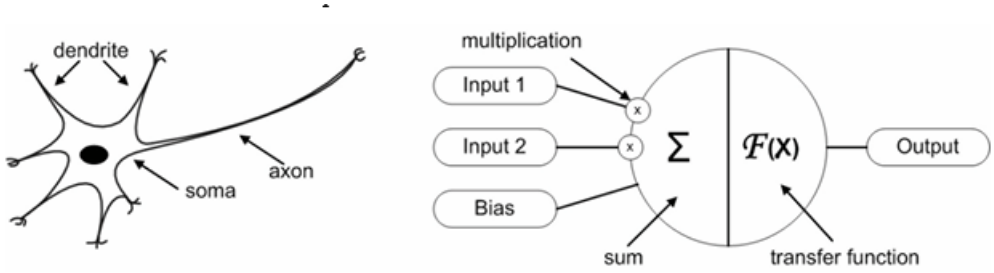

Figure 1.21: Artificial Neuron

In the thesis work, the activation function used for artificial neurons was the ReLU, an acronym for Rectified Linear Unit. This activation function is one of the most common and widely used in artificial neural networks, especially in hidden layers. Its mathematical formula is simple: ReLU(x) = max(0, x), where x is the neuron's input.

The main characteristic of the ReLU function is that it returns 0 for all negative input values and returns the input itself for positive values. This means that the function is linear for positive values and non-linear for negative values. This allows ReLU to overcome some of the gradient vanishing problems encountered with other activation functions, such as the sigmoid or hyperbolic tangent, especially in deep neural networks.

1.6.2 Multilayer Perceptron

A Multilayer Perceptron, also known as a neural network, is a structure composed of several layers of neurons, where the output of one neuron in a layer becomes the input for the neurons in the next layer.

In the last layer, called the output layer, the activation may vary depending on the type of problem: for regression, no activation function is generally applied, while for binary classification, the Sigmoid function is commonly used. For multiclass classification, the Softmax function is often adopted to ensure that the sum of the predictions for all classes equals 1. The basic architecture of Multilayer Perceptrons

involves each unit in one layer being connected to all units in the next layer, with key parameters of the architecture including the number of hidden layers and the number of neurons in each layer.

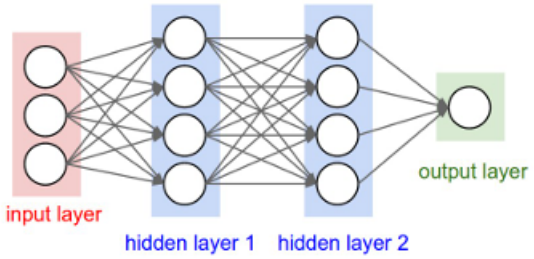

Figure 1.22: ANN Basic Architecture

Chapter 2

State of Art

2.1 sEMG Wearable Devices in Rehabilitation

In the field of rehabilitation, evaluating patients presents significant challenges, primarily due to constraints within clinical settings [28] [29]. In response to these challenges, wearable technology emerges as a compelling solution for the objective assessment and monitoring of patients both within and outside clinical environments. Leveraging wearable devices, healthcare professionals can access a wealth of detailed information on patients' impairments, facilitating the identification and optimization of rehabilitation therapies.

In addition, wearable technology plays a crucial role in stroke rehabilitation [30], addressing the specific challenges faced by patients recovering from this debilitating condition. By providing objective data on patients' motor capabilities, these devices enable healthcare professionals to tailor interventions more effectively to individual needs. For stroke survivors, wearable technology facilitates continuous monitoring of motor function, allowing for early detection of progress or setbacks. Moreover, the portability and convenience of wearable devices empower patients to engage in rehabilitation exercises outside of supervised sessions, promoting independence and active participation in their recovery journey.

In the field of wearable real-time monitoring systems, signals such as ECG, EMG and EEG are also used. These biosignals are acquired and analyzed to extract relevant information for observation, diagnosis and treatment of patients [31]. However, traditional monitoring systems often suffer from drawbacks such as slow data acquisition and transmission, inefficient power consumption, and bulky size, which limit their versatility and widespread adoption.

An example of the use of biosignals within a wearable system for monitoring and rehabilitation of upper limbs is provided by Zhao et al. [32], who introduced a robotic glove for assisted training capable of capturing EMG and ECG signals. The

ECG/EMG signals collected undergo a series of processing steps including filtering, amplification, and digitization before being wirelessly transmitted to a smartphone or laptop using a low-energy Bluetooth module. Additionally, a dedicated software platform is developed to analyze and visualize the ECG/EMG data, which is seamlessly integrated into the control system of the robotic glove. Throughout the training process, the EMG sensor monitors various hand activities, while the ECG sensor tracks changes in the user's physiological status. This innovative system showcases its feasibility and effectiveness in monitoring physiological signals during upper limb rehabilitation, offering valuable insights for tailoring rehabilitation strategies to meet individual treatment needs.

Regarding the proposed portable and wireless acquisition system, Smith et al. [33] proposed a solution to register important physiological signals. The acquisition system mainly consists of a portable device, a graphic user interface (GUI), and an application program for displaying the signals on a notebook (NB) computer or a smart device. Essential characteristics of the portable device include eight measuring channels, a powerful microcontroller unit, a lithium battery, Bluetooth 3.0 data transmission, and a built-in 2 GB flash memory. Major advantages of the proposed system are the capability of combining it with an NB computer or a smartphone to display the signals being measured in real-time, and superior mobility due to its independent power system. Briefly, this acquisition system offers consumers or users a convenient and portable studying tool to measure dynamic vital signals of interest in psychological and physiological research fields."

The Myo armband gathers EMG signals and motion-related inertial data, transmitting them via Bluetooth to the gateway (Intel UPS-GWS01). The gateway filters and extracts information from the data before sending it to the cloud server.

2.2 sEMG-based classification of hand motions using deep-learning techniques

The classification of hand motions based on surface electromyography (sEMG) signals using deep-learning techniques represents a cutting-edge approach in the field of prosthetics and rehabilitation engineering. By harnessing the power of deep-learning algorithms, which excel at extracting complex patterns from large datasets, researchers aim to develop robust and accurate systems capable of decoding the user's intended hand movements with high precision.

In a study [34] conducted on patients with trans-radial amputation, it was demonstrated that it is possible to decode individual flexion and extension movements of each finger with an accuracy greater than 90 % using exclusively surface electromyography signals. An EMG array of bipolar Ag–AgCl electrodes was placed on the subject's right arm according to the European recommendations for sEMG.

This was implemented by dividing the forearm into five distinct levels where levels I through V were characterized by 32, 28, 24, 19, and 12 electrodes, respectively.

The central theme in the field of hand movement classification is the optimal configuration for signal acquisition and in this context, paper [35] gives a comparison of six acquisition setups. The article aimed to assist researchers in selecting the appropriate acquisition setup for the classification of hand movement class. The acquisition setups are based on four different sEMG electrodes and were used to record more than 50 hand movements from intact subjects with a standardized acquisition protocol. Comparable classification results are obtained with three acquisition setups, including the Delsys Trigno, the Cometa Wave, and the cost-effective configuration composed of two Myo armbands. The Myo armband consists of 8 medical-grade stainless steel sEMG single differential electrodes. Implementing the Double Myo Setup required overcoming two main difficulties: managing timestamps and software limitations. The Double Myo configuration involves wearing two armbands, positioned on the upper and lower arm, respectively, providing uniform muscle mapping.

Myo Armband is also used individually in [36] for the classification and recognition of hand gestures using electromyography (EMG) signals to control upper limb prostheses. In this research, EMG signals were captured via an embedded system while wearing the Myo Armband, enabling the observation of hand movements. The study involved 10 healthy subjects performing various upper limb movements, and after extracting EMG data, supervised classification techniques were applied to recognize different hand gestures. The classification achieved an overall accuracy of 83.9 % using ensemble (bagged tree) classifier.

Chapter 3

System Description

The thesis project focuses on applications of real-time Functional Electrical Stimulation (FES) and online modulation of stimulation patterns. The primary objective is to develop a bio-mimetic system for FES control based on surface ElectroMyoGraphic (sEMG) signals aimed at rehabilitating hand movements.

The starting point of the project is an existing system, designed for event-driven sEMG-based FES control, which employs the Average Threshold Crossing (ATC) technique. This paradigm allows an online and real-time FES intensity modulation [37].

In this setup, the surface ElectroMyoGraphic (sEMG) signal goes through direct processing, extracting the ATC profile, on a wearable acquisition board before being wirelessly transmitted to the control unit. By integrating the ATC method directly on-board, there is a reduction in both data size and transmission load. This integration facilitates the development of energy-efficient biomedical acquisition systems.

The control platform enables the modulation of stimulation current intensity solely based on ATC information, which has demonstrated a high correlation with muscle force, as evidenced in previous research [22]. Subsequently, the control unit is capable of dynamically updating stimulation parameters with each transmission of new ATC data points. Furthermore, the system is equipped with a user-friendly graphical interface (GUI), providing oversight of the stimulation process and allowing for parameter selection.

Figure 3.1: System Overview: the hardware part is composed of the sEMG acquisition system and the electrical stimulator. The acquisition devices communicate via Bluetooth with the control platform, while the stimulator uses a USB cable for the connection.

The goal of this thesis project is to extend the applicability of the previous system to the hand-forearm region to create a system useful for the recovery of hand motor functionality. This primarily requires the development of an acquisition system suitable for the intricate motor control of the hand, which involves the coordination of numerous muscles. This implies an increase in the overall complexity of the system.

The thesis work focused on the development of the acquisition system for FES control, integrating the synchronous management of acquisition devices required for monitoring muscles in the hand-forearm district. To this end, a dedicated software for the interaction with the acquisition units was developed, starting from an existing version provided by the research group. The software was further improved with the introduction of a classifier, obtained using Machine Learning techniques.

The classifier, in the final system, will be interposed between the acquisition unit and the stimulation unit, at the level of the control unit. Its introduction is necessary to manage the system's complexity and make the information derived from the input ATC signals, usable for stimulation. The classification result can be used to select the stimulation channels to be activated, using the parameters obtained from the processing of ATC data in the control unit.

In conclusion, the stimulation phase was introduced, trying to simulate the operation of the integrated system, to set the stimulation channel selection according to the classification result obtained by the control unit.

The primary approach through which the system is conceived is the therapist-patient application [38], where the therapist utilizes the muscle information from a healthy individual to configure the stimulation parameters to be applied to a second individual (the patient), Figure 3.2.

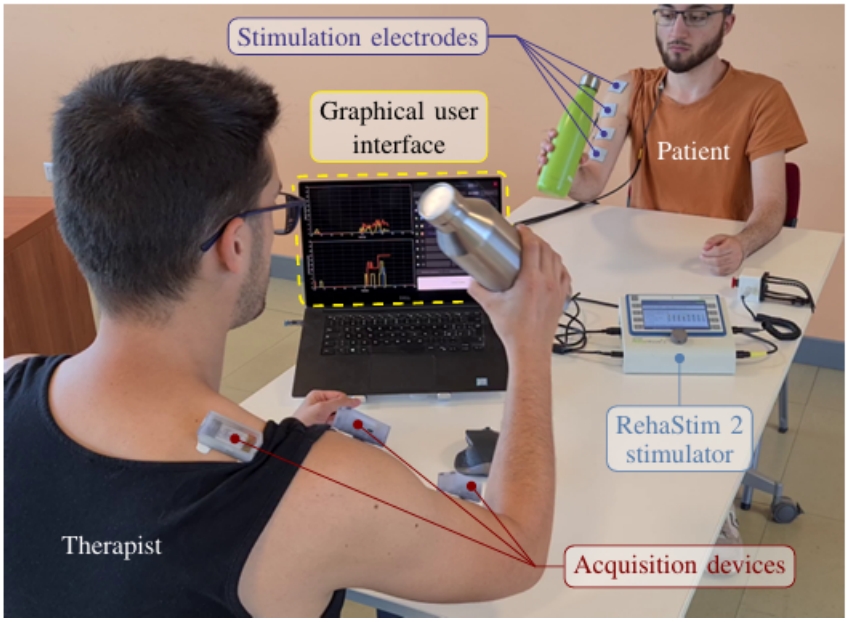

Figure 3.2: Therapist-Patient controlled stimulation [39].The *acquisition devices* are applied on the therapist's muscles, to extract the sEMG signal and determine the ATC values. These data are sent to the control unit where they are displayed in the *Graphic User Interface (GUI)*. The control unit computes the stimulation parameters that are sent via USB to the *RehaStim 2 stimulator* and applied through the *stimulation electrodes* on the patient.

3.1 Acquisition System Devices

This section will describe the devices included in the FES acquisition system.

The design of the acquisition system architectures for the FES system is derived from an anatomical study described in 1.1. Subsequently, the bio-electric signal extracted from the muscles identified as pivotal for hand motor control was individually acquired to determine optimal electrode placement conditions and verify their effective activation and associated movements.

Following these targeted acquisitions, the muscles to be included in the overall acquisition system have been definitively identified. These muscles can be divided into 3 subgroups based on their location in the hand-forearm region, which also determines the type of acquisition device used. All acquisition devices were made available by the eLioNS Laboratory research group.

The first subgroup includes the following muscles: *Extensor Pollicis Longus*, *Extensor Pollicis Brevis*, *Abductor Pollicis Longus*, and *Proper Extensor Indicis*.

These muscles are located in close proximity, in the distal part of the dorsal forearm, Figure 1.5. Therefore, their sEMG/ATC signals were acquired using the same device, called Apollux. This wearable acquisition unit applies the Average Threshold Crossing (ATC) parameter extraction technique to the sEMG signal and transmits the result to the control unit.

The Apollux device, used as shown in the Figure 3.3, consists of two essential elements [40]:

- Analog Front End (AFE): This circuit detects the sEMG signal and extracts the quasi-digital Threshold Crossing (TC) signal. The raw signal conditioning circuit is designed for differential signal acquisition, applying signal filtering with a passband between 70 Hz and 400 Hz and a default gain of 500V/V (which can be increased by x2, x3, or x4). The last stage of AFE is a threshold comparator used to obtain the TC signal, an intermediate stage of the ATC technique. The threshold applied by the comparator is established following calibration.
- Digital Processing Unit: This component performs the calculation of ATC values and their transmission. The Apollux3 Blue MCU [41] is utilized for its extremely low-power characteristics.

The components of the device are housed within a case that gives it a compact shape with size 57.8mm × 25.2mm × 22.1mm [23], facilitating the wearability of the Apollux without causing limitations in the execution of movements. Finally, data transmission to the control unit occurs via Bluetooth Low Energy (BLE) technology [42], with ATC values updated every 130 ms.

Figure 3.3: Real-time acquisition using Apollux devices: two ATC profile extracted from *Gastrocnemius Medialis* and *Soleus* muscles [43]

The second subgroup of muscles, necessary for motor control of the hand, is located within the hand itself. These muscles are referred to as intrinsic, and among them, those of interest for the acquisition system are located in the thumb, e.g. *Opponens Pollicis*, *Abductor Pollicis Brevis*, and little finger, e.g. *Abductor Digiti Minimi*. Bio-electrical signals from the thumb muscles are extracted with two acquisition devices, while an additional device is used for those in the little finger. During the preliminary study of these muscles, the need to modify the structure of the integrated Apollux emerged. The case is poorly suited for such a distal application, making electrode adhesion unstable and hindering accurate signal acquisition.

To extend the acquisition area and include the hand, it was decided to separate the components within the case and connect the cables to allow the acquisition area to be occupied only by the active electrodes. The resulting device configuration is shown in Figure 3.4

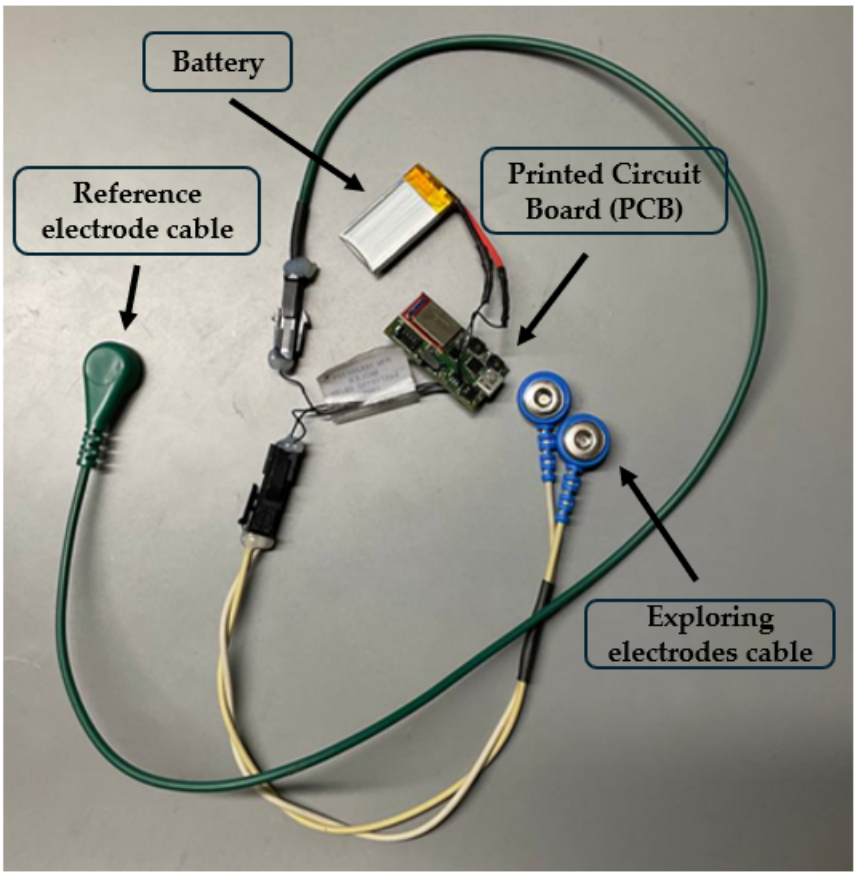

Figure 3.4: Modification of the Apollux device by removing the components from the case so that only the electrodes can be applied at the acquisition point. Improved adhesion and preservation of electrode skin contact.

Finally, a device called Armband, again made available by the eLiONS Lab. research group, was chosen to complete the acquisition system. The third subgroup of muscles comprises the extrinsic musculature located in the forearm, Figure 1.7. These muscles are responsible for controlling the flexion and extension movements of the fingers; moreover, there are additional muscles that, although mainly responsible for motor control of the wrist, are important for the recognition and execution of finger movements.

The Armband, Figure 3.5, has been designed as a circular ring to fit around the forearm, consisting of seven units: one acting as the master board, responsible for providing a wireless interface with the user and controlling all operations, and the remaining six serving as its slaves, which execute commands sent by the master.

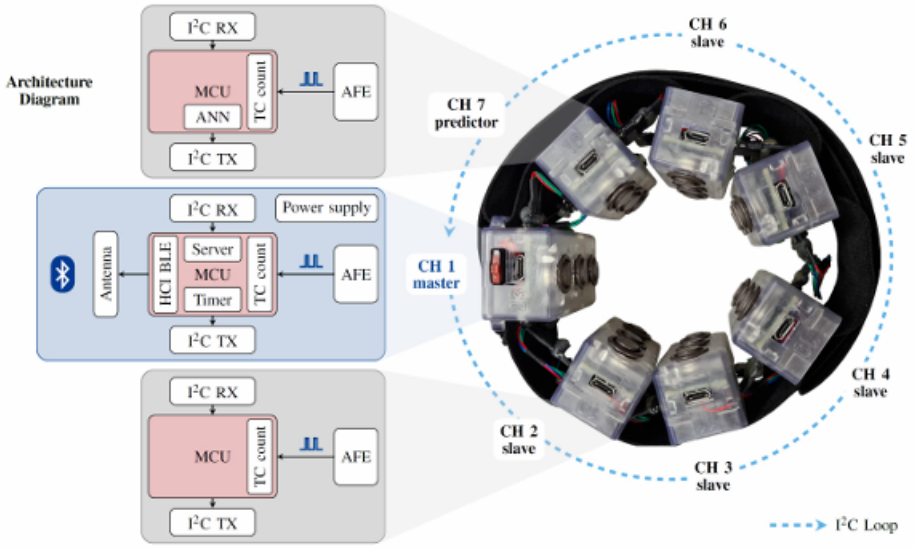

Figure 3.5: Armband acquisition device. Power and I2C communication wires electrically connect the boards, while the elastic band physically keeps the modules in the proper position [44].

The overall acquisition system architecture and the studies leading to the precise positioning of the acquisition units will be described in detail in Chapter 4.

3.2 Classifier for Hand Movement Recognition

During the project's development, a classifier was integrated at the control unit level. In this way, the control platform has additional information related to the movement being performed, predicted through the ATC data sent from the acquisition devices.

The information on the predicted movement can be useful for the overall control of the electrical stimulator. This allows stimulation to be administrated in the patient only after movements have been recognized through the distribution of ATC values among the acquisition channels.

Another application of the predicted class parameters involves the employment of the electrical stimulator, which, in the previous FES control system, required the modulation of stimulation parameters (e.g. pulse width, amplitude). In that case, the one-to-one relationship between stimulation channels and acquisition channels allows for stimulation to be conducted by updating stimulation parameters exclusively in correspondence to channels where muscle activation is recorded.

Due to the complex architecture of the acquisition system developed in this project, movement classification can be employed to determine the channels of the stimulator to activate. Consequently, the selection of activated channels, applying the stimulation parameters computed using the same procedure as the previous system, is movement-dependent.

Hence, the additional information required for stimulator control can be obtained by using a classifier capable of determining the performed movement. In this context, the classifier, by providing information regarding the movement performed during its acquisition, acts as a filter between the acquisition and stimulation unit.

Therefore, the classifier must be capable of providing real-time predictions to align with the overall system's use. The control unit should provide the ATC data as input to the classifier, which should base its prediction on the ATC data.

3.3 Functional Electrical Stimulation

The FES system utilizes the RehaStim2 [45], manufactured by HASOMED$_{@}$, as its electrical stimulator. This device is compliant with EU guidelines MDD 93/42/EWG and is classified as a class IIa medical device, with an applied part type BF (body floating). Equipped with a built-in rechargeable battery, the RehaStim2 is portable, making it suitable for integration with bio-signal acquisition systems, which are often susceptible to power-line interference.

The RehaStim2 can interface with a PC via the ScienceMode2 serial communication protocol, enabling direct control of stimulation parameters. It features two independent current generators, each connected to 4 stimulation channels, totaling 8 stimulation channels that can operate simultaneously. To ensure safety, the stimulator conducts a tissue impedance check before each stimulation pulse. If the impedance deviates from the expected range, stimulation is automatically halted. Additionally, an emergency button is provided for immediate cessation of stimulation if needed.

The stimulation waveform produced by the RehaStim2 is biphasic rectangular pulses with a balanced charge, ensuring effective and controlled muscle activation.

The user-controlled stimulation parameters are reported in Table 6.1.

Parameter	Range	Step
Current Intensity	0 - 130 mA	2 mA
Pulse Width	20 - 500 μs	10 μs
Frequency	10 - 50 Hz	5 Hz

Table 3.1: RehaStim2 stimulation parameters

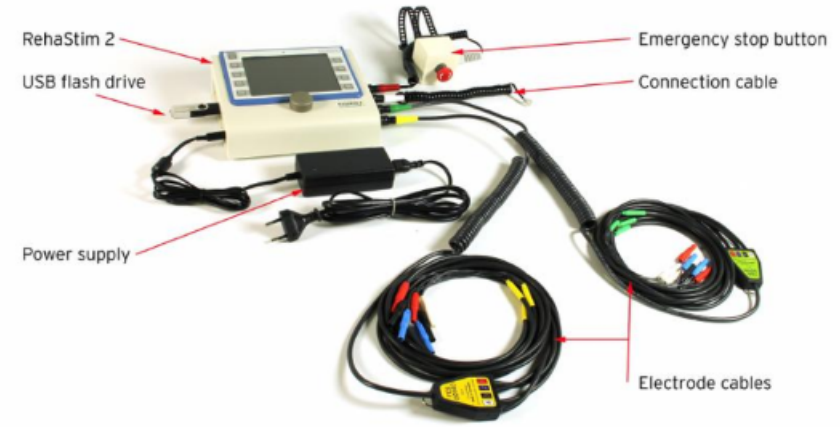

Figure 3.6: Stimulator RehaStim2 [46]

The following chapters will be organized as follows:

- Chapter 4: "Acquisition System Description". This chapter will outline the structure of the acquisition unit and its devices, explaining the preliminary study phase. Finally, the protocol used for the acquisitions carried out on the subjects will be described.
- Chapter 5: "Acquisition protocol & software adaptation". This chapter will describe in the first part the software and its functioning. Next, information regarding the experimental protocol and selected movements will be provided.
- Chapter 6: "Machine Learning and Neural Network". In this chapter, the characteristics of the developed classifier and the training methods used will be described.

Chapter 4

Acquisition System Description

4.1 Study on Electrode Placement for sEMG Signal Acquisition in the Forearm-Hand Region

This chapter will focus on describing the architecture of the acquisition system, designed in the thesis work. Starting from the anatomical structure of the hand, Section 1.1, the steps that led to the definition of the system will be outlined. This includes the selection of appropriate devices, introduced in Section 2.1, their positioning, and ultimately, the definition of the overall architecture of the acquisition system.

4.1.1 Muscle Identification and Signal Acquisition

Understanding the anatomical structure of the hand is crucial as it forms the foundational premise for subsequent phases of this thesis. Building upon this theoretical foundation, a practical investigation followed to capture the essential muscles involved in hand movements. Efforts were directed at identifying pivotal muscles for motor control of the hand in the forearm-hand region using the *Apollux* device [23], introduced in the previous Section 3.1, for sEMG/ATC signal acquisition. This phase involved meticulous probing to identify optimal locations for acquisition devices, ensuring accurate capture of muscle activation patterns.

Subsequent analysis aimed to elucidate the relationship between muscle activation profiles and corresponding movements, studying the interaction between muscle activity and motor control.

- Flexor muscles of the fingers: these muscles are situated in the anterior forearm. Particularly, the objective was to activate the *Flexor Digitorum Superficialis* and *Flexor Digitorum Profundus* muscles through flexion of the fingers at all joint levels and evaluate the intensity of acquisitions while moving along the proximal fiber. Two *Apollux* devices were employed to assess any differences in acquisition intensity as shown in Figure 4.1. From this analysis, it emerged that a more distal positioning better identified the activation of these muscles, information that will be utilized subsequently in the development of the thesis project.

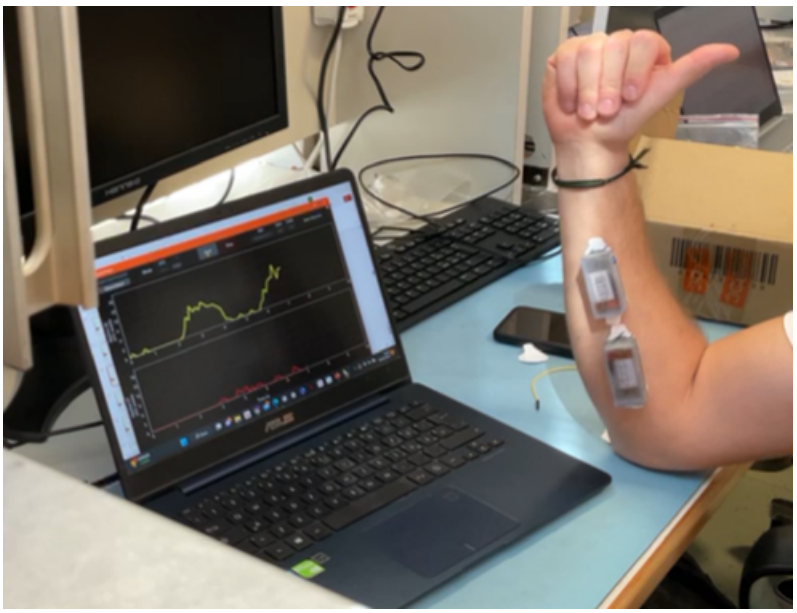

Figure 4.1: The image shows the comparison of signals taken along the muscle fibers of the *Flexor Digitorum Superficialis* at different distances along the forearm. The two *Apollux* have the same amplification value to show the difference in signals amplitude. (red line proximal device - yellow line distal device)

- Extension movement of the fingers, Figure 4.2: according to theoretical information, this movement is controlled by the muscles *Extensor Digiti Minimi* and *Extensor Digitorum Communis*. These muscles are located in the dorsal forearm, and following the placement of the device, based on visual and tactile analysis of muscle morphology it was possible to test the activations of these muscles. At this stage, it emerged that it was indeed possible to detect the activation of the mentioned muscles associated with the extension of the fingers, including Little Finger, even in a selective mode.

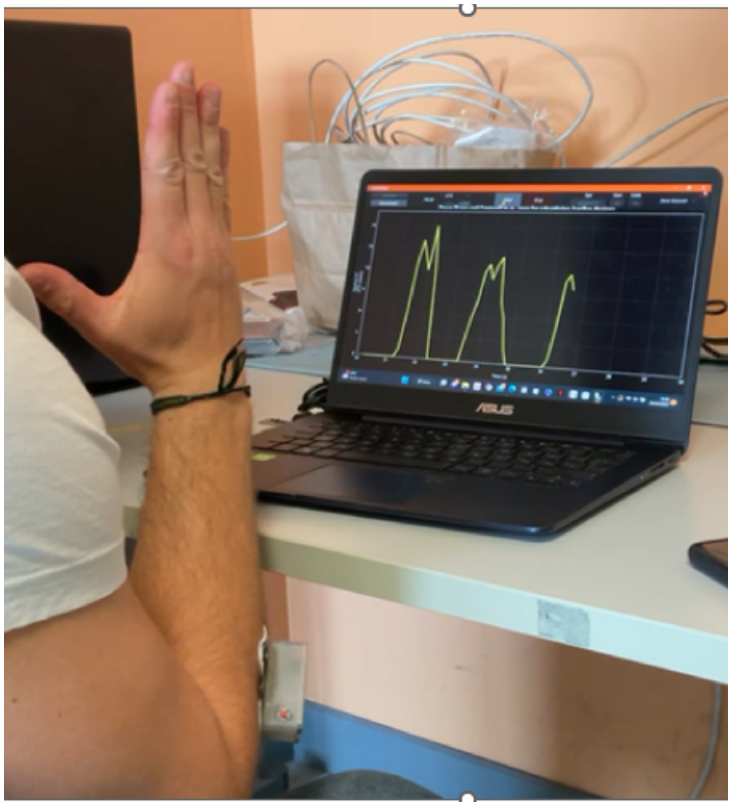

Figure 4.2: Investigation of the extensor muscles of the fingers. Acquisition device placed at muscles *Extensor Digiti Minimi* and *Extensor Digitorum Communis*.

- Muscular structure of the Thumb: In this case, the study was more intricate due to the thumb's complex muscular structure, which is divided between intrinsic (located within the hand) and extrinsic (located within the forearm) musculature, Figure 1.5. Additionally, the thumb possesses a high degree of freedom, necessitating an examination of the connection between muscle and controlled movement, as depicted in Chapter 1. Following this analysis, the first limitation of the existing acquisition unit, the integrated *Apollux*, was encountered, as it did not allow for the acquisition of intrinsic musculature. Subsequently, modifications were made to the device to overcome these limitations, already shown in Figure 3.4, whose application will be illustrated below.

  As a result, the extrinsic musculature at the distal level of the forearm was initially analyzed to assess the contribution of these muscles to movements such as abduction, extension, and opposition of the thumb using the device in the following placement, Figure 4.3.

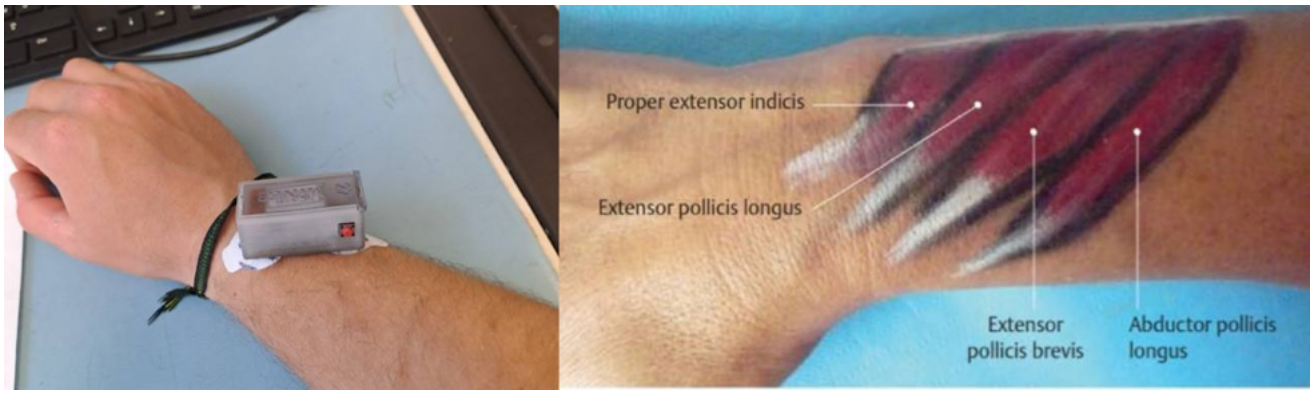

Figure 4.3: Electrode placement on the distal region of the forearm for thumb extrinsic muscles acquisition.

After this step, the significance of the acquisition point analyzed for movement such as thumb abduction and extension was confirmed. The extension of the index finger, individually is also visible with this device placement.

To complete the study of the thumb and its movements, information on the acquisition of its extrinsic musculature, represented by the long flexor of the thumb, located proximate to the anterior forearm, was added. This muscle lies adjacent to the flexor muscles of the fingers, situated at a more superficial level. By increasing the amplification value of the *Apollux*, it became possible to detect the activation of thumb flexion movement, thereby highlighting the feasibility of monitoring such movement via extrinsic musculature.

4.1.2 Device modifications for intrinsic muscle acquisition

To extend the acquisition area and include the hand, it was decided to separate the components within the container of the *Apollux* device and connect cables to allow for the acquisition zone to be solely occupied by the active electrodes. This modification enabled the extension of acquisitions to the intrinsic muscles of the hand.

In particular, the involvement of muscles controlling thumb movement was studied. Subsequently it was decided to use two acquisition devices in this region of the hand, as shown in Figure 4.4. This makes it possible to optimize the distinction of movements under thumb control, considering the large number of degrees of freedom, creating the following split between muscle and acquisition point:

- Thumb external: *Opponens Pollicis Brevis* and *Abductor Pollicis Brevis*
- Thumb internal: *Flexor Pollicis Brevis* and *Adductor Pollicis Brevis*

Figure 4.4: The figure shows the optimized acquisition system with the positioning of the electrodes about the intrinsic muscles of the thumb.

The described analysis confirmed the central role of selected muscles, in controlling thumb movements e.g. opposition, extension, abduction and adduction. In addition, modifications of the wearable device and the use of the glove allowed extended acquisitions to be carried out while maintaining high signal quality.

Following this, activation of muscles controlling little finger movement was tested, confirming the ability to extract the ATC signal from this hand region as well.

In conclusion, the delineation of muscle activation patterns and their correlation with hand movements represent a milestone in the search for robust signal acquisition methodologies. The information gained at this stage not only facilitates the identification of optimal signal acquisition locations but also deepens our understanding of the intricate interplay between muscle activity and motor control. With this knowledge, subsequent chapters will move into the development of a comprehensive hand motion recognition system, taking advantage of the insights gathered in this work.

4.2 Overall Electrode Placement and Acquisition Devices

Following the specific muscle trials described earlier and the insights gained, it is necessary to define the electrode placement for the entire hand-forearm region. This will enable us to obtain muscular information regarding the activated muscles responsible for hand movement during various hand motions.

4.2.1 Intrinsic Muscles Acquisition Units

Starting from the intrinsic hand muscles, based on the studies outlined in the previous section, it was decided to allocate three devices for signal acquisition within the hand. Specifically, two acquisition points are placed in the thumb positioned internally and externally, respectively. This decision was made considering the presence of a high number of muscles to assess the activation breadth across the two devices. Additionally, a device will be added to monitor little finger activity.

As previously explained, for the acquisition of intrinsic hand muscles, the modified Apollux device is utilized.

The described devices will occupy channels 8 to 10 in the overall system. Specifically:

- CH 8: Thumb Internal
- CH 9: Little Finger
- CH 10: Thumb External

4.2.2 Extrinsic Muscles Acquisition Units

The first group of extrinsic muscles considered for acquisition is located distally in the forearm and is formed by the following muscles:

- Extensor Pollicis Longus/Brevis
- Abductor Pollicis Longus
- Proper Extensor Indicis

This set of muscles is in close proximity, therefore it has been decided to dedicate a single device for the control of this region, which will occupy channel 11 (CH 11 Forearm Distal) in the overall system.

The muscles directly involved in the selective control of the fingers are as follows:

- Flexor Digitorum Superficialis/Profundus
- Extensor Digitorum Communis
- Extensor Digiti Minimi

Although the muscles responsible for wrist control are not explicitly mentioned, they play a secondary stabilizing role and should therefore be considered in this study. The muscles in question are:

- Extensor Carpi Ulnaris
- Extensor Carpi Radialis
- Flexor Carpi Ulnaris
- Flexor Carpi Radialis

Due to the number of muscles involved in finger movements, it was decided to utilize a device provided by the research group. The device is an armband [44], 3.1, designed as a circular ring, intended to encircle the forearm. It comprises seven units, covering channels 1 to 7 of the global system.

- CH 1: Central Anterior
- CH 2: Radial Anterior
- CH 3: Radial Posterior
- CH 4: Central Posterior
- CH 5: Ulnar Posterior
- CH 6: Medial
- CH 7: Ulnar Anterior

This decision was made following verification of the feasibility of acquiring the above-mentioned muscles at the same longitudinal position on the forearm.

4.2.3 Overall Acquisition System

The following Figure 4.5 shows the overall architecture of the acquisition system, with the optimal placement of the selected devices. The use of the system and the analysis of the extracted data will be described in the following chapters.

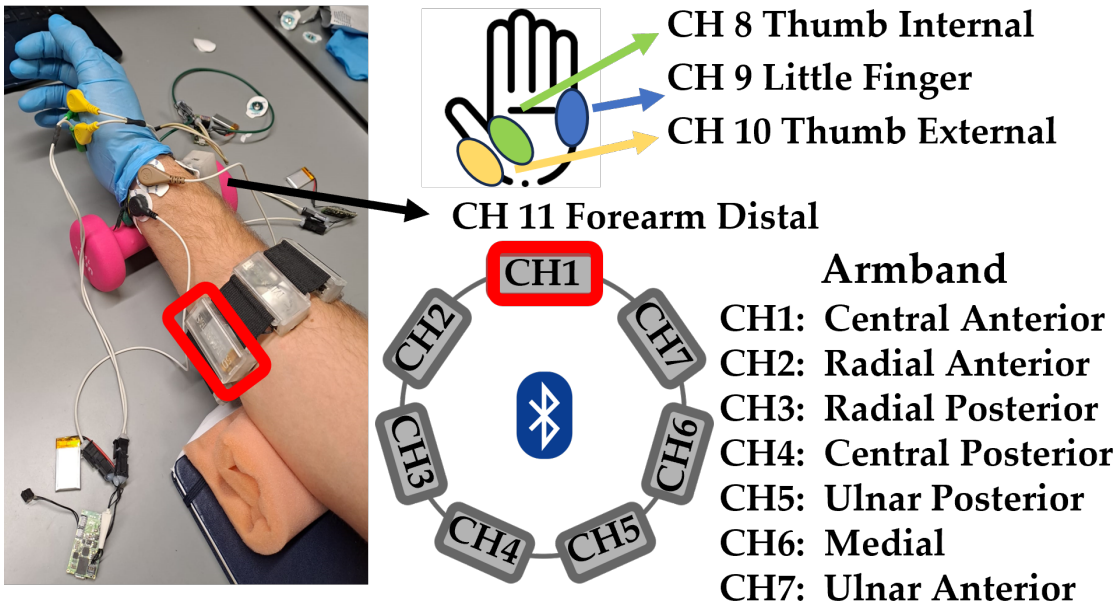

Figure 4.5: Overall Acquisition System. The figure depicts the positioning of the acquisition devices in the hand-forearm region. From distal to proximal: channels 8 to 10 for intrinsic muscles, channel 11 for the distal forearm position, and channels 1 to 7 for the armband.

Chapter 5

Acquisition protocol & software adaptation

This chapter will detail the protocol and software used to obtain the acquisitions. This software allows interaction with the acquisition system outlined in Chapter4, facilitating the synchronous usage of the five acquisition units (1 Armband and 4 Apollux).

5.1 Software and Acquisition Unit Interaction

The first section of this chapter introduces the architecture of the software utilized, which represents the merging of the two versions previously developed for controlling the identified devices individually.

Furthermore, the graphical user interface (GUI) has been customized to effectively monitor the ATC values extracted from the selected muscles during acquisitions and to set crucial parameters (e.g. AFE gain, threshold for TC) for the proper employment of the devices.

An additional interface has been adapted with the function of serving as a guide for the user during movement execution. This screen provides the subject with detailed information on the movement to be performed and the timing to follow, aiding in distinguishing between muscle contraction execution and maintaining the resting position.

5.1.1 Software Architecture

The control software has been developed using the Python programming language and is designed to run on a standard laptop, allowing direct processing of

acquired muscle data. This configuration also allows for establishing a BLE connection with the acquisition units. For this purpose, a USB BLE dongle is employed, specifically, the Nordic Semiconductors nRF52840 [47].

The distinctive feature of the software is its modularity, attributable to the architectural design that involves the use of independent units capable of communicating with each other through application programming interfaces (APIs). This approach is made possible by the Object-Oriented Programming (OOP) paradigm [48].

Method callbacks initiate all top-down functions, whereas internal bottom-up data communication relies on queues. Each layer is equipped with one or more queues tailored to the type of data and recipient, ensuring structured and organized data flow control throughout the system.

The software relies on the interaction of four main components: the *BLE*, the *acquisition units*, the *System*, and the *Graphical User Interface* (GUI).

The BLE object, situated at the lowest level of the architecture, is implemented using the Blatann module and manages device scanning and connection. During this phase, connection management is organized by dividing the connected devices (4 Apollux and 1 Armband) across two different BLE dongles. A specific connection strategy is adopted to ensure that the Armband and a single Apollux are connected to the same dongle, to balance device distribution. The acquisition unit objects are instantiated for each device, thus creating a group of objects at a parallel level. During system operation, this level comprises 5 objects: 1 Armband and 4 Apollux, which, once instantiated correctly, interface between BLE and the system, as shown in Figure 5.1.

The System object manages input/output communications with peripheral devices and their interaction. In this module, ATC data from all connected peripherals converge and can be processed differently. The first operation performed with the ATC data is their transmission to the graphical interface to obtain their real-time representation. Also at this level of the system, the classifier will be used to obtain predictions on the movement executed by the subject on the acquisition side. The implementation of the classifier within the control platform will be illustrated in the next Chapter 6.

The Graphical User Interface (GUI) was developed using the Kivy Python-compatible framework. This constitutes the user interaction level and includes widgets such as spinners, buttons, graphs, and popups.

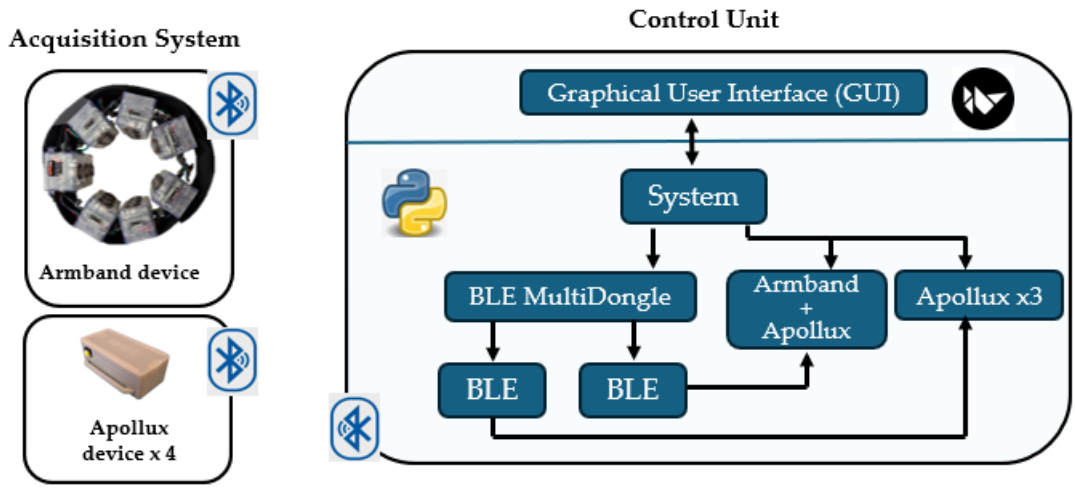

Figure 5.1: Software Architecture.The figure shows the software architecture, with the highest level occupied by the *GUI*, followed by the *System* level and *acquisition devices*, and finally, at the lowest level, two *BLE* objects.

5.1.2 Graphic User Interface (GUI)

In this section, the main functionalities of the interface, employed for conducting acquisitions, will be elucidated. Figure 5.2 showcases the initial screen of the interface, serving as the starting point for its utilization.

Figure 5.2: Graphical user interface (GUI)

- The *Connection* button begins the Bluetooth Low Energy (BLE) connection procedure with peripheral devices. During this phase, the system initially scans for peripheral devices, presenting them to the user via checkboxes. Users can then select the desired devices for connection. The connected devices are distributed in a specific order to the two BLE dongles used.
- The *Calib all* button begins the threshold calibration procedure, a fundamental operation for the proper utilization of the ATC paradigm. Conducting calibration post-connection enables users to immediately proceed with acquisitions without altering the amplification values of the acquisition units, which remain set to default values.
- The *Start* button to commence the system, initiating signal acquisition and processing following the previously described procedure until obtaining the ATC value. ATC data are displayed in the graphical interface, organized into two main columns: on the left are the acquisitions made by the wristband, while on the right are signals derived from other devices. Figure 5.3 shows the GUI while the software is running.
- The *Set Up* button allows for the modification, at any time, of the gain value applied to each acquisition device. This functionality is utilized during the setup phase of the acquisition system to tailor it to the subject.

Note the presence of two checkboxes labeled "save session" and "protocol interface," both essential for acquisitions. The former allows data to be saved in text file format, while the latter initiates an additional screen that guides the subject through the protocol."

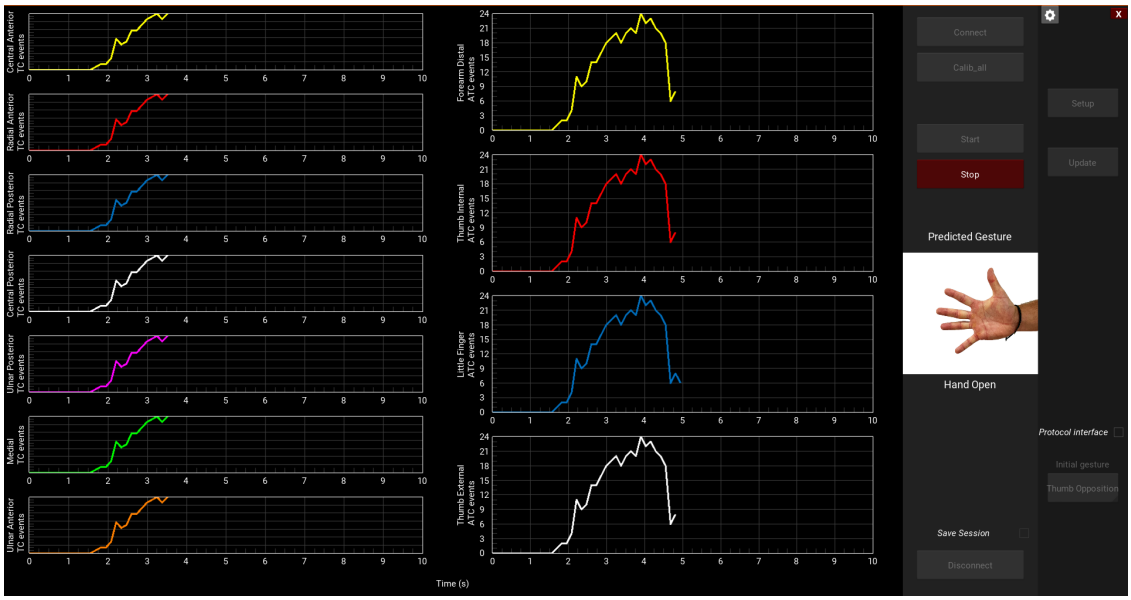

Figure 5.3: Graphical user interface (GUI) during use for performing the acquisition protocol

5.2 Experimental Protocol

After defining the positioning of the acquisition electrodes and the devices utilized, it was necessary to determine the movements to be replicated by the subjects during the acquisition protocol. For this selection, were chosen movements suitable for rehabilitation and capable of inducing selective control over individual fingers [49] [50]. The chosen movements are depicted in the following Figure 5.4.

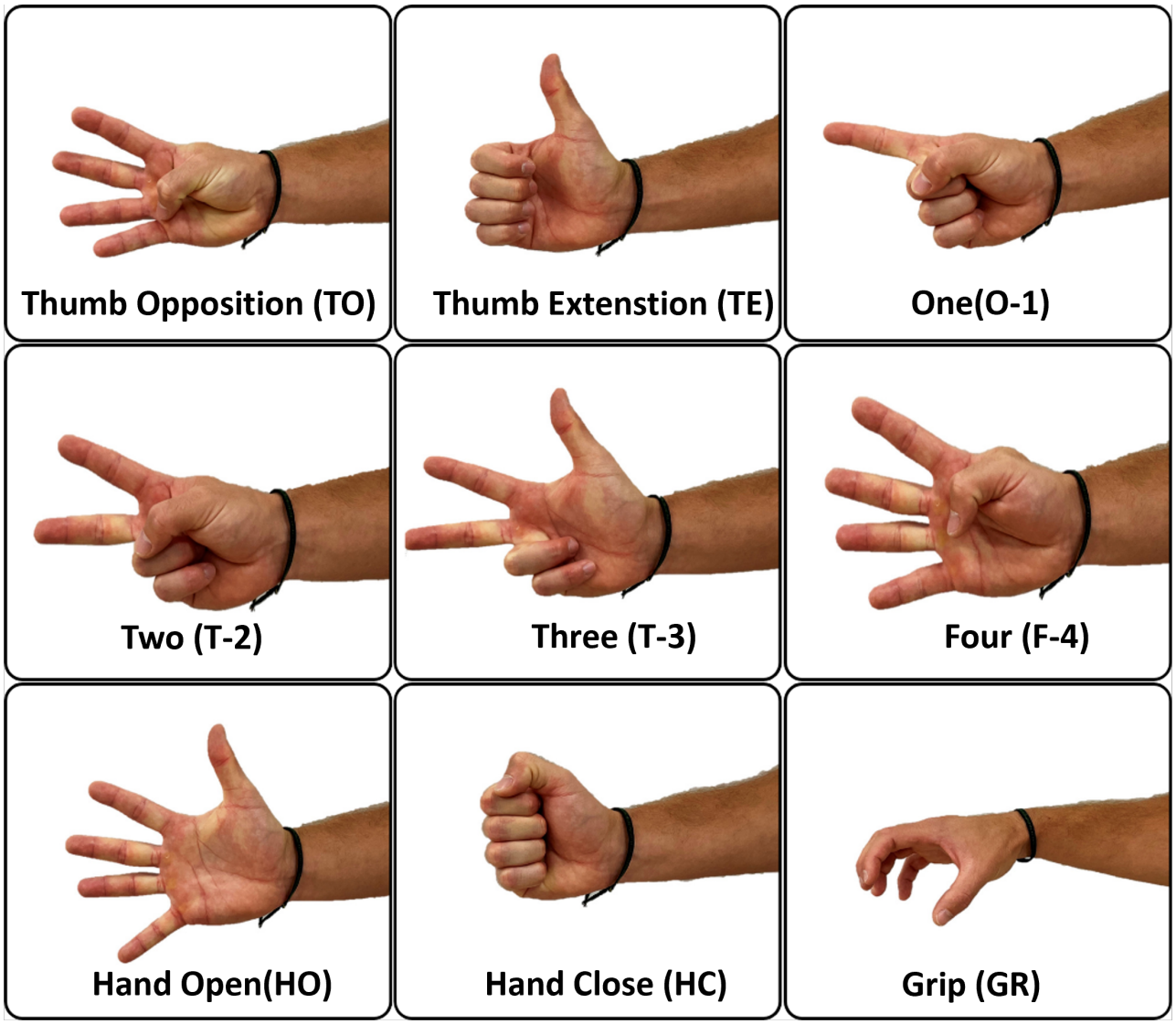

Figure 5.4: Selected Movements. *Thumb Opposition, Thumb Extension, One, Two, Three, Four, Hand Open, Hand Close, Grip*

The procedure for preparing the subjects for the acquisitions has been divided into several phases. Initially, the correct positioning of the armband was carried out, which, in addition to considering the distance on the longitudinal axis, must ensure a correspondence between the channels and the muscles involved in the acquisition. Therefore, this phase is divided into two steps:

- Measurement of the palmar forearm, particularly the junction axis between the elbow and wrist. Identification of the point at approximately one-third of the total calculated distance, starting from the elbow. This serves as the reference for positioning along the longitudinal axis.

- To ensure correspondence between channels and acquired muscles, it was chosen to maximize activation of the finger flexors on CH 1 and extensors on CH 4. Therefore, the placement of the 'Flexor Digitorum Superficialis' muscle on the forearm was identified, through palpation and visual analysis of activated muscle fibers with a specific movement. For this measurement, the actual positioning of the acquisitions was reproduced to avoid issues due to relative displacement between electrode and muscle fiber.

Based on the explained measurements, the preliminary positioning of the armband was carried out.

Subsequently, pairs of electrodes were placed for the acquisition of signals from the intrinsic muscles (CH8 - CH9 - CH10 in Figure 4.5), using a latex glove to ensure electrode adherence throughout the protocol duration. Holes were made in the glove corresponding to the electrodes to allow cable connection, and reference electrodes were positioned on the palmar side of the wrist.

Finally, the integrated Apollux for CH11 in Figure 4.5 was placed on the distal forearm. Once the electrode positioning phase was completed, the cables were connected, and the acquisition system was ready for use. Throughout the procedure, proper positioning of the hand-forearm district was maintained, with the forearm horizontally positioned and the hand in a neutral position, supported to maximize the range of motion and allow relaxation during rest phases. Additionally, the elbow was slightly elevated to maintain the armband in place.

Once the positioning for ATC signal acquisition is completed, the devices are connected to the control unit and undergo an initial calibration, keeping all gains at a unity value. Next, by starting the ATC signal acquisitions and verifying the activations on the GUI, the second step of verifying the correct positioning of the armband takes place. The subject is then asked to perform finger flexion and extension movements, making sure that the maximum activation occurs on CH1 and CH4 channels, respectively. In this regard, the armband can be rotated slightly until the desired result is achieved.

At this point, all the necessary operations for conducting the acquisitions correctly have been completed, and the subject can undergo the general test. This latter consists of executing the nine movements depicted in Figure 5.4. Each movement is performed for 3 consecutive repetitions and must be maintained for a total time of 5 seconds. There are also 5 seconds of rest between repetitions of the same movement, while the rest period at the change of movement lasts ten seconds. During the rest phase, the subject must completely relax the hand, maintaining the ATC profile on the baseline.

All subjects underwent a trial acquisition to become familiar with the procedure

and movements, considering the difficulties in properly relaxing the hand and adhering to the timing of movement execution precisely. Additionally, the trial was used to adjust the gains of the devices, if necessary.

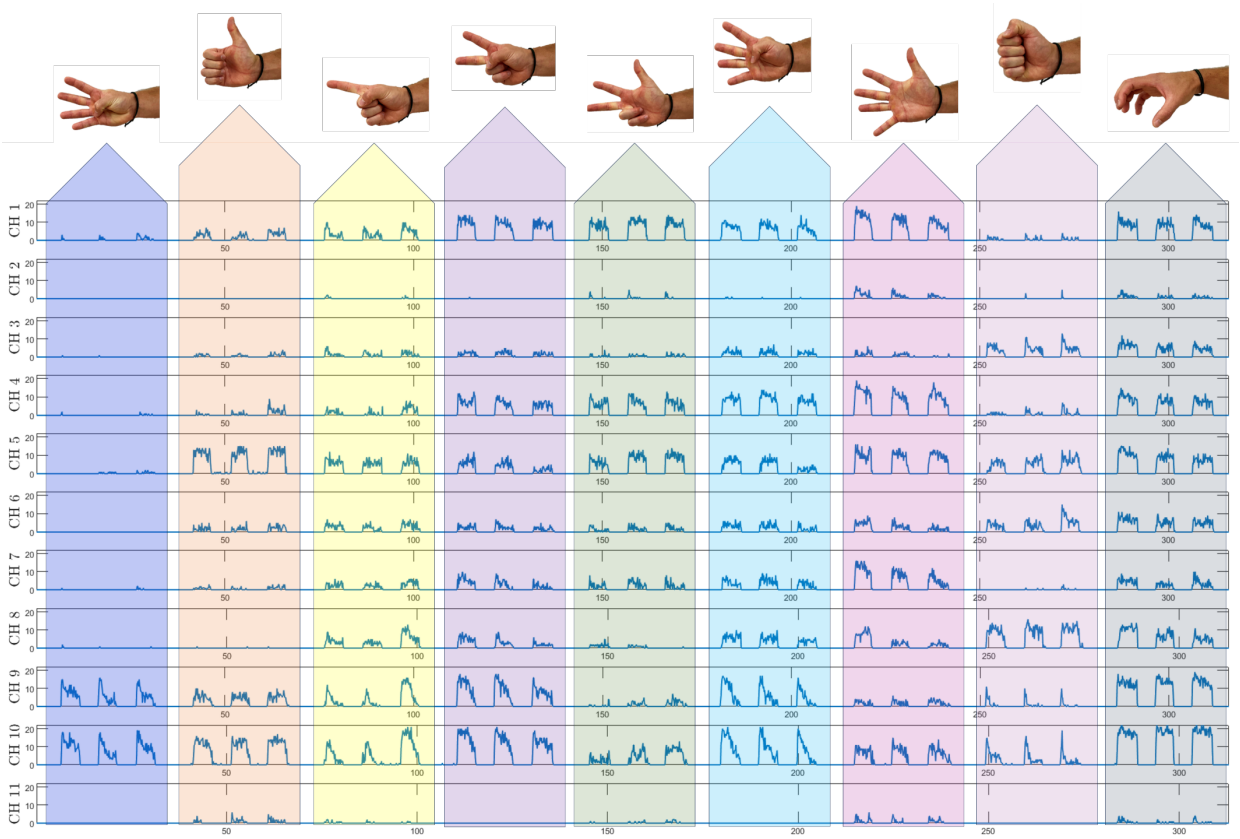

Figure 5.5: ATC profiles obtained from the acquisition system with the execution of the protocol.

Chapter 6

Machine Learning and Neural Network

The main advantage brought by the classifier concerns the overall control of the electrical stimulator. Indeed, this allows inducing an impulse in the patient only after verifying that the input ATC data into the control unit are related to the execution, by the therapist, of a movement for rehabilitative purposes.

Furthermore, the class predicted by the classifier can be integrated into the processing of incoming ATC data in the control unit, adding a stimulation control factor to it.

In the original FES system, the control unit modulates the stimulation parameters that are transmitted to the stimulator. The presence of a one-to-one correspondence between acquisition and stimulation channels implies that stimulation is induced at the channels that have recorded muscle activation.

Using the classifier is possible to detect motion information and, based on this, select the muscles to be stimulated. This will ensure the maintenance of the stimulation pattern defined by the control unit. Therefore, the decision was made to integrate a classifier capable of distinguishing the nine movements performed during the protocol and the idle state.

It is important to emphasize that the neural networks were trained using only the ATC values as the sole feature. This enabled real-time classification leveraging the ATC data transmitted to the control unit every 130 ms. To evaluate the performance of the models, the index associated with each sample during acquisition, identifying the movement performed, was used. This allowed assigning a corresponding class of membership to each ATC sample, using the same samples to segment the signals based on the associated movement.

This chapter initially examines the preliminary analyses conducted on the acquired signals to assess the suitability of a machine learning-based approach. Subsequently, the databases used for training the models and the methodologies employed to optimize the neural networks will be described.

6.1 Preliminary Analysis

This section will describe the preliminary analysis conducted, using MATLAB®, to assess the feasibility of applying machine learning methods to the acquired signals for classifier development. For preliminary analysis, two main aspects were considered:

1. Variability of muscle activation across different channels during the performed movements.
2. The repeatability of executing repetitions within the same movement.

6.1.1 Variability of muscle activation across different channels

To compute the first information, the starting point is the ATC profile from the acquisitions, organized to obtain a dataset containing the ATC values associated with each channel and the reference index called *Class*. The latter is saved by the software during its operation and allows each ATC sample to be associated with the corresponding motion.

Next, the labeling of the dataset is adjusted based on the norm parameter, which is associated with each sampling instant. This parameter allows to evaluate the muscle activation that occurred on the overall acquisition system, computed on the ATC value group belonging to the same instant. The Equation 6.1 shows the expression used to calculate *NormValue*, where Ch_{x} is the X_{th} channel of the acquisition system [44].

$$\mathrm{NormValue} = \sqrt{\sum_{i=1}^{Nchannels} Ch_i^2} \tag{6.1}$$

By applying a threshold to the obtained norm value, the labeling of the dataset can be changed. The overthreshold values are kept with unchanged *Class* values while the remainder are associated with the class that corresponds to the rest status (*Idle*), having a low overall activation value. The approach described is as follows 6.2:

$$\text{Class} = \begin{cases} \text{Actual Class}, & \text{if } NormValue > \text{Th} \\ \text{Idle}, & \text{if } NormValue \leq \text{Th} \end{cases} \tag{6.2}$$

Next, indexes are used to segment signals by movement. The signal segments associated with the same movements are used to extract the *median* and 40_{th} and 60_{th} *percentile* values. These values are represented within a *Radar Plot* Figure 6.1 that combines information from all acquired channels, extracted from the raw signals of each subject. The graph illustrates the spatial distribution of activations for each movement executed during the protocol.

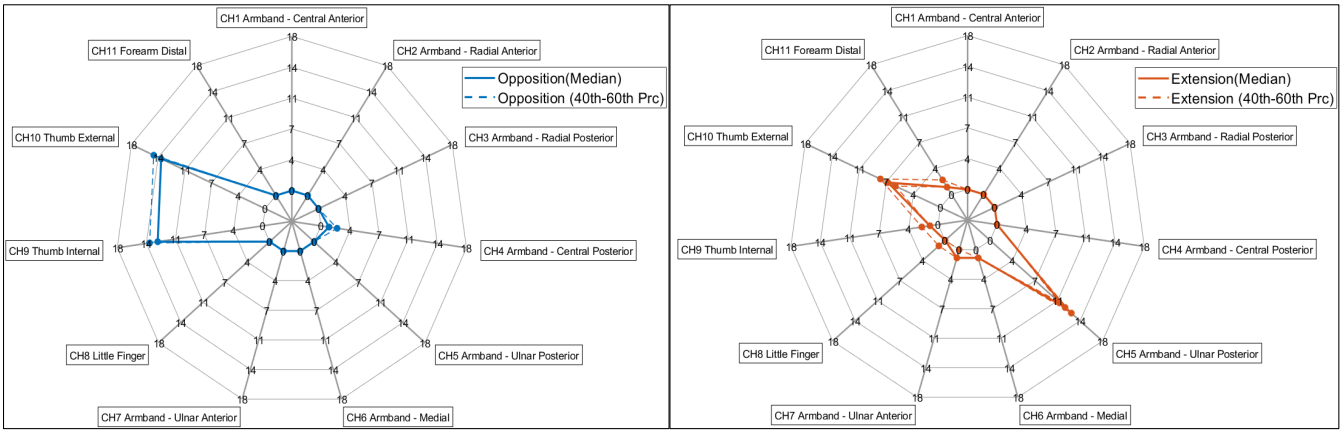

Figure 6.1: Radar-Plot Single-Subject obtained from a dataset with idle norm threshold 7

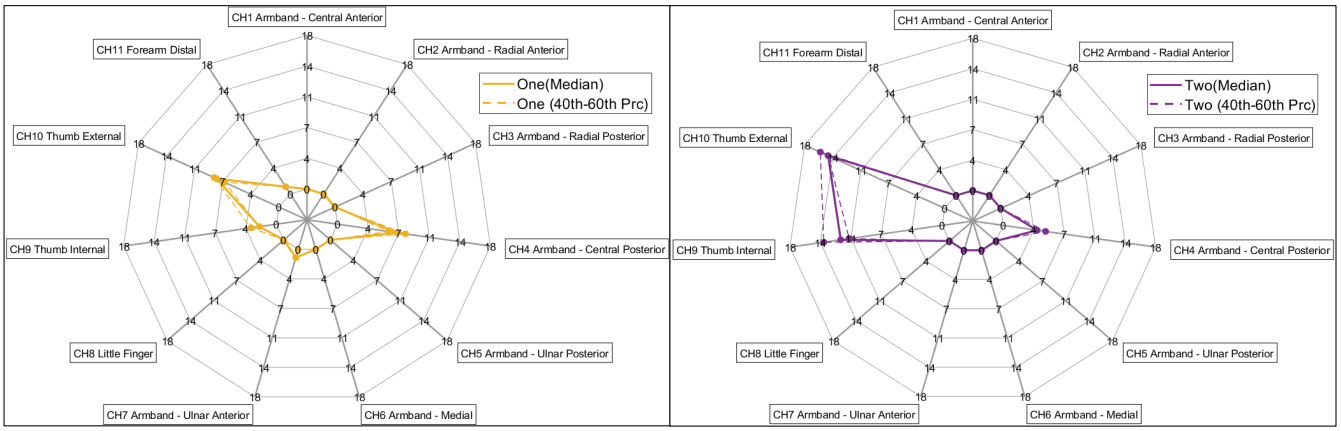

Figure 6.2: Radar-Plot Single-Subject obtained from a dataset with idle norm threshold 7

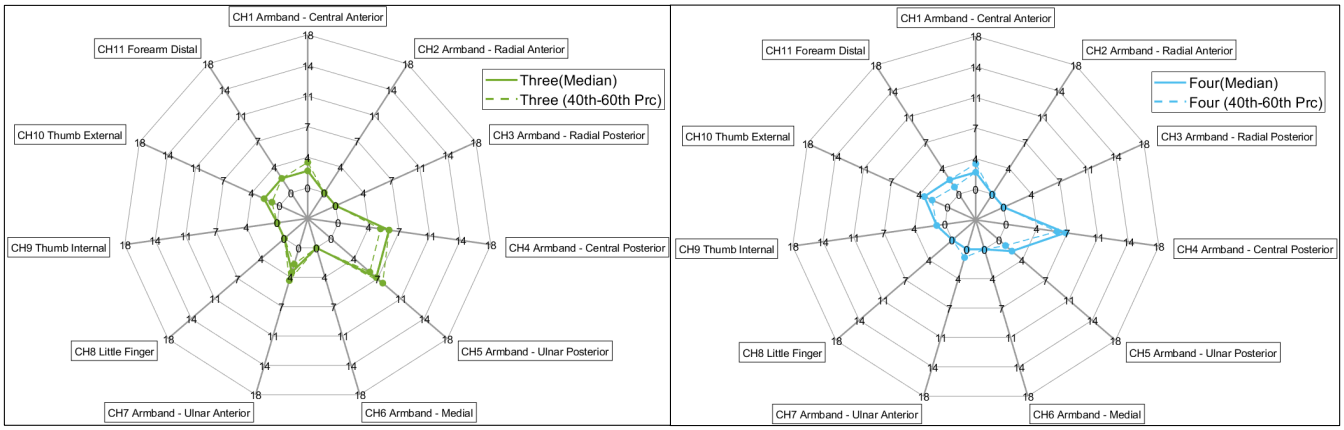

Figure 6.3: Radar-Plot Single-Subject obtained from a dataset with idle norm threshold 7

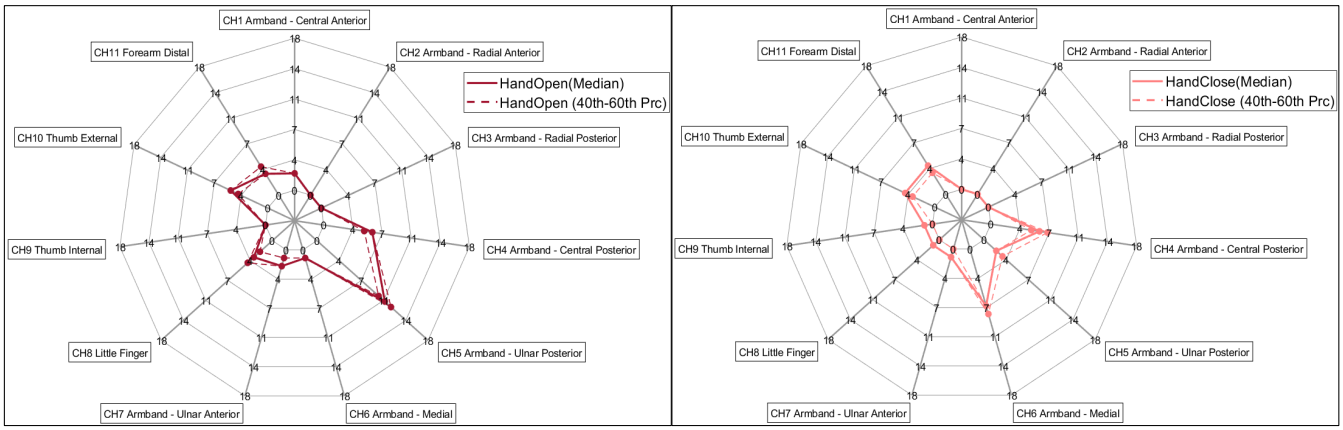

Figure 6.4: Radar-Plot Single-Subject obtained from a dataset with idle norm threshold 7

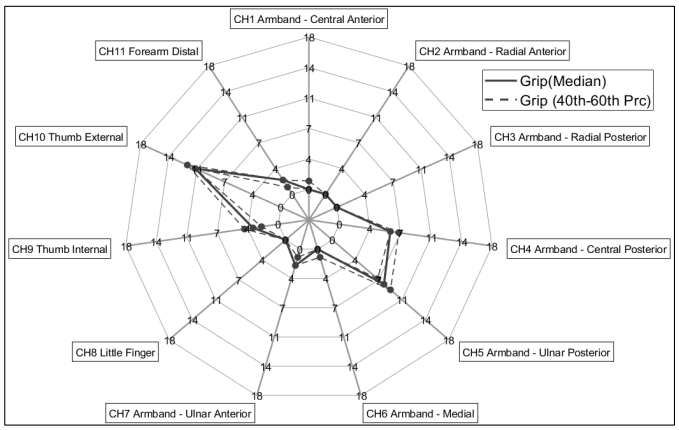

Figure 6.5: Radar-Plot Single-Subject obtained from a dataset with idle norm threshold 7

Through the analysis of the Radar Plot results, it is possible to examine the spatial distribution of muscle activations within the acquisition system. It is crucial to verify any differences in activation profiles among various movements to develop a reliable classifier. This constitutes a fundamental assumption for the classifier, which will rely on the distribution of ATC values across different acquisition channels to accurately predict the executed movement.

The Radar Plot shown in Figure 6.1 displays distinct profiles for each movement overall. Therefore, this can be considered a positive result for the preliminary analysis before implementing the classifier.

6.1.2 Movements Repeatability

The second element of interest for the preliminary analysis concerns the verification of the movement's repeatability belonging to the same movement. To accomplish this, the signals have been processed to obtain measures of similarity following the procedure outlined in [9].

The following steps are executed:

1. Creation of movement matrices referenced to the repetition of a specific movement as shown in Figure 6.6. The procedure for motion segmentation is based on Class values. The obtained signal windows, matrices containing the ATC values extracted from all channels of the acquisition system, are norm-checked to exclude low activation instants.

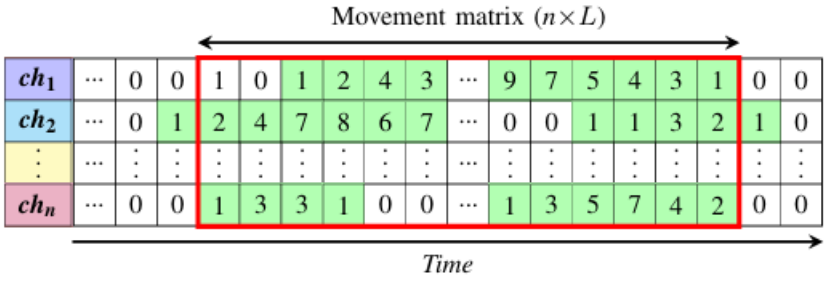

Figure 6.6: The segmentation result for each movement, a *similarity matrix* containing the ATC values of the channels from Ch_1 to Ch_n. Rows highlighted in green represent activations, while the red box denotes the extracted matrix following the initial segmentation with the application of norm value control, excluding phases of low activation [51].

2. Computation of Normalized Channel-wise Cross-correlation (NCC) defined in Equation 6.3 between X and Y, which provides the measure of channel-by-channel similarity as a function of the relative lag (τ) [51].

$$\mathrm{CC}_{xy}[\mathrm{ch},(\tau)] = \frac{\sum_m (X_{ch}[m+\tau]Y_{ch})}{\max\{|X_{ch}|^2, |Y_{ch}|^2\}} \tag{6.3}$$

3. Computing W_{xy} vector, defined in 6.4, quantifies the contribution of each channel to the whole movement with values from 0 to 1 [51].

$$\mathrm{W}_{xy}[\mathrm{ch}] = \frac{\sum_{\kappa}(X_{ch}[ch+\kappa]) + \sum_{m}(Y_{ch}[ch+m])}{\sum_{ch}(\sum_{k}(X_{ch}[ch+\kappa]) + \sum_{m}(Y_{ch}[ch+m]))} \tag{6.4}$$

4. Calculation of the matrix product of the matrices obtained in the previous steps, extraction of the maximum value to obtain the Similarity Index (SI_{xy}) 6.5. This measure represents the overall similarity between two movement matrices (X, Y) and lies within the range of 0 to 1 [51].

$$\mathrm{SI}_{xy} = \max(CC_{xy}^{T} \times W_{xy}) \tag{6.5}$$

The following figures show the results of the similarity values obtained from the comparison of 12 subjects. Each submatrix, sized 9x9, represents the similarity value obtained from comparing individual repetitions (9 for each subject) performed by a pair of subjects. The matrices on the diagonal, which have higher average values, refer to the comparison between repetitions performed by the same subject.

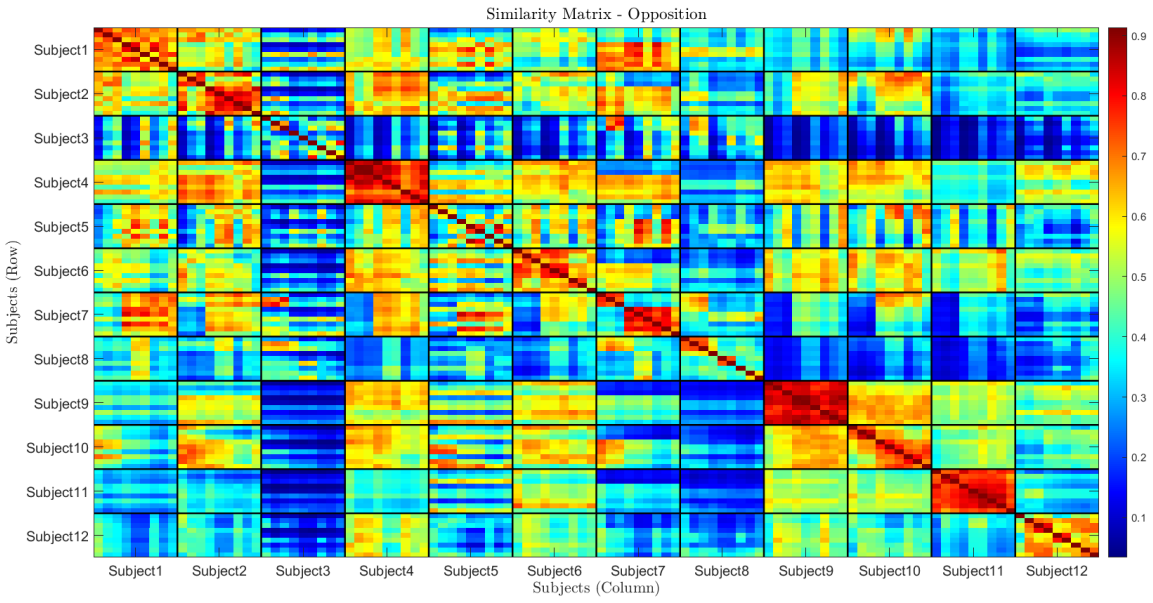

Figure 6.7: *Opposition* movement similarity matrix

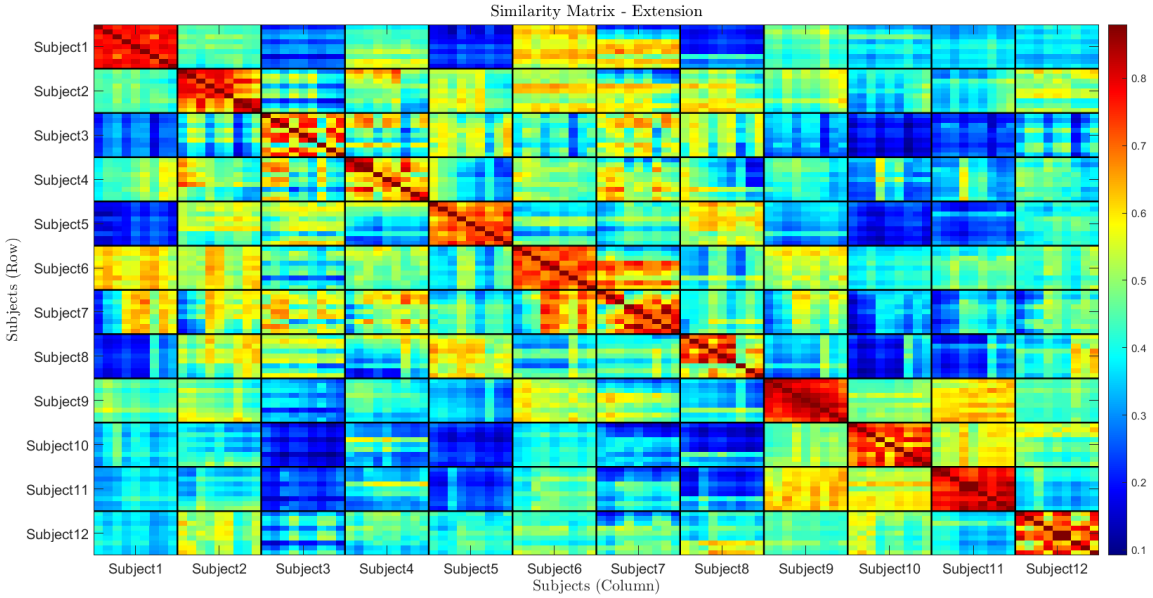

Figure 6.8: *Extension* movement similarity matrix

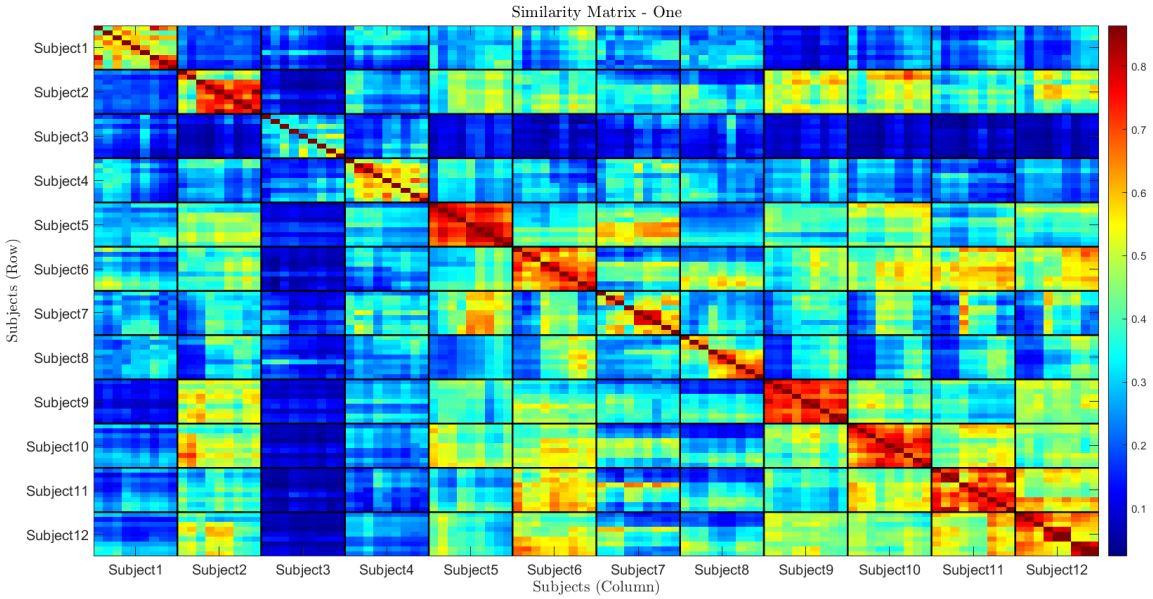

Figure 6.9: *One* movement similarity matrix

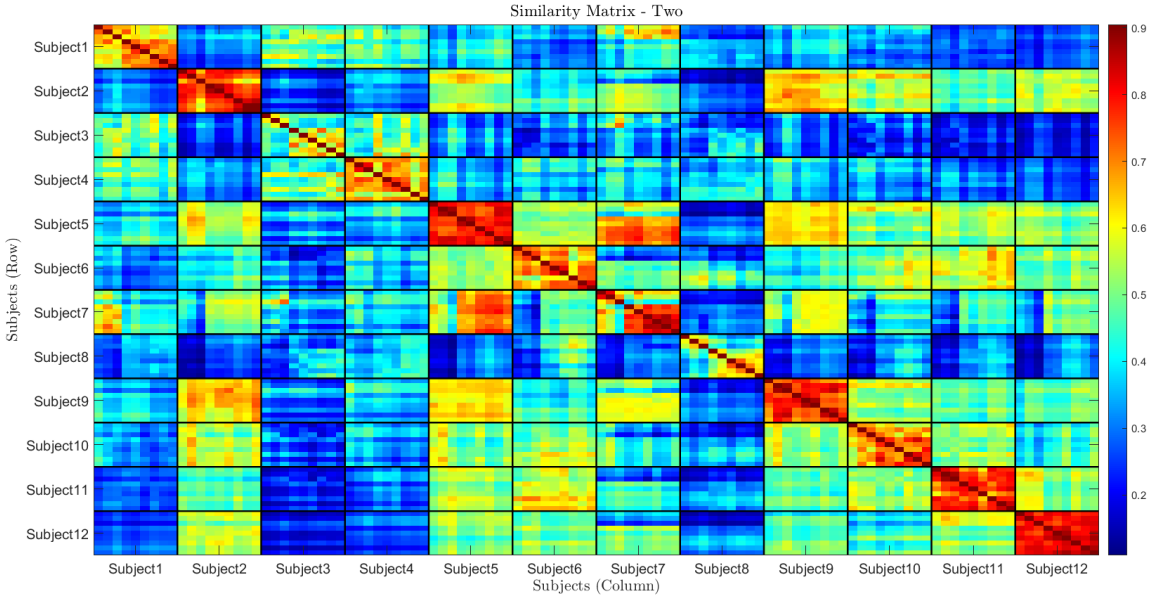

Figure 6.10: *Two* movement similarity matrix

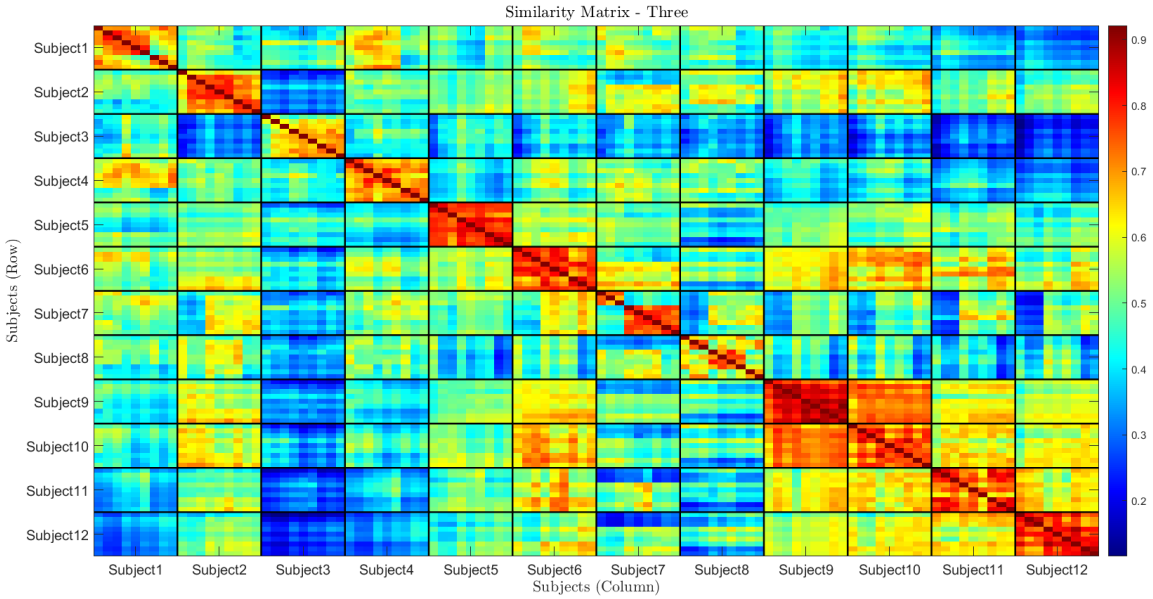

Figure 6.11: *Three* movement similarity matrix

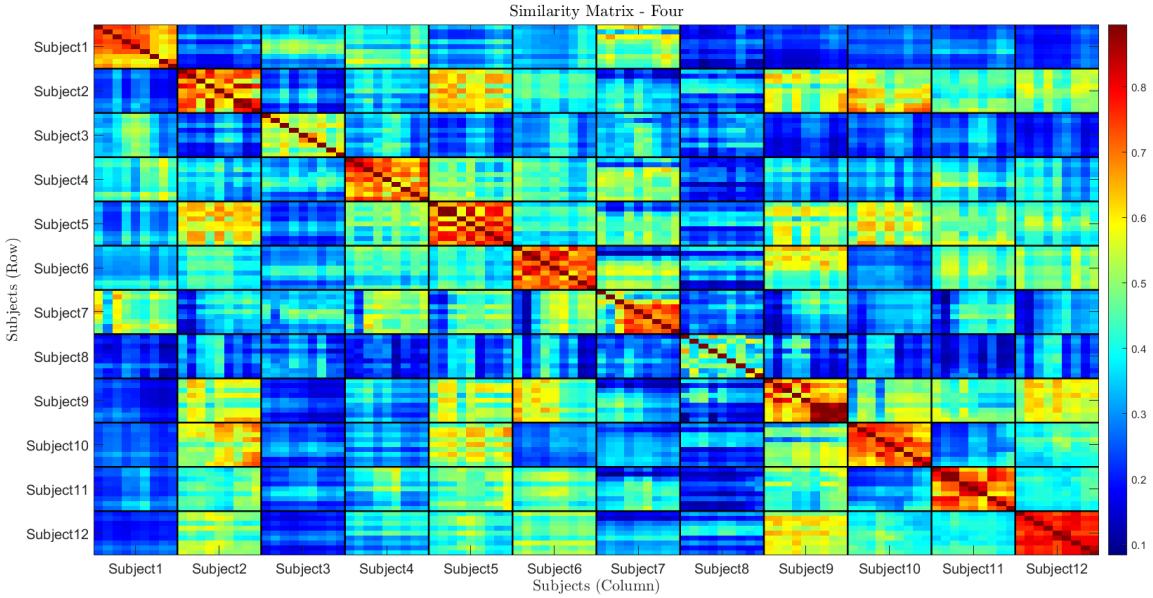

Figure 6.12: *Four* movement similarity matrix

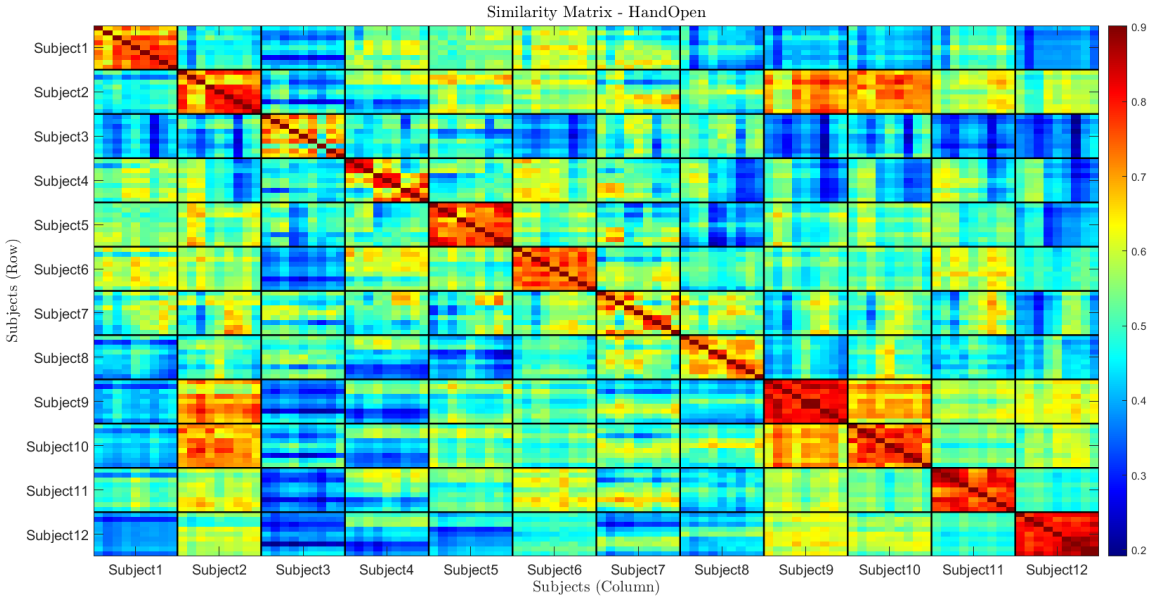

Figure 6.13: *Hand Open* movement similarity matrix

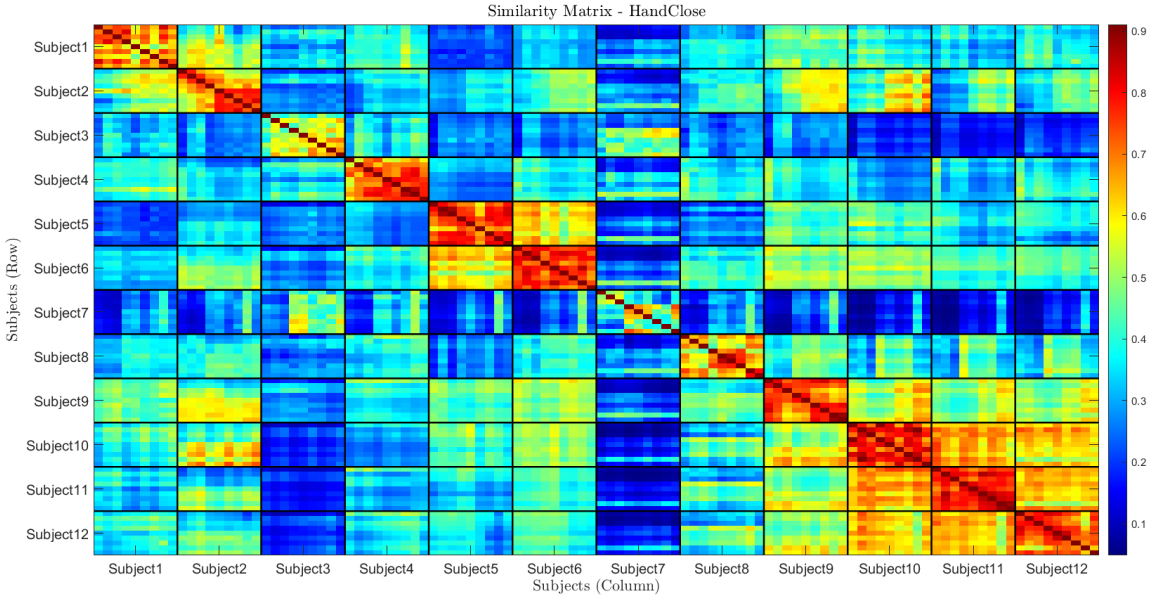

Figure 6.14: *Hand Close* movement similarity matrix

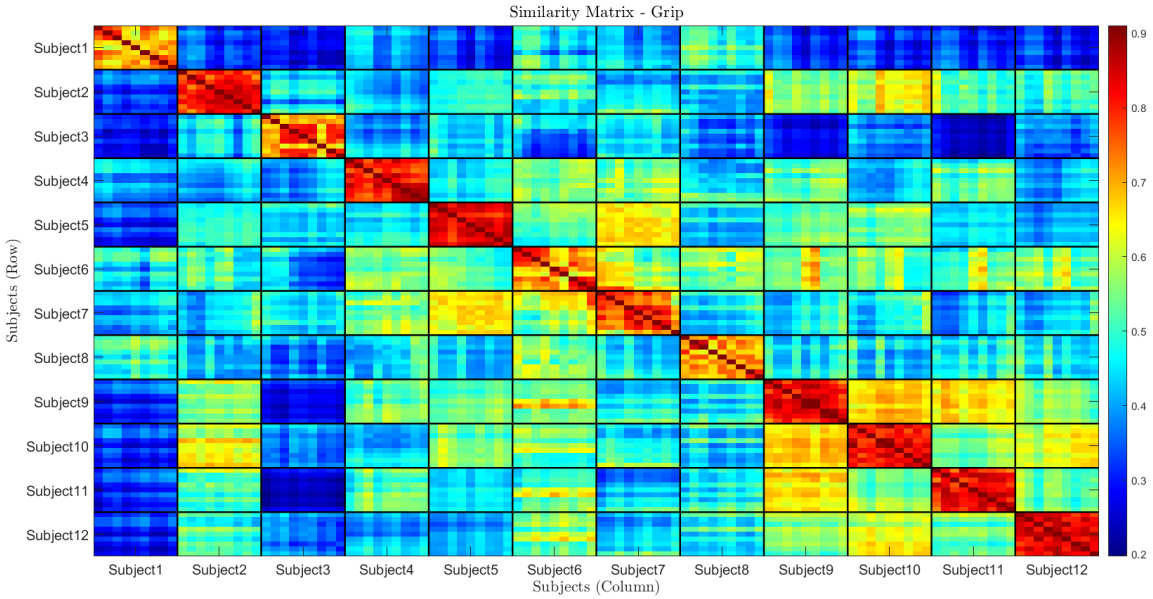

Figure 6.15: *Grip* movement similarity matrix

Referring to the figures provided, a notable inter-subject variability is observed across all movements. However, in some movements e.g. opposition, extension, three, hand open, hand closed, and grip, there are pairs of subjects with similarity values in the sub-matrix that display values ranging between 0.55 and 0.7 in the majority of comparisons.

Based on these observations, it was decided to evaluate whether a classifier could effectively handle the high inter-subject variability, partially leveraging information from subjects with higher similarity. Additionally, it will be significant to examine how the distribution of subjects between the training and test sets impacts the performance of the developed classifier.

Furthermore, regarding intra-subject variability, numerous instances are noted where repetitions executed by individual subjects exhibited high repeatability, with similarity values between 0.65 and 0.85. A comprehensive analysis of such occurrences will be conducted, with an expansion of available data associated with a single individual.

6.2 Database Preparation

During the thesis project, two distinct datasets were created. In the first case, 12 different subjects were involved, while in the second case, all the signals used were derived from the same subject.

Data collection adhered strictly to ethical guidelines, approved by the Bioethics Committee of the University of Turin [52]. Every participant received detailed information regarding the physical safety of the acquisition devices and the anonymization procedures applied to their data. This was done in compliance with the experimental protocol and for the purposes permitted by the study.

In both cases, the procedure for preparing the dataset for the neural network training phase was the same. The acquisition data, saved by the software in text file format, were organized to form a labeled dataset where each group of ATC values, belonging to the same instant, has a Class value associated with the performed movement. Starting from the labeled dataset, two procedures were adopted to vary the dataset type and assess its performance. In the first case, the labeling was modified by applying different thresholds to the norm. In the second case, datasets were created by excluding the contribution of some acquisition channels.

Threshold-based labeling applied to the norm

The labeling was modified, as previously explained, by applying a threshold to the norm value. This operation was performed for threshold values of 1, 3, 5, 7, 9,

and 11, resulting in 6 datasets, varied only by the threshold value applied during labeling 6.2.

This allows for classification to be performed on an optimized dataset, finding the threshold value that best fits the classification.

By varying the threshold value applied to the norm, an imbalance in the classes is observed in the resulting datasets. An increase in the threshold value leads to a greater number of ATC values associated with the *Idle Class* during labeling. Therefore, to maximize classifier performance, class balancing was implemented during dataset preparation [53].

As the threshold value increases, the subject must also increase the intensity of the contraction to maintain the presence of the movement within the dataset and prevent all samples associated with the movement from being classified as idle. This condition creates a too high dependence on the force generated by the subjects. Therefore, threshold values higher than those listed above were not tested.

Dataset reduction: Channel subset generation

Datasets containing a subset of available acquisition channels were created. This approach was adopted to precisely evaluate the actual contribution of each channel in the classification task.

The objective of the project is to achieve accurate classification while minimizing the number of input channels. Since wearability [54] is a key element in the development of the overall system for FES control.

Channels with the following characteristics were excluded:

- High variability in activations. Assessment of variability was initially observed during subject acquisitions by visually checking activations and considering inter-subject differences. In addition, a more analytical analysis was conducted by examining the percentile values represented in the radar plot 6.1. From this analysis, the decision was made to exclude the device placed on the little finger (CH9). Indeed, the activations recorded by this acquisition unit show significant variability in several movements, e.g. four, hand open, hand close and grip. In addition, removing this device could improve the overall wearability of the acquisition system.

- Low activation values were observed across all movements. For this assessment, the radar plot was also utilized, leading to the decision to exclude the device positioned on the thumb internal (CH8). In this case, limited activation was recorded across multiple movements.

In this way, the following datasets were obtained:

1. Dataset All Channel: All Channel used.

2. Dataset Little Finger Out: Channel of the little finger excluded.
3. Dataset Thumb Internal Out: Channel of the thumb internal excluded.
4. Dataset Thumb Internal and Little Finger Out: Both previous channels excluded.

Through this process, a set of datasets was obtained, each of which was adapted to specific criteria, enabling in-depth analysis and optimization for the classification task under study.

6.2.1 Multi Subject Dataset

For the construction of the dataset, 12 subjects, all aged between 24 and 27 years old, were involved. Each subject completed three full sessions of data collection, resulting in a total of nine repetitions for each movement. This approach facilitated gathering a diverse range of data from multiple sources, ensuring a comprehensive representation of muscle activation.

The next step is to apply this dataset configuration by varying the distribution of subjects in the training and testing phases. Considering the large number of possible solutions, five distributions were randomly evaluated.

6.2.2 Single Subject Dataset

Conversely, the second dataset was assembled solely from acquisitions of a single subject. This dataset configuration was designed with future application of the developed device in mind within the thesis project. As the system is intended for therapist-patient interaction, with classification applied to signals exclusively from the same individual, this specific dataset setup was adopted.

However, despite this focus on a single subject, it is imperative to consider the classification problem from a broader perspective. Potential future developments may necessitate extending the analysis to multiple subjects. Such an approach would enable the exploration of challenges and opportunities in classification across a broader population, facilitating more generalizable conclusions and preparation for potential future scenarios [**art26**].

6.3 Offline Training and Network Optimization

The training phase of the machine learning model, utilizing the various datasets obtained, was conducted within the MATLAB® environment.

To optimize the efficiency of the Artificial Neural Network (ANN), the Deep Learning™ Toolbox was used, allowing for precise customization of the network

structure and training parameters. A 5-fold cross-validation [55] strategy was adopted, where the dataset is divided into five equal parts. Each part is alternately used as a test set, while the remaining four are used for training. This process is repeated for all possible combinations of dataset parts, ensuring a comprehensive evaluation of the model's performance on different data.

This methodology helps to reduce the risk of overfitting [56] and provides a more accurate assessment of the model's performance. The chosen gradient optimizer is the Adam algorithm, with an initial learning rate set to 0.03, which automatically decreases every 10 epochs to enhance training accuracy. Additionally, a patience parameter of 5 was set, which interrupts the training process if the validation error remains stagnant for 5 consecutive samples, optimizing the overall efficiency of the procedure.

Subsequently, a training phase was initiated to evaluate various network architectures to optimize performance. During this process, various network configurations were examined, varying the number of hidden layers from 2 to 4 and the number of neurons in each layer from 10 to 150. These different configurations were applied to all datasets, each characterized by different normalization values of the idle state, to also perform optimization of this parameter.

In the next paragraphs, the results obtained from the training and optimization phase of the network architecture will be reported.

To maximize the performance of the classifier, according to the accuracy value, the following parameters should be selected:

- Optimal value used as threshold for rest condition in the dataset (*Idle Norm*).
- Hidden layer size.
- Number of neurons within the hidden layers

Two types of graphs are used to determine the listed parameters:

1. The first figure (Figure 6.16 and 6.19) illustrates the various ANN architectures, characterized by variations in the number of hidden layers and the number of neurons within each layer. The graph relates the accuracy achieved from each network, trained using datasets varying in terms of the threshold used to normalize the "idle" state in the dataset. Linear interpolation of the trend curves is performed, focusing on central idle values, to identify a potential plateau. This graph enables us to determine the most suitable idle-norm value for the dataset to enhance classification performance.
2. The second figure (Figure 6.16 and 6.18) presents the accuracy values obtained from three distinct neural models, each with a different number of hidden

layers. These models have been trained with a specific idle-norm value selected based on the first graph. This graph allows us to evaluate which number of neurons within the hidden layers maximizes classification performance.

This procedure was applied to all types of datasets, varying by idle-norm value and selected channels.

6.3.1 Network Optimization Multi-Subject Dataset

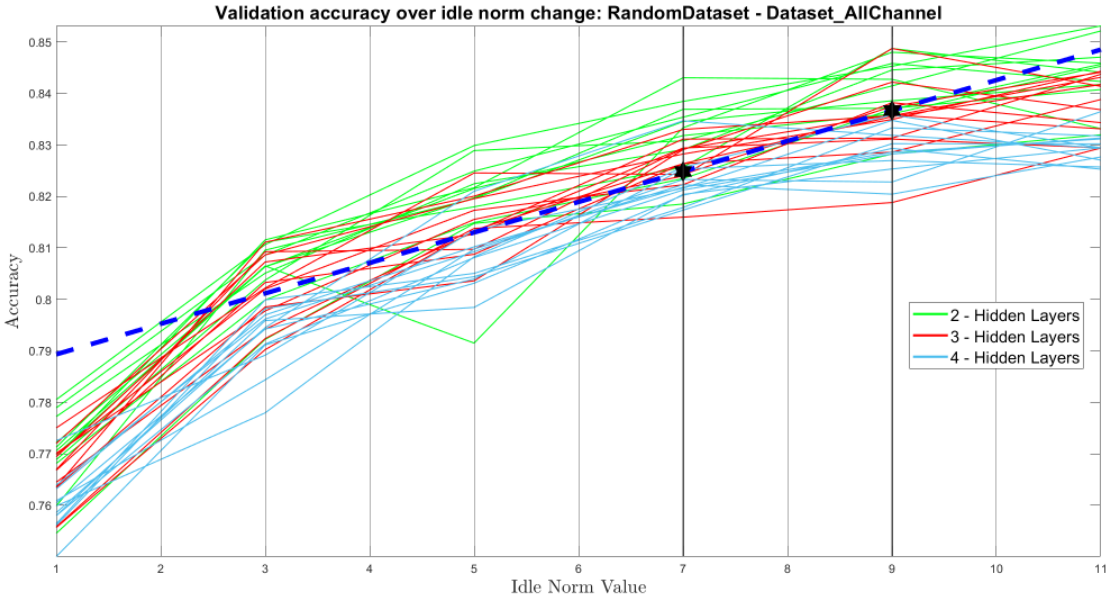

Figure 6.16: ANN validation accuracy of all configurations trained. Each line represents a single network structure, which is trained with an input dataset ranging from idle norm 1 up to 11

From the observation of Figure 6.16, it emerges that *idle norm* values between 7 and 9 are the most effective for classifying movements using this dataset. Higher values tend to deviate from the increasing trend of linear interpolation. Additionally, models with two hidden layers generally exhibit higher accuracy values. Based on these observations and the identification of optimal idle-norm values, further examination of the remaining parameters is conducted to select the optimized model.

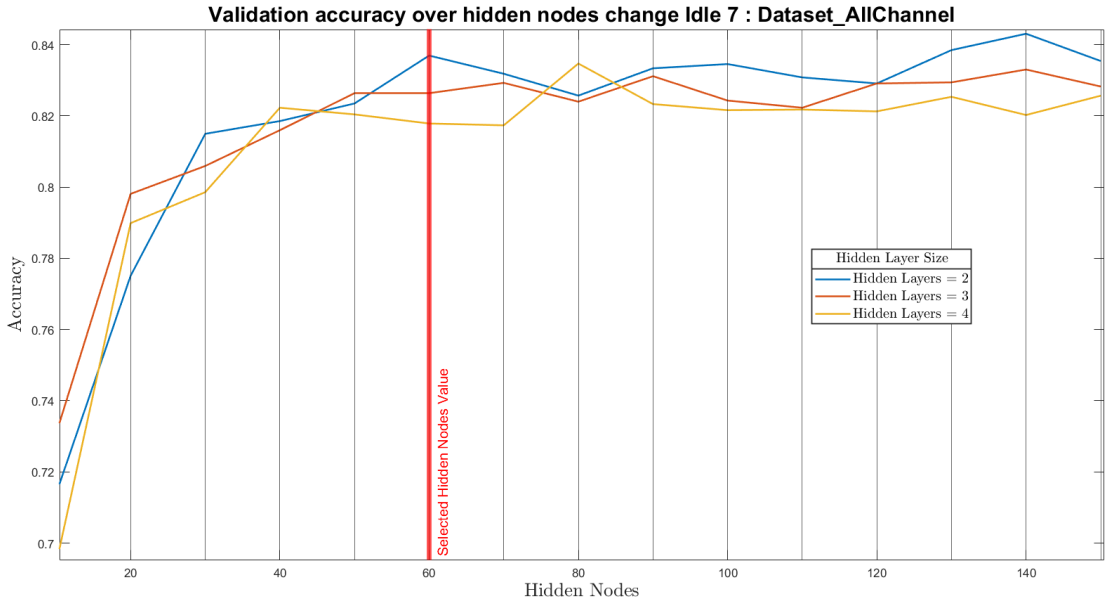

Figure 6.17: ANN validation accuracy for a defined idle norm (i.e., 7). The performance behavior is highlighted at varying the network configuration.

This graph confirms that having two hidden layers is the best choice for the network architecture. Furthermore, it facilitates the identification of the optimal number of neurons used, which corresponds to the vertical red line in the figure. The choice of neuron numbers should be based on the concept of balancing model complexity and generalization ability, which is fundamental in the field of machine learning and neural networks [57]. Model complexity refers to its ability to fit the training data, while generalization ability refers to its ability to make accurate predictions on data not seen during training.

6.3.2 Network Optimization Single Subject Dataset

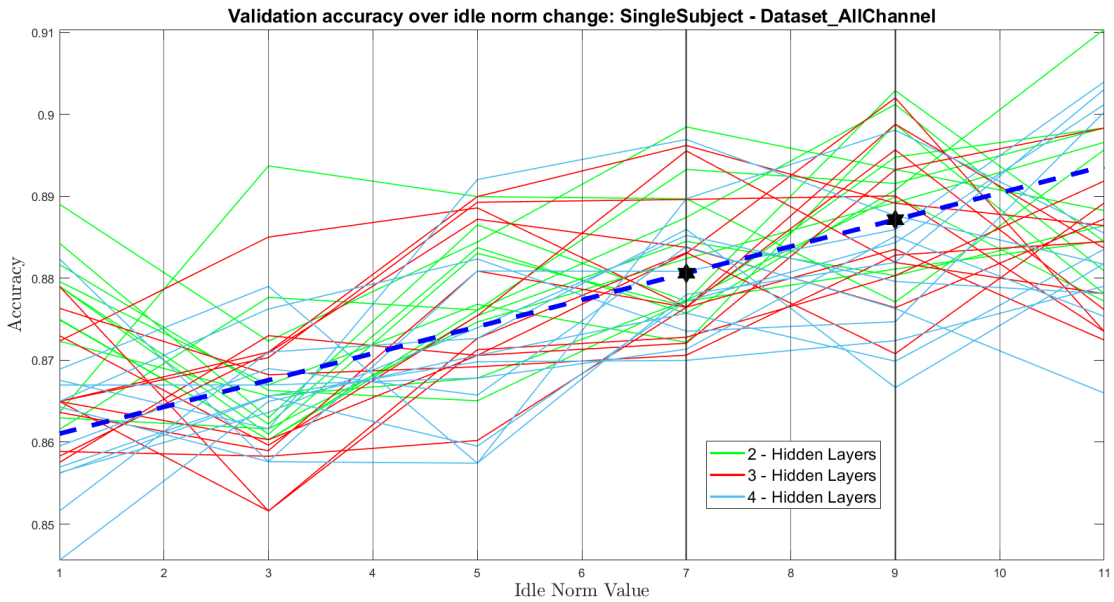

Figure 6.18: ANN validation accuracy of all configurations trained. Each line represents a single network structure, which is trained with an input dataset ranging from idle norm 1 up to 11

In the figure, a less pronounced division is observed, compared to the multi-subject case, based on the number of hidden layers that define the network architecture. In this case, as well, the values for the idle state limits that best fit the characteristics of the dataset are 7 and 9, just like in the previous Figure 6.16.

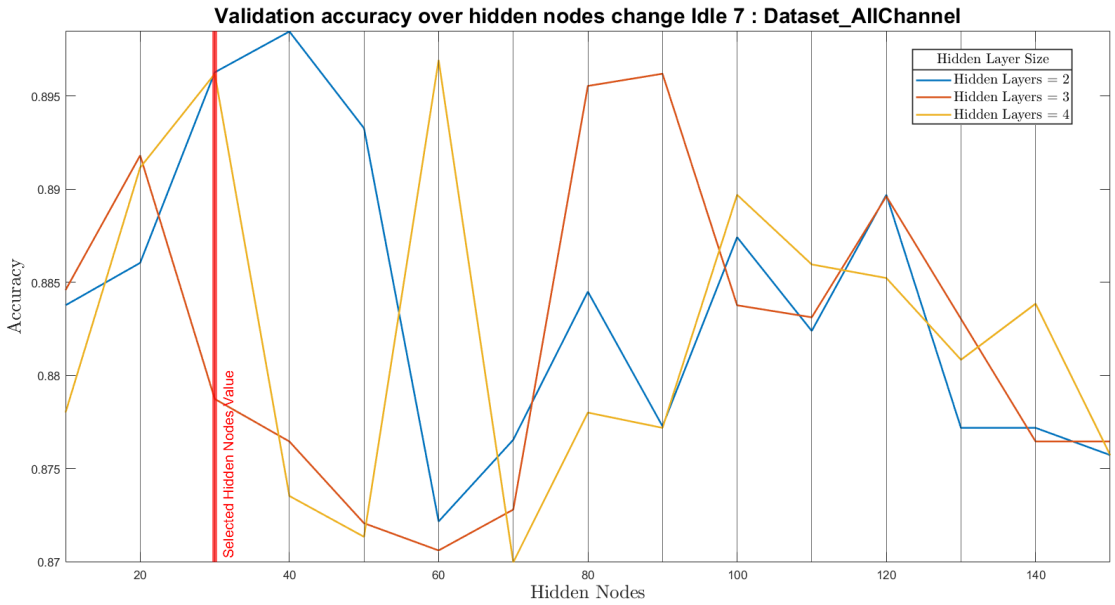

Figure 6.19: ANN validation accuracy for a defined idle norm (i.e., 7). The performance behavior is highlighted at varying the network configuration.

The irregular trend in accuracy values shown in Figure 6.19 could be attributed to overfitting, which increases as the number of neurons in the hidden layers increases [42]. The graph displays that maximum accuracy values are achieved with a lower number of neurons in the hidden layers, compared to the multi-subject dataset.

This trend implies an overfitting problem, in which the neural network may excessively adjust its parameters to the training data, thereby compromising its generalization ability. This tendency to overfitting is justified by considering the characteristics of the dataset. The latter includes signals from the same subject, thus exhibiting reduced variability. Therefore, it is plausible that a less complex structure is sufficient to achieve good performance, as shown by the results.

Network Optimization		
	Single-Subject Dataset	Multi-Subjects Dataset
Hidden Layers Size	2-4	2
Hidden Layers Nodes	20-30	60-80
Idle-Norm Value	7-9	7-9

Table 6.1: The table shows the values identified, with the previously described analysis, which will be used in the testing phase.

Chapter 7

Results and Discussion

This chapter presents the results obtained from classifying movements in offline and online modes. During the testing phase, in both modalities, the acquisition protocol described in Section 5.2 was followed, using the acquisition system previously described in Chapter 4.

For the execution of the offline test, the optimized models based on the procedure described in Section 6.3 were used. The classifier results (*Pred Class*) were compared with the movement indices (*True Class*), which constitute the labeling of the databases and were assigned to each ATC value by the software during the acquisitions.

The classification performance was evaluated considering four parameters:

- **Accuracy (ACC)**: Measures the ratio of correctly predicted instances to the total number of instances.

$$\text{Accuracy} = \frac{\text{Number of correct predictions}}{\text{Total number of predictions}} \tag{7.1}$$

- **Precision**: Measures the ratio of correctly predicted positive observations to the total predicted positive observations.

$$\text{Precision} = \frac{\text{True Positives}}{\text{True Positives} + \text{False Positives}} \tag{7.2}$$

- **Recall**: Measures the ratio of correctly predicted positive observations to the all observations in actual class.

$$\text{Recall} = \frac{\text{True Positives}}{\text{True Positives} + \text{False Negatives}} \tag{7.3}$$

- **F1-score**: Harmonic mean of precision and recall, providing a balance between the two metrics.

$$\text{F1-score} = \frac{2 \times \text{Precision} \times \text{Recall}}{\text{Precision} + \text{Recall}} \tag{7.4}$$

The online tests were conducted following the implementation of the classifier with the best performance in the software. To evaluate the classification, a visual approach was used, comparing in real-time the classification result, which appears as an image within the graphical interface, with the movement performed by the subject.

7.1 Multi Subjects

This section of the results is dedicated to the analysis of the performance obtained considering the datasets composed of the 12 subjects involved. In this case, four types of datasets were used, varying the number of selected channels. Each of them was trained and tested by varying the distribution of subjects between the training and test sets, with five random distributions.

The first part explains the selection of the best dataset in terms of subject distribution and channels used. The second part, on the other hand, reports the performance obtained by the best model.

7.1.1 Database Reduction and Subjects Distribution

The classification of hand movements using the dataset consisting of 12 subjects was conducted by randomly varying the distribution of subjects between the training and test sets, maintaining a ratio of 9 and 3 subjects, respectively. The following table 7.1 summarizes the five distributions applied for the creation of the test sets. The complementary subjects to those included in the table were included in the training set of the respective models.

Random Subjects Distribution	
Testset - 1	Subject 9 - 10 - 11
Testset - 2	Subject 1 - 8 - 12
Testset - 3	Subject 2 - 3 - 12
Testset - 4	Subject 3 - 7 - 8
Testset - 5	Subject 1 - 2 - 9

Table 7.1: The table displays the distribution of subjects, obtained randomly, within the test set.

Furthermore, datasets were created using subsets of channels compared to those available using the full version of the acquisition system. This was done to assess the actual improvement in performance brought about by the use of specific acquisition devices. Four types of datasets were therefore obtained, applying variations in the number of channels used, the versions used are as follows:

- Type I: Testset *All Channel*:

- Type II: Testset *Little Finger Out*
- Type III: Testset *Thumb Internal Out*
- Type IV: Testset *Little Finger & Thumb Internal Out*

These two modes of dataset manipulation have been previously described in Section 6.2.

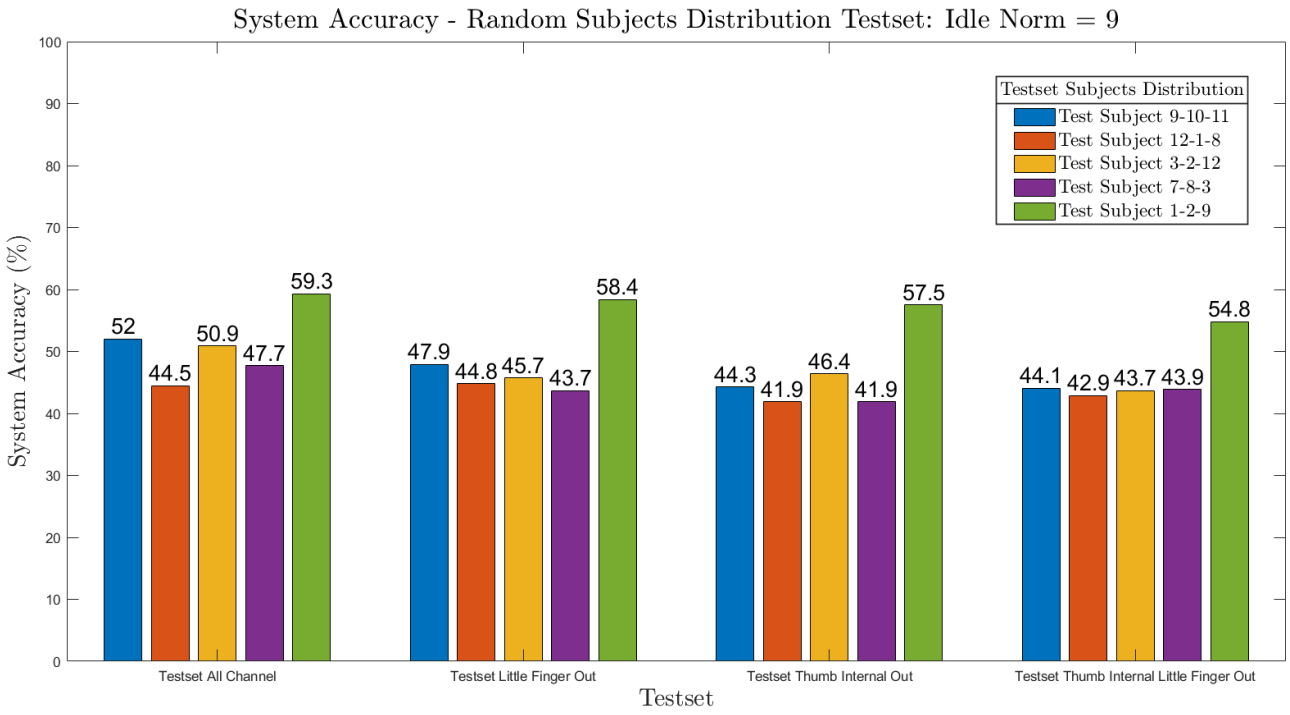

Figure 7.1: The histogram represents the average accuracy value obtained from the best models, trained for each type of dataset. Test sets differ in the distribution of subjects and acquisition channels used.

Analyzing the best performances obtained, with the distribution of subjects that optimizes the classifier's capabilities, comparable results are observed from the first three types of datasets. The accuracy value, considering the all system, reaches 59.3%, 58.4%, and 57.5% respectively. However, excluding two devices, the classifier fails to maintain the level of previous cases and its performance slightly decreases to 54.8%.

Considering the results related to the same dataset type, a strong variability is observed due to the distribution of subjects used. Therefore, an investigation has been initiated to understand the cause of this difference and identify justifications within the dataset and the signals acquired from individual subjects.

To this end, datasets containing the maximum number of channels, which achieve the best performance, were considered. Among these, two random subject distribution scenarios characterized by significant differences in terms of overall accuracy and selected subjects were chosen. Consequently, datasets with distributions 4 and 5, represented respectively in violet and green in the figure, were examined.

The analysis's starting point was observing the confusion matrix to identify potential divergences in the recognition of specific movements.Figure 7.2 and Figure 7.3 report confusion matrices of subjects distribution 5 and 4 respectively.

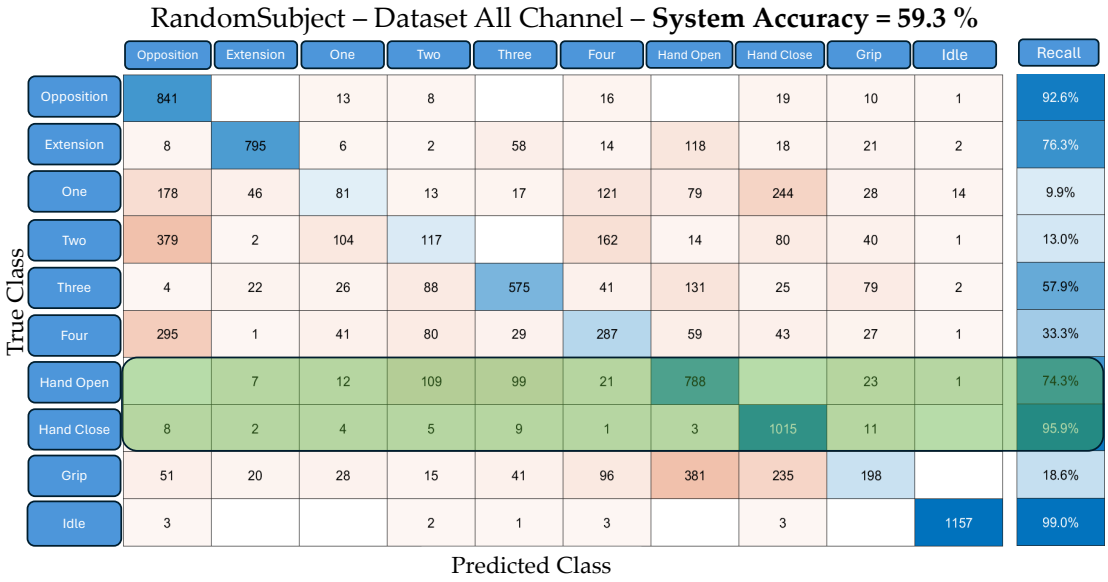

Figure 7.2: Offline test results of classifying 9 movements and the idle state.*Subjects Distribution number 5.*The *hand open* and *hand close* movements are highlighted in the table.

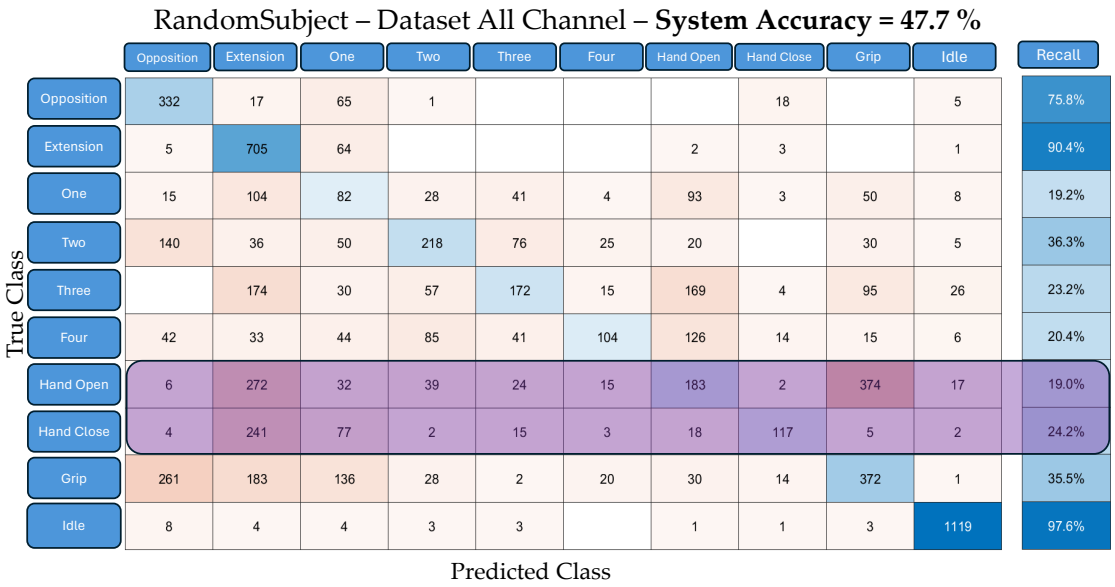

Figure 7.3: Offline test results of classifying 9 movements and the idle state. *Subjects Distribution number 4*.The *hand open* and *hand close* movements are highlighted in the table.

From this initial observation, two movements, *hand open* and *hand closed*, were identified. With the first distribution, these movements are correctly classified in 76.3% and 95.9% of cases respectively (recall percentage values). However, with the second distribution of subjects, these same movements achieve only 19% and 24.2% of correct classifications.

Based on this finding, similarity matrices were analyzed to verify if this type of result was reflected in the similarity values obtained, Figure 6.14, Figure6.13. Therefore, it was checked whether, with the distribution used, there was a correspondence between the train and test sets of at least one pair of subjects with high similarity values (ranging between 0.5 and 0.7). It is observed that the distribution that optimizes performance has this correspondence, while it is lacking in the second case, where for the movements in question, none of the subjects included in the test set share a subject with high similarity in the training set. Therefore, even the analysis of similarity measures confirms the results obtained in the confusion matrix.

To conclude the analysis, the spatial distributions of muscle activations were observed considering the individual subjects of the test set, compared with the average activations obtained from the training set subjects. The following Figure 7.4 and Figure 7.5 show these comparisons applied to the two distributions of the

subjects under examination, distribution 5 and 4 respectively.

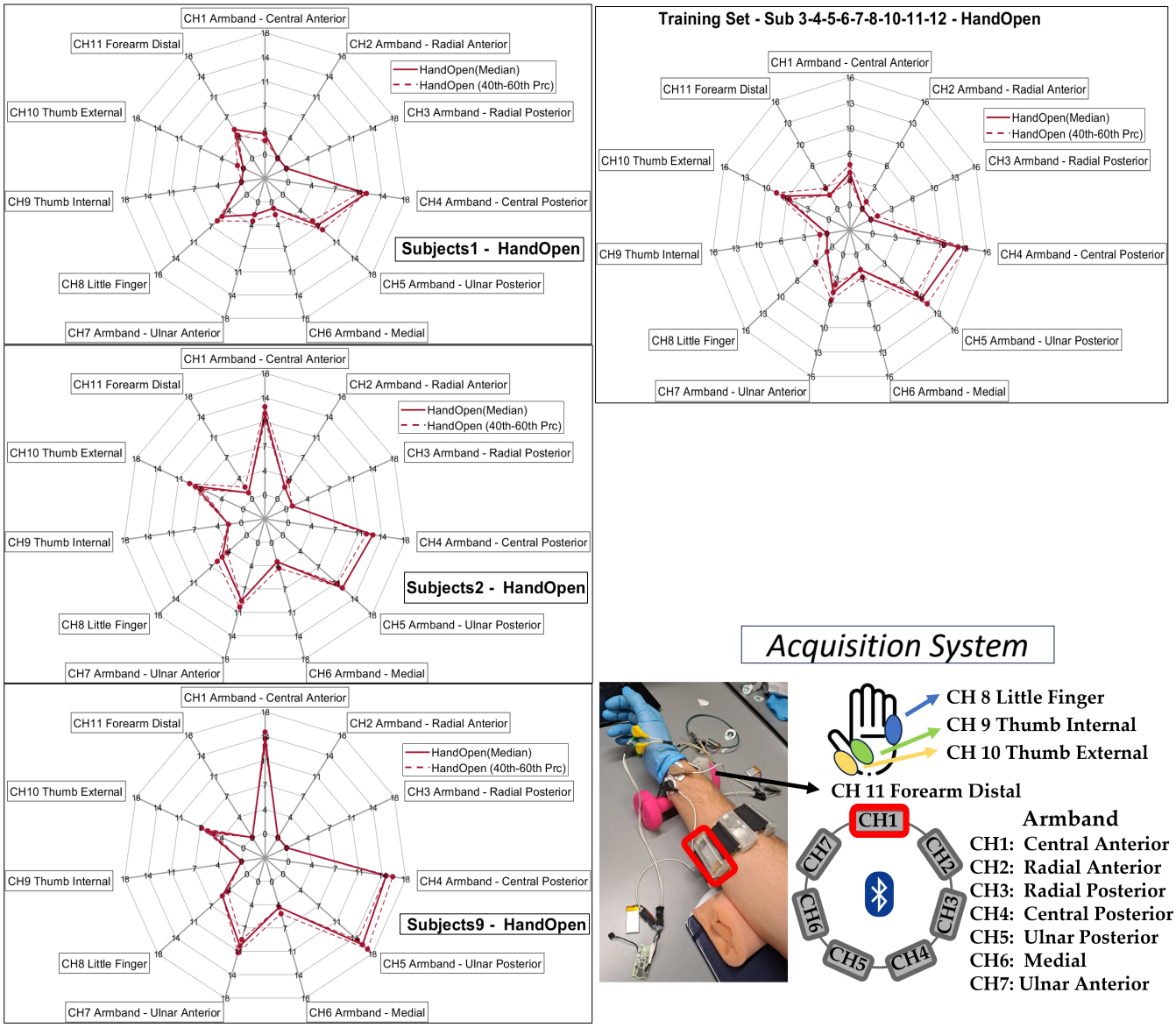

Figure 7.4: The figure shows the spatial distributions of activations on individual subjects comprising the test set, referring to the *hand open* movement. The radar plot represents, for each channel, the median value and the 40th and 60th percentiles extracted from the ATC profile. On the right side, there is the general radar plot of the training set and the image of the overall acquisition system. *Subjects Distribution number 5.*

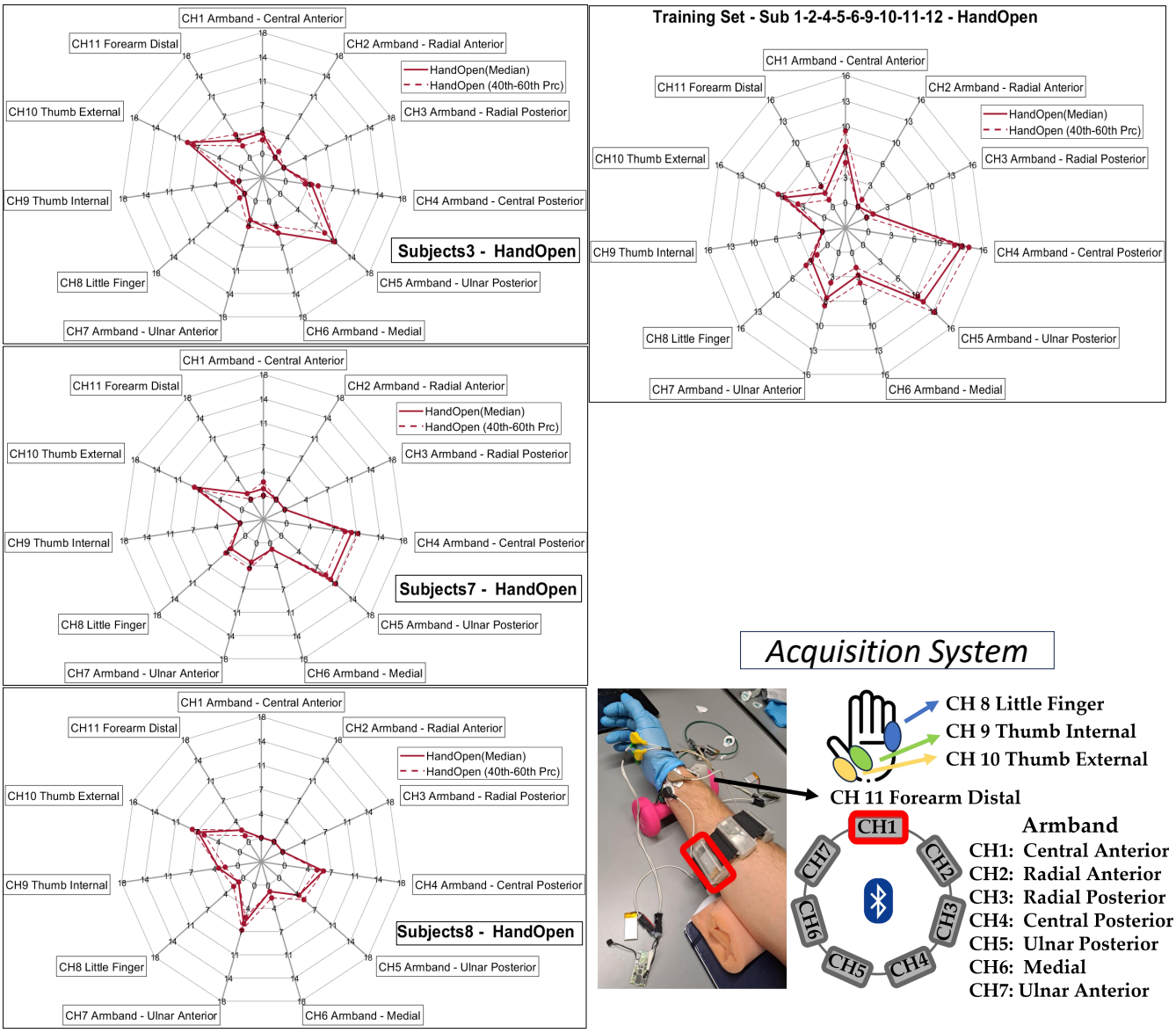

Figure 7.5: The figure shows the spatial distributions of activations on individual subjects comprising the test set, referring to the *hand open* movement. The radar plot represents, for each channel, the median value and the 40th and 60th percentiles extracted from the ATC profile. On the right side, there is the general radar plot of the training set and the image of the overall acquisition system. *Subjects Distribution number 4*

In Figure 7.4, which considers the case where movement classification yields the best results, there is a greater similarity between the activations. Indeed, the shape drawn by the radar plots related to the subjects of the test set is comparable to

the representative radar plot of the training set. This does not happen with the distribution of subjects number 4, Figure 7.5, where subjects exhibit significantly different activations in some channels, e.g., *CH1 Armband Central Anterior*, *CH8 Little Finger*.

In conclusion, these divergence, at the level of specific channels identified through the radar plot, were confirmed by observations of the ATC profiles obtained from the acquisitions.

The differences identified in the case of CH8 associated with the little finger are due to the variability in the activation of the *Abductor Digiti Minimi*, which is strongly dependent on the way the movement is performed and difficult to control compared to other muscles. The use of this channel may therefore lead to an improvement in classifier performance, but it also makes them more susceptible to variability.

The differences in CH1, associated with the *Flexor Digitorum Superficialis* responsible for finger flexion, may be specific to the subject and unpredictable, as they involve flexor muscles not directly involved in the hand opening movement.

7.1.2 Best Classifier Performance

The results, pertaining to all three subjects in the test set, for the classifier that achieved the best performance, are presented. Figure 7.6 displays the confusion matrix, providing an overview of the model's predictions at the individual class level. Subsequently, a Table 7.2 is presented containing the average precision, recall, and F1-score values, as well as those for each individual movement. The accuracy parameter has been exclusively calculated in relation to the overall system in order to evaluate the overall performance of the classifier, and therefore it is not included in the table. The chosen model architecture features two hidden layers, each comprising 90 neurons.

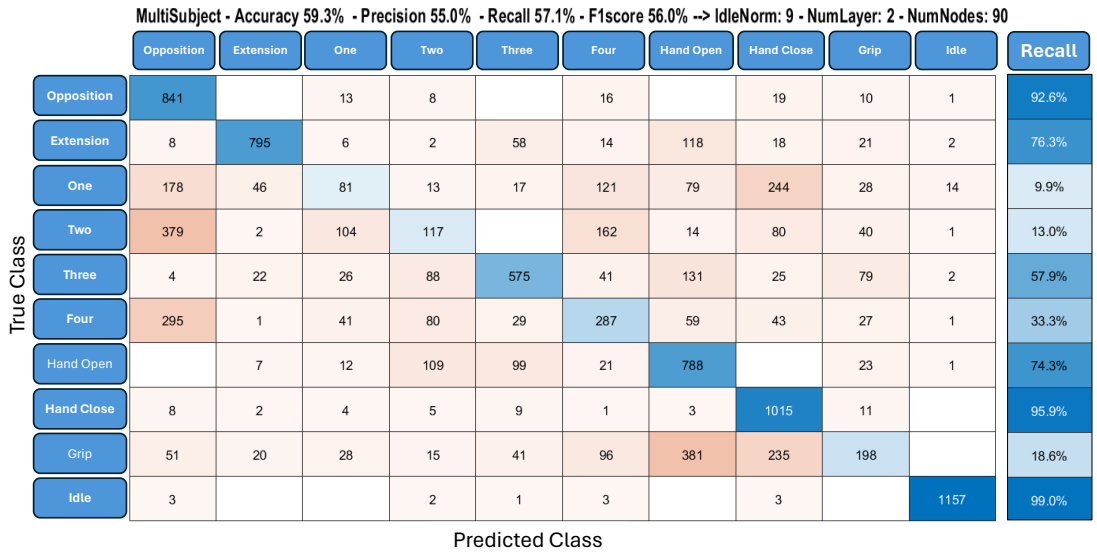

Figure 7.6: Confusion Matrix reporting the classification results obtained on the three subjects of the test set. The best model trained using the *Dataset All Channel* is utilized.

Table 7.2: Evaluation metrics (%)

Movement	Precision(%)	Recall(%)	F1-score(%)
Opposition	47.56	92.62	62.88
Extension	88.83	76.30	82.09
One	25.71	9.87	14.26
Two	26.65	13.01	17.49
Three	69.36	57.91	63.12
Four	37.66	33.26	35.32
Hand Open	50.10	74.34	59.86
Hand Close	60.35	95.94	74.09
Grip	45.31	18.59	26.37
Idle	98.13	98.97	98.55
Avg	**55.0**	**57.1**	**56.0**

The recognition of movements is subjected to high variability. Some classes exhibit high recall values, as seen in the case of *opposition* and *hand close* with 92.6% and 95.9%, respectively. Other movements such as *extension* and *hand open* have intermediate values of 76.3% and 74.3%. However, the remaining movements are poorly recognized by the model used, which is why it was not feasible to utilize the

classifier for real-time testing.

In conclusion, the tests aimed at verifying the feasibility of using a classifier capable of handling inter-subject variability were not satisfactory for extending applications by integrating the classifier within the control unit. This was noted considering the significant impact on performance caused by the distribution of subjects, as described previously. To optimize classification, it is necessary to standardize movements in order to limit variability that cannot be entirely mitigated by considering anatomical differences among subjects.

7.2 Single Subject

This second part of the results is dedicated to the performance obtained based on the dataset constructed for a single subject. The subject underwent the acquisition protocol eight times, two of which were used for the offline testing phase.

7.2.1 Best Classifier Performance

For the test to be conducted, it is necessary to first establish the threshold value applied in the normalization process of the dataset's resting state (*idle norm*), which optimizes the distinction of the performed movements. Figure 7.7 shows the threshold value set at 7 as the best solution.

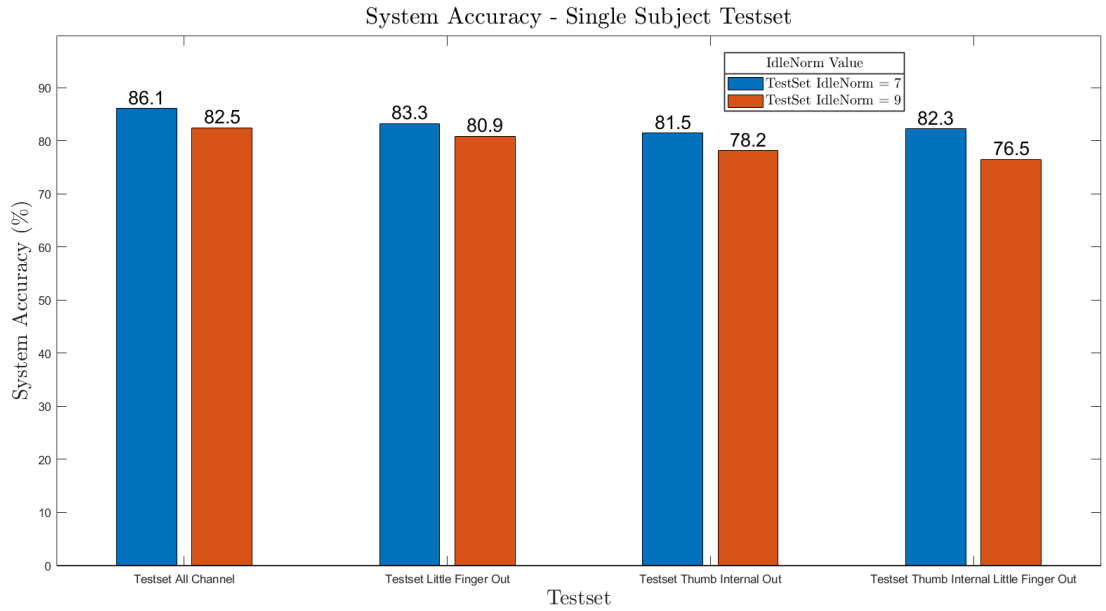

Figure 7.7: The histogram represents the results, in terms of accuracy, obtained from different types of datasets, in terms of *Idle norm* value as threshold applied on the rest condition.

In this case, all the results are comparable, showing a variability ranging from 76.5% in the case of datasets with the exclusion of two channels to 86.1% in the case of the complete dataset. There is coherence in terms of performance compared to the multi-subject scenario, as the use of the complete acquisition system also yields the best results in predicting movements in this case. The following Figure 7.8 presents the confusion matrix where the classifier can be evaluated based on the previously indicated parameters (precision, recall, f1-score), considering individual movements. As in the previous case, accuracy is computed only on average terms, for the general evaluation of multi-class prediction.

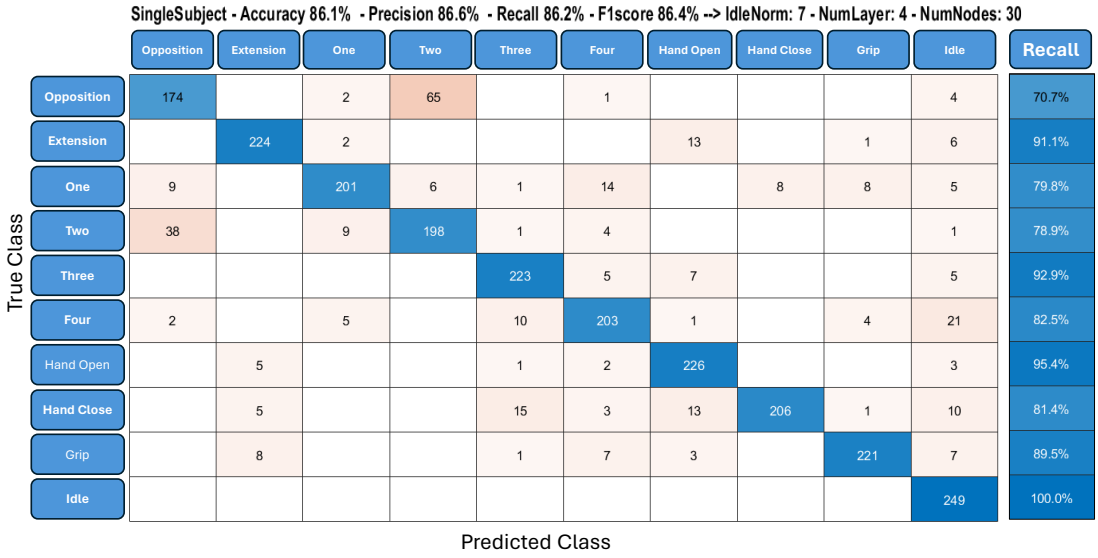

Figure 7.8

Table 7.3: Evaluation metrics (%)

Movement	Precision (%)	Recall (%)	F1-Score (%)
Opposition	78.03	70.73	74.2
Extension	92.56	91.06	91.8
One	91.78	79.76	85.35
Two	73.61	78.88	76.15
Three	88.49	92.92	90.65
Four	84.94	82.52	83.71
Hand Open	85.93	95.36	90.4
Hand Close	96.26	81.42	88.22
Grip	94.04	89.47	91.7
Idle	80.06	100	88.93
Avg	**86.97**	**85.32**	**85.9**

From the offline test, it is observed that, on average, all movements exhibit high probabilities of being correctly predicted by the classifier. The movement with the lowest recall value, equivalent to 70.7%, is opposition. The remaining classes are identified correctly between 78.9% (*One*) and 95.4% (*Hand Open*). Considering these reported values, the classifier was tested online as reported in the following paragraph

7.2.2 Real-time Hand Movements Classification

To achieve the online test, the best model of the classifier has been integrated into the software. This allows verifying the system's ability to correctly predict the movement executed by the subject from the acquisition side. The classification is based solely on the ATC values sent to the control unit every 130 ms. The classifier is integrated at the *System* layer, and the predicted class value is subsequently sent, through a queue, to the GUI where it is used to update the image associated with the predicted movement.

In order to stabilize the classification and minimize the probability of error, it was decided to introduce a control within the system. Each predicted class value is compared with a group of the last obtained class values; only if the group of values matches the last predicted one, the movement is effectively considered classified. It remains to establish the number of consecutive predictions necessary to consider the classification occurred, using the predicted class value. A higher value increases the likelihood of accurately recognizing the performed movement but creates a longer latency time in the predicted movement variation. Conversely, lower numbers of consecutive predictions of the same type may not allow stable classification, which would be problematic for the use of the classifier within the overall system. Numbers of consecutive classifications equivalent to 3-4-5 have been evaluated to assess actual changes in classification performance.

In order to evaluate hand movement recognition, two complete acquisition sessions were conducted for each consecutive prediction value (3-4-5). The results obtained are displayed through a confusion matrix from which precision, recall, and f1-score values are extracted for each movement.

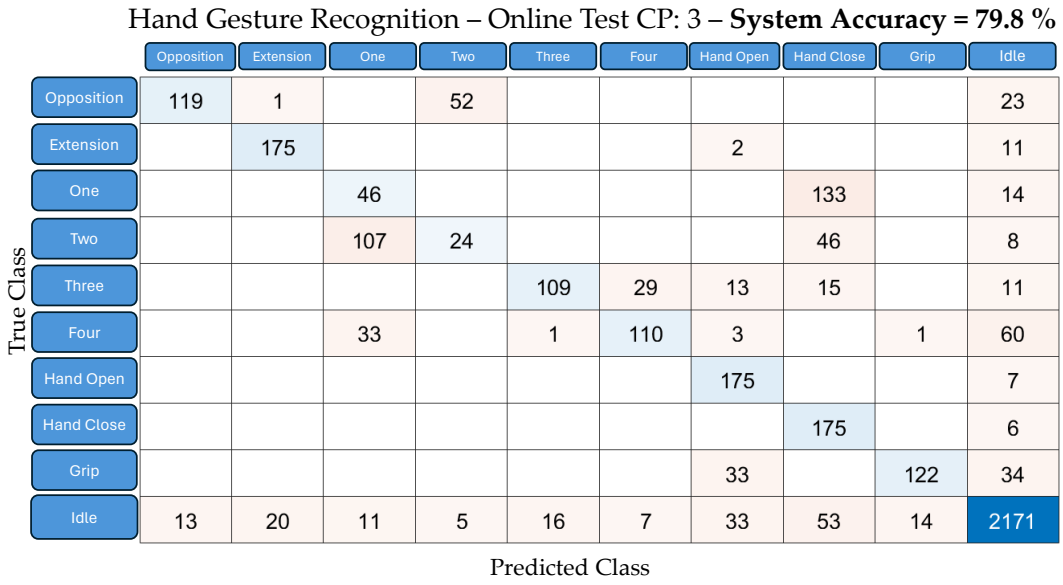

Figure 7.9: The Confusion Matrix reports the real-time classification results for two sessions of the experimental protocol. The value of consecutive predictions of the same class required to obtain the actual classification. *Consecutive Prediction* (CP) = 3.

Table 7.4: Movement Recognition Metrics - *Consecutive Prediction* (CP): 3

Movements	Precision (%)	Recall (%)	F1-Score (%)
Opposition	90.15	61.03	72.78
Extension	89.29	93.08	91.15
One	23.35	23.83	23.59
Two	29.63	12.97	18.05
Three	86.51	61.58	71.95
Four	75.34	52.89	62.15
Hand Open	67.57	96.15	79.37
Hand Close	41.47	96.69	58.04
Grip	89.05	64.55	74.85
Idle	92.58	92.66	92.62
Avg	**68.50**	**65.50**	**67.00**

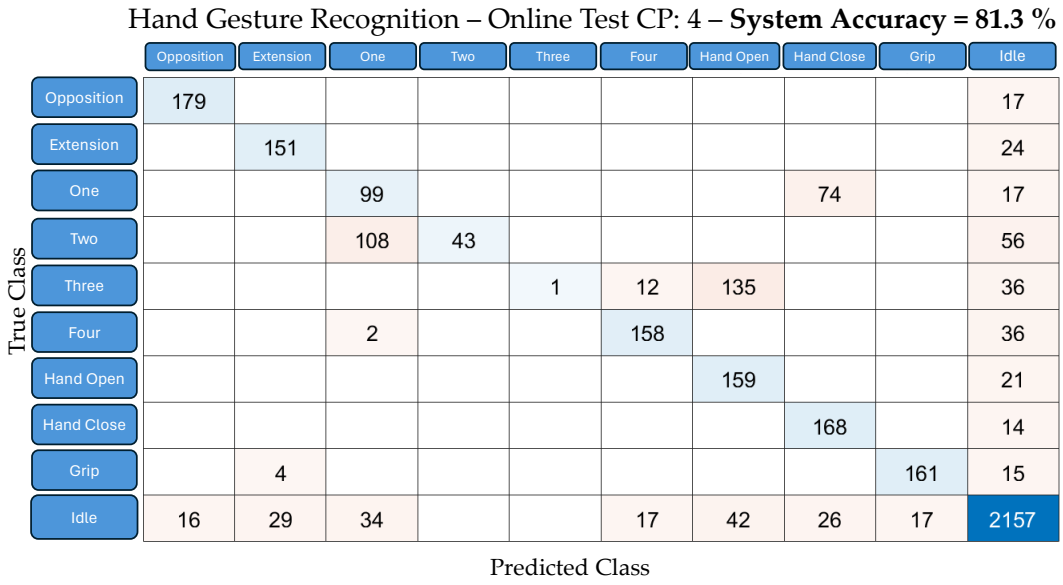

Figure 7.10: The Confusion Matrix reports the real-time classification results for two sessions of the experimental protocol. The value of consecutive predictions of the same class required to obtain the actual classification. *Consecutive Prediction* (CP) = 4.

Table 7.5: Movement Recognition Metrics - *Consecutive Prediction* (CP): 4

Movements	Precision(%)	Recall(%)	F1-Score(%)
Opposition	91.80	91.33	91.56
Extension	82.07	86.29	84.12
One	40.74	52.11	45.73
Two	100.00	20.77	34.40
Three	100.00	0.54	1.08
Four	84.49	80.61	82.51
Hand Open	47.32	88.33	61.63
Hand Close	62.69	92.31	74.67
Grip	90.45	89.44	89.94
Idle	90.14	92.26	91.19
Avg	**79.00**	**69.40**	**73.90**

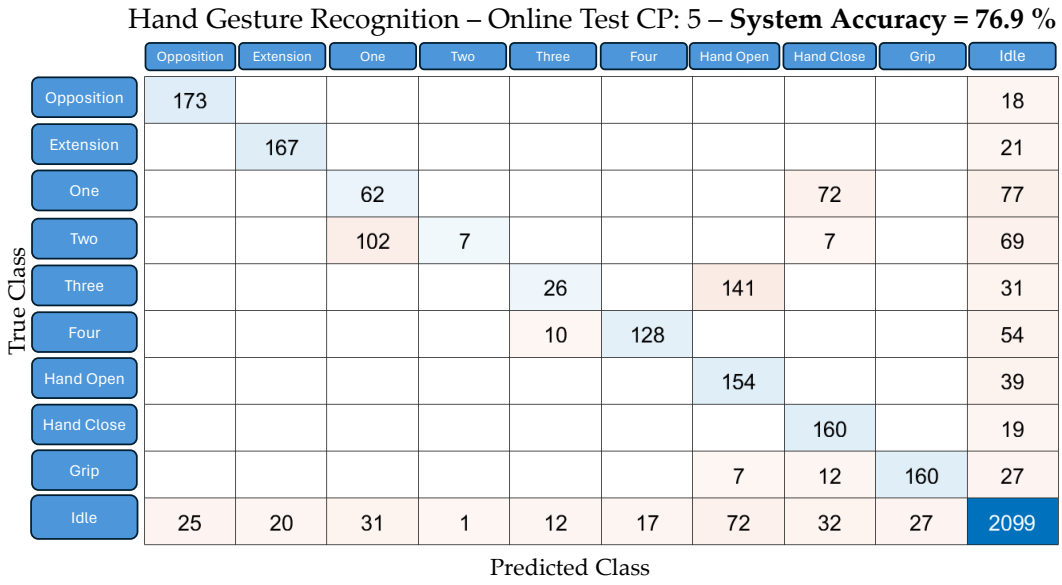

Figure 7.11: The Confusion Matrix reports the real-time classification results for two sessions of the experimental protocol. The value of consecutive predictions of the same class required to obtain the actual classification. *Consecutive Prediction* (CP) = 5.

Table 7.6: Metriche di riconoscimento dei movimenti - *Consecutive Prediction* (CP): 5

Movements	Precision (%)	Recall (%)	F1-Score (%)
Opposition	87.37	90.58	88.95
Extension	89.31	88.83	89.07
One	31.80	29.38	30.54
Two	87.50	3.78	7.25
Three	54.17	13.13	21.14
Four	88.28	66.67	75.96
Hand Open	41.18	79.79	54.32
Hand Close	56.54	89.39	69.26
Grip	85.56	77.67	81.43
Idle	85.53	89.85	87.64
Average	**70.70**	**62.90**	**66.60**

Analyzing the results, movements e.g. opposition, one, two, three, four, grip, are observed to have been recognized differently in the three tests.This variability is due to the precision with which the movement must be executed for correct recognition by the classifier; in these cases, variability in execution leads to performance instability.

Other movements, such as extension, hand open, hand close, consistently showed high performance across all three tests. This is attributed to the clear distinction in their recognition compared to other movements and the greater reproducibility of the gesture. In these cases, observing the confusion matrix, it is noticed that classification errors occur during the transition phase from the resting phase preceding the movement activation. However, these errors are inherent in the classification technique implemented. The movement remains classified correctly without being identified as a different type of gesture.

From the results obtained based on classification data collected from online tests, the CP value that yielded the best performance is 4. Utilizing this parameter, six out of the ten target movements were successfully recognized. It is observed from the confusion matrix that the sources of error, as anticipated, stem from a delay in the transition between muscle activation and rest states during the execution of the experimental protocol.

The remaining movements (One, Two, Three) were recognized in an unstable manner by the control unit. This instability is attributed to the complexity of the movements and their similarity to others, necessitating selective control of individual fingers during gesture execution.

Despite this, real-time classification analysis allows testing hand movement recognition in the real context of use within the system, highlighting the need to increase the stability of the mentioned movements to be able to use the system with all nine selected gestures.

Chapter 8

Conclusion and Future Perspective

During the thesis project, the development of a real-time and sEMG-based system for Functional Electrical Stimulation (FES) control was initiated. The anatomical area targeted by the system is the hand. Therefore, following a detailed study of hand anatomy and muscular structure, the architecture of the sEMG signal acquisition system was defined. The architecture consists of 5 independent devices, which are used synchronously through software enabling interaction with the devices and visualization of the obtained data within a Graphical User Interface (GUI).

The data of interest, transmitted to the control unit via bluetooth, are obtained from the sEMG signal to which the ATC paradigm is applied. This paradigm allows computing parameters closely related to muscle activation and generated force. The extracted parameters are used for modulating stimulation parameters.

After completing the initial phase dedicated to the development of the acquisition system and software adaptation, the project focused on integrating a classifier within the control unit. Therefore, 9 movements were selected and performed by 12 subjects involved in the experimentation, suitably organized within an acquisition protocol. The classifier training phase was divided into two areas: the first focused on creating a multi-subject dataset, while the second focused on a specific and personalized dataset for a single individual.

The specific approach to individual subjects was adopted based on the primary mode of system usage, the therapist-patient mode. This method of carrying out rehabilitation activities involves using the acquisition system on the therapist, who, by performing movements, directly determines the stimulation parameters administered to the patient. This way, the stimulation is directly controlled by the information obtained from the therapist's muscle activations.

To maximize performance, a phase of model optimization was conducted to define key elements of the neural network architecture, chosen as the machine learning model for multi-class classification. Additionally, different types of datasets were evaluated based on the number of devices used. For the multi-subject case, various subject distributions between training and test sets were also randomly tested, maintaining a distribution of 9 and 3 subjects, respectively, between the two training and test set.

Finally, classifier performance was evaluated based on the results obtained in the previous optimization phase. At this stage of the work, criticalities emerged in the classifier's ability to address the high intersubject variability, already observed in the preliminary phases of model training analysis. Therefore, integration of the multi-class model within the control unit was not pursued, and no online tests were conducted in this regard.

In the context of the dataset built on the individual subject, however, the results were significantly better, with an average accuracy value of 86.1%. The best model was then integrated into the control unit and tested in real-time mode, showing promising prospects for integrating the classifier into the overall system.

The continuation of the project has, as its primary objective, the integration of the classifier within the overall system, in order to test its functionalities applied to electrical stimulation.

The classifier primarily serves as a control function for the application of electrical stimulation to the patient. In this way, stimulation can only be initiated after the movement has been recognized, ensuring that the ATC signals input into the control unit derive from the execution of a movement for rehabilitative purposes.

Furthermore, considering the high number of acquisition channels, it will be necessary to condense the information contained in the ATC data within the stimulation channels, which are different in number and positioning compared to the acquisition channels. Therefore, the predicted class information from the classifier can be used as an additional parameter for modulating the FES parameters.

The integration with FES was initiated in the final phase of the project, providing a preliminary solution for integrating the predicted class index for stimulation control.

Bibliography

[1] Isabela Campanini et al. "Surface EMG in clinical assessment and neurorehabilitation: Barriers limiting its use". In: *Frontiers in Neurology* 11 (2020). DOI: 10.3389/fneur.2020.00934.

[2] Chim H. *Hand and Wrist Anatomy and Biomechanics: A Comprehensive Guide.* Plast Reconstr Surg., 2017. DOI: 10.1097/PRS.0000000000003745.

[3] V.K. Nanayakkara et al. "The role of morphology of the thumb in anthropomorphic grasping: A Review". In: *Frontiers in Mechanical Engineering* 3 (2017). DOI: 10.3389/fmech.2017.00005.

[4] Donald A. Neumann and Troy Bielefeld. "The carpometacarpal joint of the thumb: Stability, deformity, and therapeutic intervention". In: *Journal of Orthopaedic & Sports Physical Therapy* 33.7 (2003), pp. 386–399. DOI: 10.2519/jospt.2003.33.7.386.

[5] Donald A. Neumann and Troy Bielefeld. "The carpometacarpal joint of the thumb: Stability, deformity, and therapeutic intervention". In: *Journal of Orthopaedic & Sports Physical Therapy* 33.7 (2003), pp. 386–399. DOI: 10.2519/jospt.2003.33.7.386.

[6] Dee Unglaub Silverthorn. *Fisiologia Umana: Un Approccio Integrato.* Milano: Pearson, 2020.

[7] Anatomy and Physiology I. *Skeletal Muscle.* URL: https://courses.lumenlearning.com/suny-ap1/chapter/skeletal-muscle/.

[8] Bujuìs. *Biology.* URL: https://byjus.com/question-answer/explain-the-mechanism-of-muscle-contraction-with-diagram/.

[9] Gerald Loeb. "The Motor Unit and Muscle Action". In: *Principles of Neural Science.* McGraw-Hill Education, 2014. URL: https://neurology.mhmedical.com/content.aspx?bookid=1049&sectionid=59138664.

[10] G. Kamen and D.C.C. Du. "Independence of motor unit recruitment and rate modulation during precision force control". In: *Neuroscience* 88.2 (1999), pp. 643–653. ISSN: 0306-4522. DOI: https://doi.org/10.1016/S0306-4522(98)00248-6. URL: https://www.sciencedirect.com/science/article/pii/S0306452298002486.

[11] Vladimir Medved, Sara Medved, and Ida Kovač. "Critical Appraisal of Surface Electromyography (sEMG) as a Taught Subject and Clinical Tool in Medicine and Kinesiology". In: *Frontiers in Neurology* 11 (2020). ISSN: 1664-2295. DOI: 10.3389/fneur.2020.560363. URL: https://www.frontiersin.org/journals/neurology/articles/10.3389/fneur.2020.560363.

[12] Marco Antonio Cavalcanti Garcia and Taian Vieira. "Surface electromyography: Why, when and how to use it". In: *Revista Andaluza de Medicina del Deporte* 4 (Apr. 2011), pp. 17–28.

[13] Kerry R. Mills. "The basics of electromyography". In: *Journal of Neurology, Neurosurgery & Psychiatry* 76.suppl_2 (2005), pp. ii32–ii35. DOI: 10.1136/jnnp.2005.069211.

[14] Núria Massó et al. "Surface electromyography applications in the sport". In: *ApuntsMed Esport* 45 (Jan. 2010).

[15] Anjana Goen and D. Tiwari. "Review of Surface Electromyogram Signals: Its Analysis and Applications". In: *International Journal of Electrical, Computer, Energetic, Electronic and Communication Engineering* 7 (Jan. 2013), pp. 1429–1437.

[16] "Experimental studies of alternating and direct current impedance properties of Ag/AgCl electrodes". In: *Applied Mechanics and Materials* 778 (2015), pp. 110–115. DOI: 10.4028/WWW.SCIENTIFIC.NET/AMM.778.110.

[17] N. Landra et al. "A biomimetic multichannel synergistic calibration for event-driven functional electrical stimulation". In: *2022 IEEE Biomedical Circuits and Systems Conference (BioCAS)* (2022). Preprint. DOI: 10.1109/biocas54905.2022.9948634.

[18] C Assambo et al. "Determination of the parameters of the skin-electrode impedance model for ECG measurement". In: (2007), pp. 90–95. URL: https://api.semanticscholar.org/CorpusID:1854725.

[19] Muhammad Zahak Jamal. "Signal Acquisition Using Surface EMG and Circuit Design Considerations for Robotic Prosthesis". In: (2012). Ed. by Ganesh R. Naik. DOI: 10.5772/52556. URL: https://doi.org/10.5772/52556.

[20] J. Kilby, K. Prasad, and G. Mawston. "Multi-channel surface electromyography electrodes: A Review". In: *IEEE Sensors Journal* 16.14 (2016), pp. 5510–5519. DOI: 10.1109/jsen.2016.2569072.

[21] A. Prestia et al. "Raspberry pi based modular system for multichannel event-driven functional electrical stimulation control". In: *2022 44th Annual International Conference of the IEEE Engineering in Medicine & Biology Society (EMBC)* (2022). Preprint. DOI: 10.1109/embc48229.2022.9871852.

[22] S. Sapienza et al. "On integration and validation of a very low complexity ATC UWB system for muscle force transmission". In: *IEEE Transactions on Biomedical Circuits and Systems* 10.2 (2016), pp. 497–506. DOI: 10.1109/tbcas.2015.2416918.

[23] F. Rossi et al. "Tutorial: A versatile bio-inspired system for processing and transmission of muscular information". In: *IEEE Sensors Journal* 21.20 (2021), pp. 22285–22303. DOI: 10.1109/jsen.2021.3103608.

[24] Dejan B. Popović. "Advances in functional electrical stimulation (FES)". In: *Journal of Electromyography and Kinesiology* 24.6 (2014), pp. 795–802. ISSN: 1050-6411. DOI: https://doi.org/10.1016/j.jelekin.2014.09.008.

[25] Shiyu Luo et al. "A Review of Functional Electrical Stimulation Treatment in Spinal Cord Injury". In: *NeuroMolecular Medicine* 22 (2020). DOI: 10.1007/s12017-019-08589-9.

[26] D.G. Everaert et al. "Does functional electrical stimulation for foot drop strengthen corticospinal connections?" In: *Neurorehabilitation and Neural Repair* 24.2 (2009), pp. 168–177. DOI: 10.1177/1545968309349939.

[27] Jeffrey S Knutson et al. "Efficacy of contralaterally controlled functional electrical stimulation compared to cyclic neuromuscular electrical stimulation and task-oriented training for recovery of hand function after stroke: Study protocol for a multi-site randomized controlled trial". In: *Trials* 23.1 (2022). DOI: 10.1186/s13063-022-06303-y.

[28] P. Maceira-Elvira et al. "Wearable Technology in stroke rehabilitation: Towards improved diagnosis and treatment of upper-limb motor impairment". In: *Journal of NeuroEngineering and Rehabilitation* 16.1 (2019). DOI: 10.1186/s12984-019-0612-y.

[29] Irene Campanini et al. "Surface EMG in clinical assessment and neurorehabilitation: Barriers limiting its use". In: *Frontiers in Neurology* 11 (2020). DOI: 10.3389/fneur.2020.00934.

[30] M. Al-Ayyad et al. "Electromyography Monitoring Systems in rehabilitation: A review of clinical applications, Wearable Devices and signal acquisition methodologies". In: *Electronics* 12.7 (2023), p. 1520. DOI: 10.3390/electronics12071520.

[31] Mirza Mansoor Baig, Hamid Gholamhosseini, and Martin J. Connolly. "A systematic review of wearable patient monitoring systems—current challenges and opportunities for clinical adoption". In: *Journal of Medical Systems* 41.7 (2017). DOI: 10.1007/s10916-017-0760-1.

[32] Shun Zhao et al. "Wearable physiological monitoring system based on electrocardiography and electromyography for upper limb rehabilitation training". In: *Sensors* 20.17 (2020), p. 4861. DOI: 10.3390/s20174861.

[33] Shih-Hong Liu, Jia-Jyun Wang, and Tai-Hua Tan. "A portable and wireless multi-channel acquisition system for Physiological Signal Measurements". In: *Sensors* 19.23 (2019), p. 5314. DOI: 10.3390/s19235314.

[34] Francesco V G Tenore et al. "Decoding of individuated finger movements using surface electromyography". In: *IEEE Transactions on Biomedical Engineering* 56.5 (2009), pp. 1427–1434. DOI: 10.1109/tbme.2008.2005485.

[35] Stefano Pizzolato et al. "Comparison of six electromyography acquisition setups on hand movement classification tasks". In: *PLOS ONE* 12.10 (2017). DOI: 10.1371/journal.pone.0186132.

[36] Hafiz Adnan Javaid et al. "Classification of hand movements using myo armband on an embedded platform". In: *Electronics* 10.11 (2021), p. 1322. DOI: 10.3390/electronics10111322.

[37] Fabio Rossi et al. "An Event-Driven Closed-Loop System for Real-Time FES Control". In: (2019), pp. 867–870. DOI: 10.1109/ICECS46596.2019.8965153.

[38] Keisuke Shima and Koji Shimatani. "A new approach to direct rehabilitation based on functional electrical stimulation and EMG classification". In: *2016 International Symposium on Micro-NanoMechatronics and Human Science (MHS)* (2016), pp. 1–6. URL: https://api.semanticscholar.org/CorpusID:6402828.

[39] Fabio Rossi et al. "Live Demonstration: A Real-Time Bio-Mimetic System for Multichannel FES Control". In: (2022). DOI: 10.1109/BioCAS54905.2022.9948597.

[40] A. Prestia et al. "Motion Analysis for Experimental Evaluation of an event-driven FES system". In: *IEEE Transactions on Biomedical Circuits and Systems* 16.1 (2022), pp. 3–14. DOI: 10.1109/tbcas.2021.3137027.

[41] Ambiq. *Apollo3 Blue*. n.d. URL: https://ambiq.com/apollo3-blue/.

[42] Katsuyuki Hagiwara and Kenji Fukumizu. "Relation between weight size and degree of over-fitting in neural network regression". In: *Neural Networks* (2008). DOI: https://doi.org/10.1016/j.neunet.2007.11.001. URL: https://www.sciencedirect.com/science/article/pii/S0893608007002390.

[43] Fabio Rossi. "A Bio-Inspired Processing Unit for Surface Electromyography Applications". PhD thesis. Politecnico di Torino, 2022.

[44] A. Mongardi et al. "Hand gestures recognition for human-machine interfaces: A low-power bio-inspired armband". In: *IEEE Transactions on Biomedical Circuits and Systems* 16.6 (2022), pp. 1348–1365. DOI: 10.1109/tbcas.2022.3211424.

[45] Hasomed. *RehaStim 2*. n.d. URL: https://hasomed.de/en/products/rehamove/.

[46] HASOMED gmbH. *Operation Manual RehaStim2 - User Guide*. 2012. URL: https://static1.squarespace.com/static/5f16af2c5732983b810510ef/t/625445ebc1f33f681fa9ec3e/1649690115682/RehaMove2_User+Manual_2.4._ENG_CM_20170201.pdf.

[47] Nordic Semiconductor. *nRF52840 Dongle*. n.d. URL: https://www.nordicsemi.com/Products/Development-hardware/nRF52840-Dongle.

[48] Steven F Lott and Dusty Phillips. *Python Object-Oriented Programming: Build robust and maintainable object-oriented Python applications and libraries*. Packt Publishing Ltd, 2021.

[49] E. Ekstrand et al. "Perceived ability to perform daily hand activities after stroke and associated factors: A cross-sectional study". In: *BMC Neurology* 16.1 (2016). DOI: 10.1186/s12883-016-0733-x.

[50] H. Eschmann et al. "Thumb and finger movement is reduced after stroke: An observational study". In: *PLOS ONE* 14.6 (2019). DOI: 10.1371/journal.pone.0217969.

[51] N. Landra and altri. "Una calibrazione sinergica biomimetica multicanale per la stimolazione elettrica funzionale basata su eventi". In: *2022 IEEE Biomedical Circuits and Systems Conference (BioCAS) [Preprint]* (2022). DOI: 10.1109/biocas54905.2022.9948634.

[52] Università degli Studi di Torino. *Comitato di bioetica dell'ateneo*. n.d. URL: https://www.unito.it/ricerca-e-innovazione/fare-ricerca-unito/comitato-di-bioetica-dellateneo.

[53] Z. Nematzadeh, R. Ibrahim, and A. Selamat. "Comparative studies on breast cancer classifications with K-fold cross validations using Machine Learning Techniques". In: *2015 10th Asian Control Conference (ASCC)* (2015). Preprint. DOI: 10.1109/ascc.2015.7244654.

[54] Hiren Kumar Thakkar et al. *Chapter 11 - Applications of wearable technologies in healthcare: an analytical study*. Ed. by Akash Kumar Bhoi et al. Intelligent Data-Centric Systems. Academic Press, 2022. DOI: https://doi.org/10.1016/B978-0-323-90548-0.00001-2. URL: https://www.sciencedirect.com/science/article/pii/B9780323905480000012.

[55] Z. Nematzadeh, R. Ibrahim, and A. Selamat. "Comparative studies on breast cancer classifications with K-fold cross validations using Machine Learning Techniques". In: *2015 10th Asian Control Conference (ASCC)* (2015). Preprint. DOI: 10.1109/ascc.2015.7244654.

[56] Benyamin Ghojogh and Mark Crowley. "The theory behind overfitting, cross validation, regularization, bagging, and boosting: tutorial". In: *arXiv preprint arXiv:1905.12787* (2019). DOI: https://doi.org/10.1016/j.engappai.2006.06.005.

[57] P.G. Benardos and G.-C. Vosniakos. "Optimizing feedforward artificial neural network architecture". In: *Engineering Applications of Artificial Intelligence* (2007). DOI: https://doi.org/10.1016/j.engappai.2006.06.005. URL: https://www.sciencedirect.com/science/article/pii/S0952197606001072.